

A Lead Selenide Thin Film for Photovoltaic Application

A Thesis

Presented to
the faculty of the School of Engineering and Applied Science
University of Virginia

in partial fulfillment
of the requirements for the degree

Master of Science

by

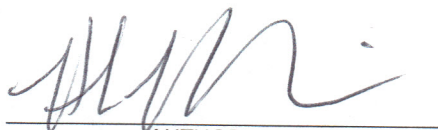
Helena Arifa Khazdozian

August

2013

APPROVAL SHEET

The thesis
is submitted in partial fulfillment of the requirements
for the degree of
Master of Science


AUTHOR

The thesis has been read and approved by the examining committee:

Tatiana Globus

Advisor

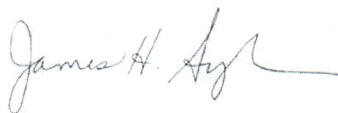
Paxton Marshall

Lloyd R. Harriott

Mool C. Gupta

Jerome Ferrance

Accepted for the School of Engineering and Applied Science:



Dean, School of Engineering and Applied Science

August
2013

Acknowledgements

I would like to acknowledge the guidance and support of my co-advisors Tatiana Globus and Paxton Marshall, who have served as inspirations to me throughout this process. I would like to thank my examination committee, Lloyd Harriott, Mool Gupta, and Jerome Ferrance, for taking the time to review my work. In particular, thanks to the chair of this committee, Lloyd Harriott, for his input throughout the research process. I would like to thank Jerome Ferrance for his invaluable contribution to this work. I would like to thank Mool Gupta and Joe Campbell for the gracious use of their laboratories. Additionally, I would like to acknowledge Naser Alijabbari and Andre Slonopas who have collaborated with me on this work and served as values resources.

And last, but not least, I would like to thank Niki Scutt. Without his love, support and patience, this would not have been possible.

Abstract

Currently, the United States is highly dependent on fossil fuels for the majority of its energy needs. This problem has many negative consequences for our nation. In order for solar energy to be cost competitive with fossil fuels, the manufacturing and material costs must be reduced while the conversion efficiency is increased. Thin film lead selenide was investigated for photovoltaic application. If incorporated into a heterojunction solar cell, PbSe has the potential to reduce overall costs through the use of less material and a low cost, low temperature deposition technique, as well as the potential to increase conversion efficiency due to the potential of carrier multiplication in PbSe quantum dots.

P-type polycrystalline PbSe thin films have been fabricated by chemical bath deposition. The electrical properties of these PbSe thin films can be reproducibly controlled through variation of the deposition conditions. P-type PbSe thin films with hole densities varying from 4.28×10^{17} to $1.91 \times 10^{19} \text{ cm}^{-3}$ have been achieved. The results suggest that PbSe thin films were also fabricated in which both electrons and holes contribute to conduction. High hole mobility for polycrystalline PbSe has been achieved. Additionally, proof of concept has been demonstrated for a heterojunction composed of p-type nanocrystalline PbSe and n-type monocrystalline Si. The heterojunction between the two highly doped semiconductors exhibits rectifying behavior, laying the foundation for future investigation of such a heterojunction.

Table of Contents

| | |
|---|-----|
| Acknowledgements..... | i |
| Abstract..... | ii |
| Table of Contents..... | iii |
| 1. Introduction | 1 |
| 1.1 Long Term Goals..... | 1 |
| 1.2 Goals of this Research | 1 |
| 1.3 PbSe – A Lead Chalcogenide | 2 |
| 2. Motivation | 2 |
| 2.1 Necessity of Photovoltaics | 2 |
| 2.2 PbSe-Si Heterojunctions..... | 6 |
| 2.3 Current State of Thin Film Photovoltaic Technology..... | 6 |
| 2.3.1 Amorphous Si | 7 |
| 2.3.2 CdTe/CdS | 7 |
| 2.3.3 CIGS/[Cd/S]..... | 8 |
| 3. Background | 8 |
| 3.1 Chemical Bath Deposition | 8 |
| 3.2 Ion-by-Ion Growth | 8 |
| 3.3 Hydroxide Cluster Growth..... | 9 |
| 3.4 Chemical Reaction | 10 |
| 3.5 Factors Influencing Deposition..... | 10 |
| 4. Experimental Techniques..... | 11 |
| 4.1 Chemical Bath Deposition | 11 |
| 4.1.1 Cleaning of Glass Substrates | 11 |
| 4.1.2 Cleaning of Si Substrates | 11 |
| 4.1.3 Chemical Bath Preparation..... | 11 |
| 4.1.4 KOH as the Complexing Agent..... | 11 |
| 4.1.5 Na ₃ C ₆ H ₅ O ₇ (TSC) as the Complexing Agent..... | 12 |
| 4.1.6 Experimental Setup | 12 |
| 4.2 Hall Effect Measurement..... | 12 |
| 4.3 Interference Spectroscopy | 14 |
| 4.3.1 Reflection Fringe Measurement..... | 14 |
| 4.3.2 Transmission Fringe Measurement..... | 15 |
| 4.3.3 Thickness Calculation | 16 |
| 4.4 Heterojunction Fabrication | 17 |
| 4.4.1 Contact Formation | 17 |
| 4.5 Current-Voltage (I-V) Measurement | 17 |
| 5. Results..... | 18 |
| 5.1 PbSe on Glass | 18 |
| 5.1.1 Estimation of Electrical Properties for Two Carrier Contribution to Conduction | 19 |
| 5.1.2 Analysis of Results | 24 |
| 5.1.2.1 Variation of Time | 24 |
| 5.1.2.1.1 60°C, 1M TSC, 86mM Se: Variation of Time | 24 |
| 5.1.2.1.2 75°C, 1M TSC, 86mM Se: Variation of Time | 29 |
| 5.1.2.2 Variation of Temperature | 31 |
| 5.1.2.2.1 1hr, 1M TSC, 86mM Se: Variation of Temperature | 32 |
| 5.1.2.2.2 2hr, 1M TSC, 86mM Se: Variation of Temperature | 33 |

| | | |
|-----------|--|----|
| 5.1.2.2.3 | 3hr, 1M TSC, 86mM Se: Variation of Temperature | 33 |
| 5.1.2.3 | Variation of Concentration of the Complexing Agent, TSC | 35 |
| 5.1.2.4 | Variation of Concentration of Se | 39 |
| 5.1.2.4.1 | 2hr, 75°C, 0.7M TSC: Variation of Se | 39 |
| 5.1.2.4.2 | 2hr, 75°C, 0.75M TSC: Variation of Se | 40 |
| 5.1.2.5 | Reproducibility | 42 |
| 5.2 | PbSe-Si Heterojunction | 43 |
| 5.2.1 | Highly Doped p-type PbSe and Degenerately Doped n-type Si | 43 |
| 5.2.2 | Lightly Doped p-type PbSe and Degenerately Doped n-type Si | 46 |
| 6. | Conclusions | 48 |
| 7. | Future Work | 49 |
| 8. | References | 50 |
| 9. | Appendix | 53 |

1. Introduction

1.1 Long Term Goals

A thin film heterojunction solar cell composed of p-type PbSe and n-type Si has the potential to increase conversion efficiency while simultaneously reducing material and manufacturing costs. Single junction solar cells, like first generation solar cells, can only absorb portions of the solar spectrum which have energy equal to or greater than their band gap energy. This greatly limits the conversion efficiency of solar cells because not all incident solar radiation can be converted into electricity. Multijunction solar cells are able to absorb larger portions of the solar spectrum by utilizing several semiconductors with different band gaps. For a single junction solar cell, photons with energy greater than the band gap of the material will be absorbed, but the excess energy of the photon is lost as heat through thermal relaxation. By employing semiconductors of varying band gap energies in multijunction solar cells, more high energy photons can be absorbed, reducing the energy loss due to thermal relaxation and increasing efficiency. However, the increased material use increases the overall cost of the solar cell. A thin film heterojunction is able to balance this trade off more favorably in the direction of cost reduction.

PbSe has a narrow band gap, allowing for absorption across the entire solar spectrum, most notably in the low infrared (IR)— a region where most semiconductors employed for photovoltaics cannot absorb. Additionally, PbSe is a direct band gap semiconductor, requiring only a few microns thickness to absorb solar radiation. Pairing thin film PbSe with a thin film wide band gap semiconductor like Si allows for absorption across the entire solar spectrum while minimizing material costs. Also, PbSe can be deposited by chemical bath deposition, a low temperature, low cost technique which reduces the manufacturing costs of the solar cell.

Carrier multiplication and quantum size effects have been observed in PbSe nanocrystals [1-5]. Carrier multiplication is a phenomenon in which multiple excitons are generated from a single incident photon. The generation of up to seven excitons from a single incident photon has been observed in PbSe quantum dots [4]. If these excitons were to be effectively separated and collected in the proposed thin film heterojunction, the conversion efficiency of such solar cells could be dramatically increased. In several published works, it has been consistently observed that the band gap of PbSe increases with a decrease in nanocrystal size [5-7]. The effect of quantum confinement allows for the tuning of band gaps in PbSe quantum dots (nanocrystals less than 10nm in size). By tuning the band gap of PbSe, absorption of specific regions of the solar spectrum could be targeted.

1.2 Goals of this Research

This work aims to fabricate a reproducible p-type PbSe thin film with properties desirable for photovoltaic application and provide proof of concept of a heterojunction between this p-type PbSe thin film and n-type Si. In order to achieve the long term goal of fabricating a low cost, highly efficient thin film photovoltaic cell, deposition of PbSe must first be investigated and optimized to achieve a reproducible thin film. Several criteria must be met if the long term goals are to be achieved. To minimize the material costs of the solar cell, a thin film layer of PbSe must be deposited which is less than 1 μ m in thickness. Ideally, PbSe quantum dots, nanocrystals less than 10nm in size, will compose the nanocrystalline structure to allow for the potential of carrier multiplication and quantum confinement effects. By employing chemical bath deposition, an inexpensive, low temperature technique, the overall costs will be reduced. High mobility of carriers and a low hole density is desired. At high carrier densities, both impact recombination and radiative recombination will contribute to recombination due to the increased presence of impurities (discussed further in section 1.3). This reduces the charge carrier lifetime and in turn the mobility of the charge carriers. For this reason, highly doped PbSe is not desirable. The ideal hole density is between $1 \times 10^{17} \text{ cm}^{-3}$ and $2 \times 10^{17} \text{ cm}^{-3}$ based on the

previous work of Dr. Tatiana Globus, advisor to this work; high photoconductivity was observed within this hole density range. Finally, in order for the PbSe thin film to be practically integrated into a solar cell, it must exhibit photoconductivity.

1.3 PbSe – A Lead Chalcogenide

PbSe is a IV-VI semiconductor. It is a polar semiconductor, meaning both ionic and covalent chemical bonding are present and electrons are shared unequally by the nuclei forming these bonds; covalent bonding is predominate in the crystal [8]. PbSe has a face centered cubic structure lattice with a lattice constant of 6.12Å [9]. PbSe has a direct band gap of 0.27eV for bulk material at room temperature [11] and an intrinsic carrier density of $3 \times 10^{16} \text{ cm}^{-3}$ [12].

PbSe is one of three lead chalcogenides, or lead salts, which include PbS and PbTe. PbSe is the least researched of the three. Lead chalcogenides are characterized by narrow band gaps which make them sensitive to infrared (IR) light. For this reason, lead chalcogenides have been employed for a wide variety of applications including IR sensors, photoresistors, photodiodes, IR lasers, and thermoelectric generators. Development of lead chalcogenides photoresistors began in the late 1930s [8], but it was not until the late 1940s that PbSe was employed for such technology [13]. Lead chalcogenides make good photoresistors due to their fairly high sensitivity, short time constant, fast response, and low Ohmic resistance [8].

PbSe is a high-impedance photoconductor, making it attractive for second-generation IR detector arrays [13]. PbSe offers detection at longer wavelength ranges of 4 to 6 μm ; if cooled with liquid hydrogen this wavelength limit can be extended to 9 μm [8]. As an IR detector, PbSe can operate between temperatures of 300K and 77K. Such detectors have been interfaced with CMOS readout circuits as well. The presence of 1/f noise limits the use of such technology for scanning imagers [13]. Another application of PbSe includes photodiodes, which are formed from a p-n junction. The quantum efficiency of such a device is close to unity with a long wavelength limit of 7 μm [8]. Furthermore, PbSe has been employed as the active material in IR lasers. In lead chalcogenides, interband radiative recombination is much stronger than interband impact recombination. This is due to the high permittivity, large effective masses, and high density of states of the valence and conduction bands in lead chalcogenides. However, in PbSe only impact recombination is equally as important. Since interband radiative recombination dominates at low temperatures and low carrier densities, IR light can be emitted. Use of PbSe has allowed for the spectral range of lasers to be extended. At 12K, a wavelength of emission of 8.5 μm was reported under pressure of 5000kg/cm² for PbSe [8].

Potential application of PbSe as photographic plates, photo resistors [14-15], and photovoltaics has attracted recent interest. Interest in photovoltaic application of PbSe is largely due to the observation of quantum confinement effects in PbSe quantum dots including size quantization and carrier multiplication [1.5]. Size quantization refers the phenomenon observed in quantum dots where band gap size is dependent on the size of the quantum dot (indirectly so in the case of PbSe), which allows for tuning of the band gap by fixing the quantum dot size. Carrier multiplication is a phenomenon in which multiple excitons are generated from a single incident photon. Further discussion of solar cells which incorporate PbSe will follow in section 2.2.

2. Motivation

2.1 Necessity of Photovoltaics

Currently, the United States is dependent on fossil fuels for the majority of its energy needs as demonstrated by the figure below. This has many negative consequences for our nation ranging from

health and safety concerns to dependence on foreign oil. It also has global implications. The United States is one of the largest consumers of energy world-wide. Burning coal releases two pounds of carbon dioxide per kWh of electricity generated [16], more than any other fossil fuel. This is cause for concern because the United States burns more coal than any other fossil fuel. Though this may change with recent interest in natural gas, natural gas still emits 1.22 pounds of carbon dioxide per kWh generated [16]. Burning fossil fuels to create energy depletes the Earth of finite natural resources while releasing harmful emissions such as carbon dioxide into the atmosphere, contributing to climate change. Already many Americans struggle to pay the high price of gas, which will only increase as the availability of oil diminishes. The price of oil is also dictated by a foreign oil market. Increasing dependence on nuclear energy creates safety concerns about the disposal of hazardous waste and the utilization of nuclear technology and materials for weapons. The recent tragedy in Japan demonstrates how safety can be jeopardized due to this technology despite all the precautionary measures in place.

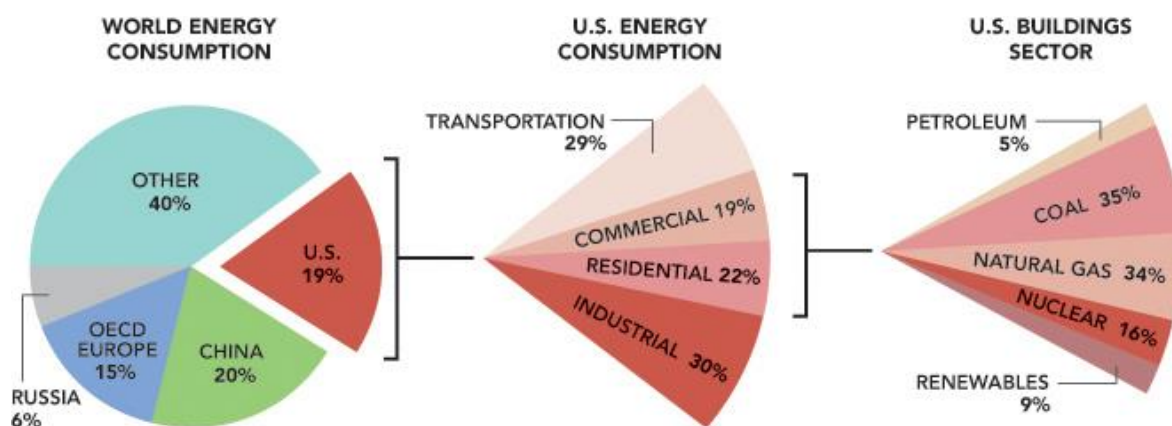


Fig. 1: Breakdown of energy consumption in the United States. (Image credit: US Department of Energy, <http://buildingsdatabook.eren.doe.gov/ChapterIntro1.aspx>)

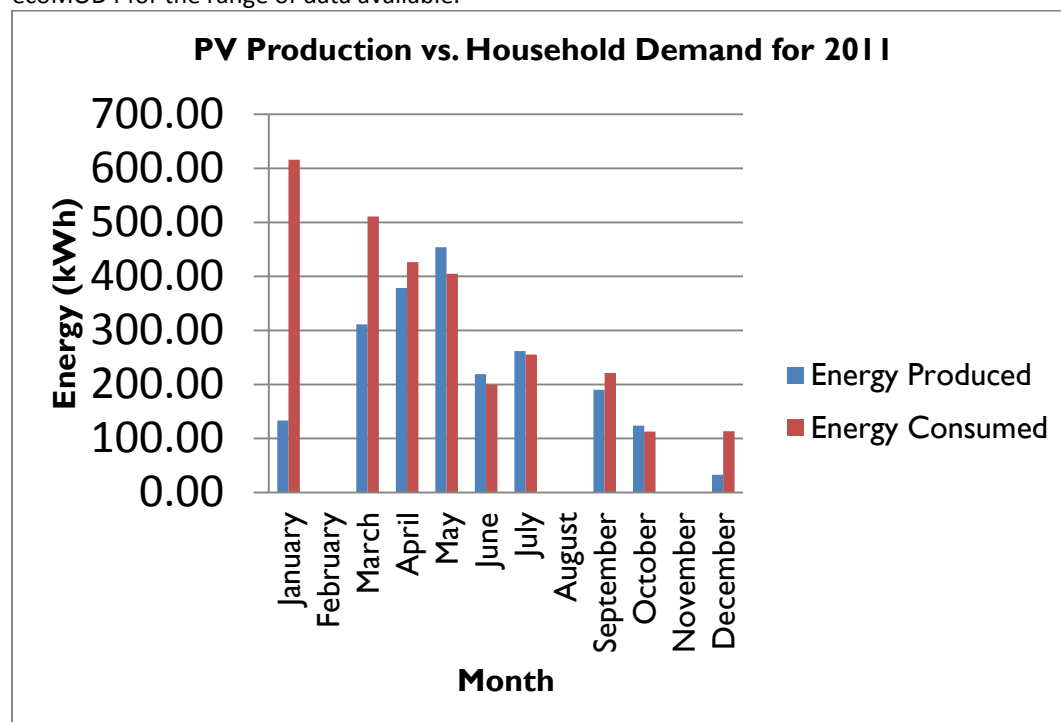
For these reasons, advancements in sustainable energy are critical to a secure, clean, safe energy future. I do not intend to argue that photovoltaics (PV) alone will solely be able to provide the energy needs for our nation. It must be a part of an approach which includes wind, hydro, solar thermal, geothermal, and other sustainable approaches to energy. Residential energy use accounts for 22% of the United States overall energy use, with buildings (commercial and residential) accounting for 41% overall (fig. 1). Reducing residential energy bills would have significant implications for our nation. First generation PVs have already demonstrated their ability to offset energy bills by reducing energy use for residential customers. The following study was conducted as part of the ecoMOD project at the University of Virginia (UVA) and presents evidence to support this claim. The ecoMOD project is an interdisciplinary effort in sustainable, affordable housing in Charlottesville, VA. As part of a greater effort to understand how to reduce energy use in residential homes, the performance of the PV system at ecoMOD4 was investigated. EcoMOD4 is an energy efficient modular home built in collaboration with Habitat for Humanity by engineering and architecture students at UVA. In addition to being built for energy efficiency, ecoMOD4 includes a geothermal heat pump – and 3.82kW PV system. The PV system at ecoMOD4 is 16% efficient and made of single crystalline silicon (c-Si) solar panels.

A study was performed comparing the energy produced by the PV system to the total energy usage in the home, or houseload, to better understand the impact of PV on reducing residential energy usage, and consequently residential energy bills (fig. 2). A monitoring system is installed at ecoMOD4, serving

to collect data on the energy consumed by the household as well as the energy produced by the PV system. This monitoring system was installed as part of the ecoMOD project's efforts to study energy efficient housing. Though there are gaps in the data available due to system downtime, enough data has been collected to determine how useful the PV system has been to the residents. From May to October, we can see that the PV system is generally producing as much electricity as the residents are using. In some cases, the PV system has even produced more energy than the residents used. As one would expect, in the late fall, winter, and early spring, the PV system is producing much less electricity, generally around 20% of the energy consumed by the residents at ecoMOD4.

Despite the reduced capacity of the PV system to produce electricity in the winter, it has been able to offset an impressive amount of carbon dioxide and reduce the energy bill for the residents at ecoMOD4 over the course of May 2010 to December 2011. Using only the available data from the monitoring system at ecoMOD4, which doesn't include days when the PV system was still producing electricity though the monitoring system was down, the amount of energy produced by the PV was calculated. On average, the PV system produces 395 kWh a month, translating to an average of \$35 saved in energy bills and 790 pounds of carbon emissions offset per month. In total, 9238 pounds of carbon dioxide, that would have otherwise been generated by the burning of coal, have been offset and approximately \$415 has been saved in energy bills considering the price of electricity in the state of Virginia was about \$0.09 per kWh in 2011 [17]. In other states with similar solar distribution the savings in energy bills would be even more dramatic, considering the average price of electricity state wide in August 2011 was about \$0.13 [17].

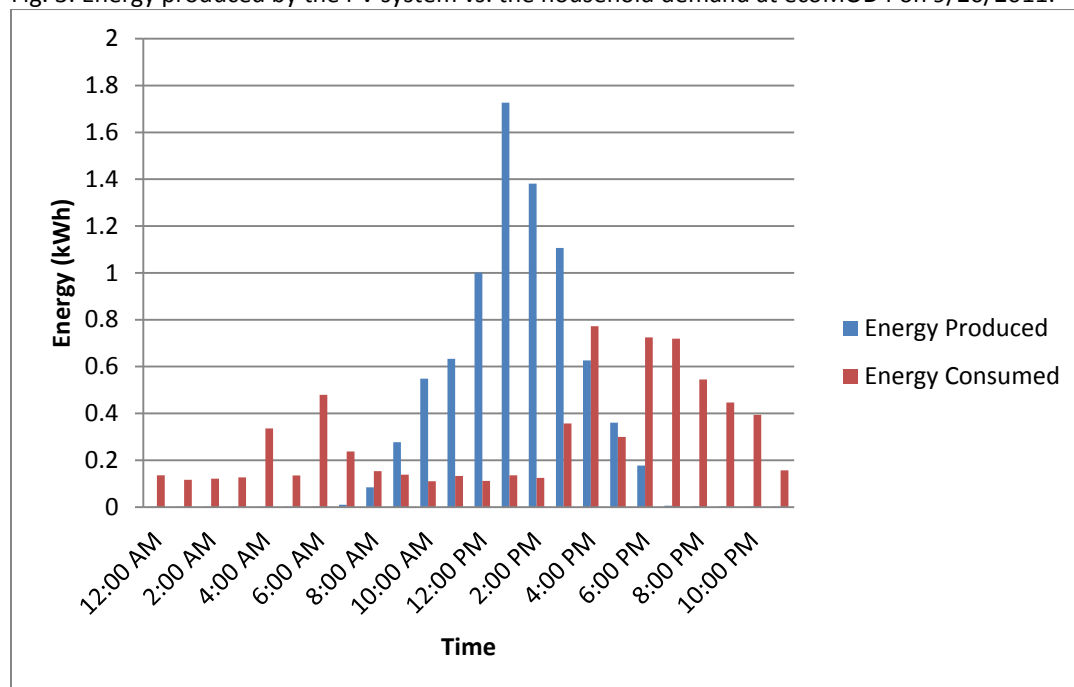
Fig. 2: Comparison of the energy produced by the PV system to the amount of energy used by the residents at ecoMOD4 for the range of data available.



There are other factors not taken into account by this data that must be considered. In general, the peak production of a PV system does not coincide with the peak demand of household energy use, as demonstrated in figure 3 below. In fact, the residents are using the least energy when the PV system is

producing the most. So even though the PV system was able to produce slightly more energy than the residents required for this particular day, it does not offset the real time usage of the residents. However, Virginia power companies provide net metering, which means that power companies buy back excess electricity produced by the PV system at the same rate that it is sold to the residents. This has a number of positive implications for the residents at ecoMOD4. On days when the PV system is producing more electricity than the residents are consuming, like on 9/20/11 in figure 3 below, the residents are actually making a net profit for the day. This PV system does not contain battery storage, but if one were to be utilized the excess energy produced by the PV system could certainly be stored and supply energy for the residents when they were using energy later in the day. Finally, the location of this PV system should be considered. Virginia happens to be a state that experiences a lot of sun, but does not reach temperatures so high that it degrades the performance of the PV system. This means PV has great potential for Virginia residents, but is not a universal solution.

Fig. 3: Energy produced by the PV system vs. the household demand at ecoMOD4 on 9/20/2011.



The PV system studied above demonstrates an impressive ability to offset much of residential energy use in Charlottesville, VA. Clearly, PVs have huge potential for providing clean energy to Americans. However, though a great deal of money could be saved on energy bills based on the analysis above, the upfront cost of a PV system makes them unaffordable to the majority of Americans. Installed PV systems cost around \$30,000 and the payback period generally is equal to or exceeds the lifetime of the system. Though tax credits can help offset these costs, it is clear that the upfront cost of such systems must be reduced dramatically if more Americans are to invest in such technology.

First generation PV systems are expensive for two major reasons: low conversion efficiency and high manufacturing and materials costs. Such systems are typically made of c-Si. One of the major drawbacks of this material is that its maximum theoretical conversion efficiency is only 32% due to its band gap energy of 1.11eV. 25% conversion efficiency under 1.5AM or 1000W/m illumination has already been achieved [18], and while 1% improvements in efficiency are extremely significant, there is not much room left for improvement in terms of cost reduction. Si itself accounts for about half the cost of solar panels, in part due to the manufacturing process. The fabrication of c-Si is achieved by plasma enhanced

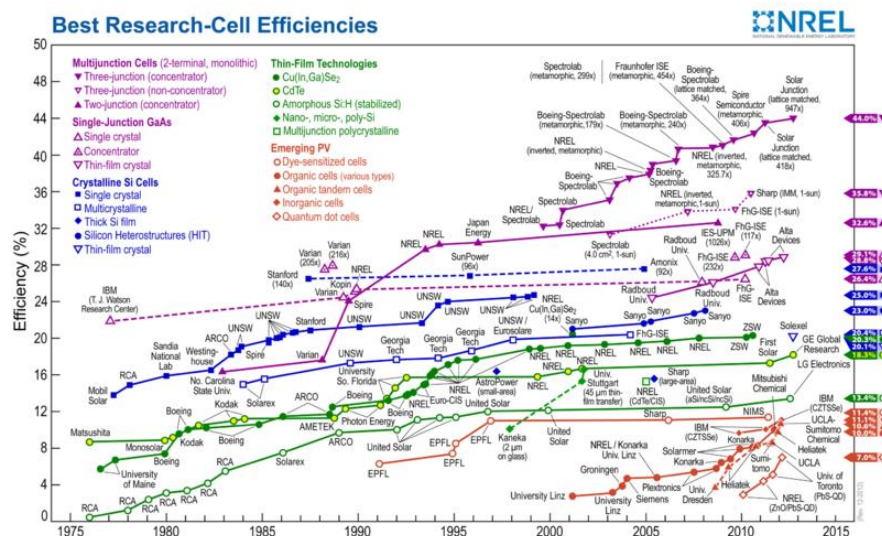
chemical vapor deposition (PECVD). PECVD is carried out at high temperatures of 900°C making the technique very costly. Thus, a viable alternative solar cell must reduce material and manufacturing costs while simultaneously increasing conversion efficiency.

2.2 PbSe-Si Heterojunctions

Heterojunctions between PbSe and Si have already been demonstrated. In general, IV-VI compound semiconductors have been investigated for a variety of applications including infrared photodetectors, photovoltaic devices, mid infrared diode lasers, and optical amplifiers [19]. As early as 1970, one such heterojunction was formed by chemical bath deposition of PbSe onto both n-type and p-type Si wafers. These diodes exhibited photoresponse [20]. More recently, several groups have investigated heterojunctions between PbSe and Si, with a strong focus on the use of PbSe nanoparticles to form the heterojunction. One paper reported that the heterojunction between p-type PbSe on p-type c-Si deposited by thermal evaporation in a vacuum behaved as a poor rectifier based on C-V and I-V characteristics, demonstrating diode like behavior [22]. Diode like behavior was also demonstrated by another group in which a built-in voltage of 0.67V and an open circuit voltage of approximately 1.2V were achieved [16]. In some of this research PbSe nanoparticles exhibit quantum size effects. Several papers reported an observable increase in the band gap with a decrease in crystals size [5,19,22]. Such quantum confinement effects are well known to allow for the tuning of band gaps in nanoparticles. Furthermore, these nanoparticles were deposited by chemical bath deposition, the deposition technique used in this work. These results demonstrate that a heterojunction between PbSe and Si can be achieved and the feasibility of the future goals of this work.

2.3 Current State of Thin Film Photovoltaic Technology

Fig. 4: Summary of efficiency of first, second, and third generation solar cells (image credit: National Renewable Energy Laboratory or NREL).



Thin films PVs, or second generation PVs, offer a great potential to reduce the overall cost of PVs by employing inexpensive deposition processes and less material. Figure 4 demonstrates the efficiencies of thin film PVs with respect to other PV technologies, including first generation solar cells. Though the efficiency of thin film PVs is slightly lower than that of first generation PVs, the cost savings benefits makes them

attractive. The efficiencies of the individual thin film technologies will be discussed shortly. There are three dominant thin film technologies in this area including amorphous Si, CdTe/CdS and copper indium gallium selenide or CIGS (often incorporating a layer of CdS). The latter two technologies share a great deal in common with the approach proposed in this paper. Both employ the use of chemical bath deposition to reduce the fabrication costs. Like PbSe, CIGS and CdTe are direct band gap semiconductors with high absorption coefficients. Thus, absorption can take place at thicknesses of only a few microns.

2.3.1 Amorphous Si

Hydrogenated amorphous silicon (a-Si:H) is not a new technology and is typically deposited by radio frequency plasma chemical vapor deposition. In 1982, a-Si:H solar cells were produced with 10% efficiency [23]. These devices are composed of p-i-n diodes rather than p-n diodes. This is due to the fact that in a p-n configuration of a-Si:H, doping is both difficult and degrades the quality of the film by the formation of dangling bonds. The intrinsic region of p-i-n device acts as the absorbing layer. The dominant transport mechanism in such a device is drift as photogenerated carriers in the intrinsic region are swept to either electrode by the built in electric field as a result of the p and n layers [24]. While initially this technology seemed promising due to its relatively high efficiencies in early development, a-Si:H solar cells suffer from the Staebler-Wronski Effect (SWE). In this effect, prolonged exposure of the a-Si:H solar cells to intense light causes a reduction in the efficiency of the device. It is generally accepted that the light exposure results in an increase in the defect density. The increase in metastable defect density causes an increase in recombination within the device, in turn reducing the efficiency. There are several models suggesting the exact cause of the formation of such metastable defects beyond the scope of this paper, but which involve the diffusion of hydrogen through the a-Si:H film [25]. The SWE is reversible through annealing [24]. One solution to the problem of SWE in a-Si:H solar cells is to utilize the material in a-Si:H based tandem and multijunction solar cells, though the additional material increases the overall cost. Microcrystalline silicon (μ c-Si:H) was investigated as an alternative to a-Si:H. Though it is easier to dope than a-Si:H, and does not typically suffer from SWE, it yielded lower efficiencies of 7.7% in 1996 [24]. More recently, a stabilized efficiency of 10.01% under 1.5AM was achieved in an a-Si:H solar cell, translating to a module efficiency of $9.2 \pm 0.19\%$. This device employed a p-i-n configuration, optimizing the thickness of the intrinsic layer and deposited on a doped LPCVD-ZnO substrate in order to achieve the stabilized efficiency [26].

Beyond the typical advantages of thin film devices, a-Si:H offers a nontoxic and abundant resource. The low temperature processing allows for the use of cheaper substrates and even flexible substrates, enabling easy integration onto a variety of building structures. Annealing at temperatures of 100-250°C can restore original efficiency of these devices [24]; however, this necessitates an additional processing step, increasing the overall cost.

2.3.2 CdTe/CdS

This technology is the most promising for PVs in terms of long term cost projections. CdTe has the optimal band gap for a material in PV application, 1.5eV [27]. At this band gap, CdTe can absorb the maximum amount of energy from the solar spectrum. Additionally, due to its simpler processing techniques, deposition on flexible substrates is possible. Polycrystalline layers of only a few microns in thickness are employed in CdTe/CdS thin film solar cells. Such solar cells typically employ a general configuration of a transparent conducting oxide (TCO) as the front contact, CdS to act as the “n-type” semiconductor, CdTe to act as the “p-type” absorber layer, and an Ohmic back contact. CdS is generally deposited by chemical bath deposition. CdTe is then deposited by closed-space sublimation to form the junction. Like CBD, this is an inexpensive yet scalable deposition method [27].

One paper reports the use of CdTe in a heterojunction thin film solar cell composed of CdS and CdTe. This heterojunction exhibited a fill factor of 72.6% and a conversion efficiency of 13.4% under 1.5AM illumination in 1991 [28]. This efficiency was quickly improved to 14.5% in 1992 [29]. The NREL has achieved $16.5 \pm 0.5\%$ efficiency under 1.5AM for a CdTe/CdS solar cell employing CTO/ZTO as the TCO rather than the traditional use of SnO_2 . This solar cell also achieved a very high fill factor of 77.34% [26]. General Electric has announced it was able to produce 12.8% efficient cells and plans to manufacture

modules with even higher efficiency in the future. Additionally, First Solar has produced record efficiency of 17.3% in the lab and plans to produce modules at 13.5-14.5% efficiency in the future [27].

2.3.3 CIGS/[CdS]

Like the CdTe/CdS devices, the CIGS thin films are polycrystalline and only a few microns in thickness. In this device configuration, a glass substrate is coated with a back contact. Molybdenum (Mo) is typically used and is deposited by sputtering. Mo is selected because the concentration of sodium is very important for growth of CIGS and for increasing the carrier density. CIGS is deposited on the back contact by three stage-coevaporation. CIGS acts as the absorber layer. CdS is typically deposited by chemical bath deposition onto the CIGS to act as a buffer layer. It has been found that the inclusion of CdS is necessary for increasing conversion efficiency. However, the role of CdS in increasing this efficiency is unclear. It is possible that the diffusion of Cd^{2+} ions into the layer of CIGS alone promotes higher efficiency or that the diffusion is resulting in the outdiffusion of Cu which is accounting for the increase in efficiency [36].

In 2008, an efficiency of 19.9% and fill factor of 81.2% was achieved [31]. Then in 2010, 20.3% efficiency under 1.5AM was achieved [26]. CIGS thin film solar cells are already commercially available through General Electric in 145W and 150W solar modules with efficiencies of 11.8% and 12.2W respectively. Additionally, these devices are cadmium free. Another commercial module is available through Solibro which achieved a world record efficiency of 17.4% for a CIGS thin film solar cell in 2011. 19.5% efficiency under 1.5AM was achieved by NREL for a CIGS solar cells incorporating a CdS buffer layer [26].

One disadvantage to this technology is the requirement of high vacuum conditions for the complex deposition techniques of CIGS. In addition to this less than cost-effective aspect of CIGS solar cells, indium is an expensive material. Finally, deposition cannot take place on flexible substrates. In CdTe and CIGS solar cells both long term stability and performance degradation has been observed. Thinner layers of both materials, less than $0.5\mu\text{m}$, are desirable in future development to further reduce costs [32].

3. Background

3.1 Chemical Bath Deposition

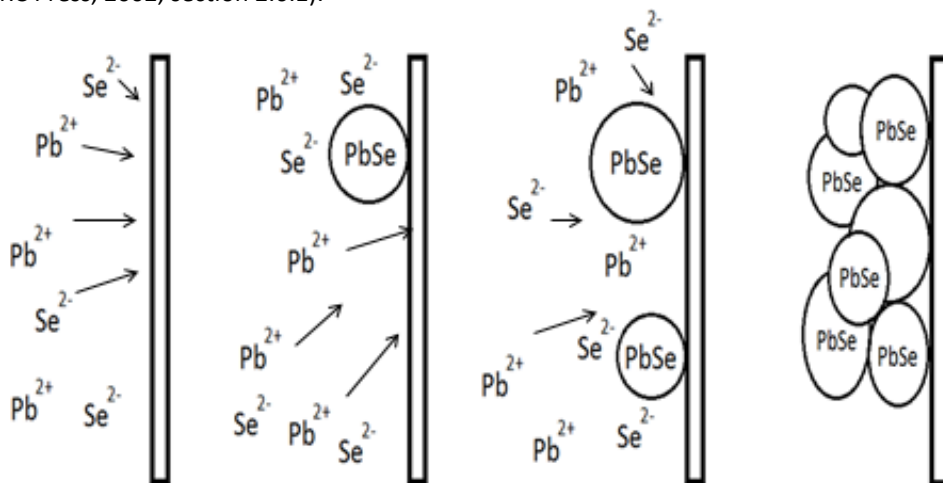
PbSe can be deposited by pyrolysis, vacuum evaporation, sputtering or chemical bath deposition (CBD) [33]. Of these techniques, CBD is the most attractive. It is a simple, low cost technique that can be executed at low temperatures. This technique has been employed for deposition of PbSe for 60 years [34]. It should be noted that the understanding of the kinetics of this technique are not greatly developed in the literature. The understanding presented in this work reflects the most recent understanding in published works. In deposition of a lead chalcogenide in general, a lead citrate (acting as the lead precursor) is complexed to control the release of the metal cation (Pb^{2+} ions) as well as to prevent the precipitation of $\text{Pb}(\text{OH})_2$. In the case of PbSe, the hydrolysis of the chalcogenide precursor, in this case sodium selenosulphate (Na_2SeSO_3), will provide the anions (Se^{2-} ions). A lead chalcogenide will precipitate provided the ionic product is greater than the solubility product, $K_{sp} \sim 10^{-38}$ for PbSe [35]. Though precipitation is expected, crystal growth can occur by one of two general deposition mechanisms: ion-by-ion growth or hydroxide cluster growth.

3.1.1 Ion-by-ion growth

As the name suggests, ion-by-ion growth occurs as a sequence of ionic reactions. Typically, ion-by-ion growth occurs when homogeneous nucleation occurs. Collisions between ions will form nuclei, which adsorb onto the substrate. However, these nuclei are intrinsically thermodynamically unstable due to their large surface area and may redissolve before growth can occur. Control of kinetics can be used to

stabilize the nuclei and prevent redissolution; this is primarily accomplished by decreasing the temperature. If the nuclei do not redissolve they will adsorb the ions that collide with them, forming crystals by the process of aggregation. Ion-by-ion growth typically results in larger crystals. Furthermore, the crystal size is directly proportional to film thickness [36].

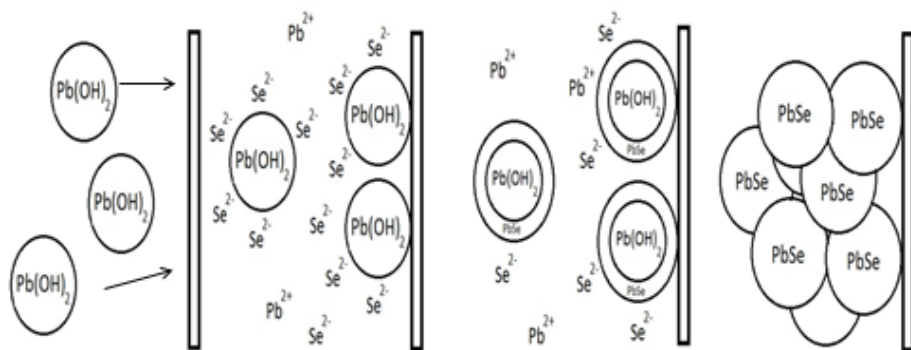
Fig. 5: Ion-by-ion growth of PbSe (adapted from G. Hodes. *Chemical Solution Deposition of Semiconductor Films*. CRC Press, 2002, section 2.6.1).



3.1.2 Hydroxide Cluster Growth

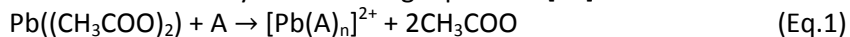
In order for hydroxide cluster growth to occur, the presence of a metal hydroxide is required. In the case of PbSe, this deposition mechanism can occur if $Pb(OH)_2$ is present as either a precipitate or colloid. Though a complexing agent is often used to prevent such a metal hydroxide from precipitating, it often exists as a colloid not visible to the naked eye. If the metal hydroxide colloid or precipitate is present, the metal hydroxide will adhere to the substrate initially. Chalcogenide anions will readily substitute for the hydroxide due to the lower resulting solubility product. This results in the formation of clusters of the lead chalcogenide. As the deposition is allowed to take place for longer periods of time, PbSe will form through the substitution reaction creating clusters of PbSe. Hydroxide cluster growth typically results in smaller crystals. Unlike ion-by-ion growth, film thickness does not greatly influence the crystal size [37].

Fig. 6: Hydroxide cluster growth of PbSe (adapted from G. Hodes. *Chemical Solution Deposition of Semiconductor Films*. CRC Press, 2002, section 2.6.1).



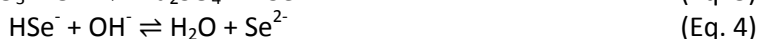
3.1.3 Chemical Reaction

While ion-by-ion growth and hydroxide cluster growth are the general mechanisms by which PbSe can be formed, the actual chemical reaction taking place is slightly more complicated. In the case of this work, Pb^{2+} and Se^{2-} ions are not readily available in aqueous form. Instead they must be created from precursors. As previously discussed the lead precursor, in this case lead acetate ($\text{Pb}(\text{CH}_3\text{COO})_2$), must be complexed to form Pb^{2+} . A variety of complexing agents may be used for this purpose. In this work, potassium hydroxide (KOH), and trisodium citrate ($\text{Na}_3\text{C}_6\text{H}_5\text{O}_7$) were employed. The formation of the complex, and consequently Pb^{2+} , can be understood by the following equations [38]:



where A represents the complexing agent and $[\text{Pb}(\text{A})_n]^{2+}$ represents the complex.

Selenourea was traditionally used to provide Se^{2-} ions for deposition of PbSe. Due to its instability and difficult preparation, sodium selenosulphate and its derivatives are now used instead [39]. In this work, sodium selenosulphate was employed as the selenide precursor. Sodium selenosulphate will hydrolyze to form Se^{2-} as described by the chemical equations below [38]



In the case of ion-by-ion growth, Pb^{2+} and Se^{2-} ions will simply form by the chemical reactions above. PbSe will form by an ionic reaction as described by the equation below, provided the ionic product is greater than the solubility product. This will result in precipitation of PbSe onto a substrate in solution. In this case the ionic reaction is an equilibrium equation, meaning that the reaction can happen forward and backwards. Therefore, redissolution can occur if the ionic product becomes lower than the solubility product.



Hydroxide cluster growth is slightly more complicated. Even in the presence of a complexing agent, some $\text{Pb}(\text{OH})_2$ may form as a colloid. In this case, Pb^{2+} ions are not readily available to form an ionic reaction with the Se^{2-} ions. Instead, PbSe will form by a substitution reaction as described above. Since the PbSe forms by substitution, rather than by an ionic reaction, the process is not one that can occur in reverse and redissolution is unlikely. In either case, the release of Se^{2-} ions controls the deposition rate [40].

3.1.4 Factors Influencing Deposition

Several factors will influence deposition including temperature, concentrations (or molarities), pH, and substrate choice. Temperature can be used to control the rate of deposition and quality of films. Like molecules of gas, increasing the temperature of the deposition bath will increase the number of collisions that occur between ions. This in turn will accelerate the chemical reaction allowing one to increase the rate of reaction by simply increasing the temperature. However, increasing the temperature can also result in poor quality films [41]. As previously mentioned, in the case of ion-by-ion growth when nuclei are first formed they are likely to redissolve before growth can occur. Decreasing temperature can stabilize the nuclei; the reverse is true for increasing temperature.

The concentration, or the molarity, of the precursors and complexing agent used is very important. The concentration of the precursors controls the concentrations of the ions necessary for either deposition mechanism to occur. The concentrations of Pb^{2+} and Se^{2-} must exceed the solubility product of PbSe for ion-by-ion growth to occur and cause precipitation of PbSe. Thus, it is important that the concentrations of the precursors and complexing agent be high enough to produce sufficient Pb^{2+} and Se^{2-} .

Furthermore, the concentration of the complexing agent should theoretically dictate which deposition mechanism will occur. If the concentration of the complexing agent is high enough to prevent any $\text{Pb}(\text{OH})_2$ from forming (as a precipitate or colloid), ion-by-ion growth should occur. If the complexing agent concentration is low, $\text{Pb}(\text{OH})_2$ will form and hydroxide cluster growth should occur.

The pH of the deposition solution plays an important role in CBD of PbSe. An alkaline chemical bath is necessary for growth to occur at all and to prevent precipitation of red Se [42]. In this work an alkali, KOH, is used to adjust the pH of the solution based on the methods of Gorer *et. al.* [5]. Finally, the substrate will also affect crystal growth. Any solid particle will act as a nucleation site making the cleanliness of the substrate extremely important, regardless of its composition. Since CBD can be carried out at low temperatures, a variety of substrates can be used including plastic, glass, oxides, and semiconductors. Typically, deposition on plastic, glass or oxides will result in polycrystalline PbSe [43]. In the case of semiconductors, epitaxial growth has been reported on Ge and Si as they possess a cubic structure similar to that of PbSe [44].

4. Experimental Techniques

4.1 Chemical Bath Deposition

PbSe thin films were deposited by chemical bath deposition (CBD) by the following means.

4.1.1 Cleaning of Glass Substrates

First glass microslides were cleaned with a cleaning solution composed of ratio 3:1:1 of deionized H_2O (DI), 30% NH_4OH and 30% H_2O_2 in a glass beaker. The glass substrates were placed in the cleaning solution which was heated to about 70°C with a hot plate. Once the solution began to bubble, the glass substrates were allowed to sit in solution for 7 minutes. Then the beaker was removed from the hot plate and each glass substrate was flipped over in the solution. The substrates were removed from the cleaning solution once it ceased to bubble. Then each substrate was placed in 50mL of DI for 2 minutes to rinse, then rinsed again with DI using a squeeze bottle and finally dried with a nitrogen spray gun. The glass substrates were stored in a petri dish lined with lint free filter papers until utilized for deposition.

4.1.2 Cleaning of Si Substrates

A 4" n-type Si wafer, polished on one side, was diced into 5x5mm samples using a dicing saw. Before deposition, each Si sample was placed in a buffered oxide etch (BOE) composed of 10:1 40% NH_4F and 49% HF for 30 seconds to remove the native oxide layer (SiO_2). Next the Si substrate was rinsed in DI for 2 minutes. Finally the Si was dried with a nitrogen spray gun and adhered to a cleaned glass substrate using electrical tape so that it could be placed in a 50mL beaker for deposition. This cleaning procedure was performed immediately before being placed in deposition solution to prevent a native oxide layer from reforming on the Si.

4.1.3 Chemical Bath Preparation

CBD of PbSe thin films was performed based on the method of Gorer *et. al.*, who investigated the optical and structural (but not electrical) properties of nanocrystalline thin film PbSe [5]. In this method, three complexing agents were employed for deposition including trisodium citrate (TSC), potassium hydroxide (KOH), and potassium nitriolotriacetate (NTA). Only KOH and TSC were used as complexing agents in this work.

4.1.4 KOH as the Complexing Agent

Initially KOH was utilized as the complexing agent in the deposition bath. Deposition solution for one PbSe thin film was prepared as follows: 2000 μL 2.0M KOH, 2000 μL 0.2M Na_2SeSO_3 , 400 μL DI and 600 μL

0.5M $\text{Pb}(\text{CH}_3\text{COO})_2$. The deposition was carried out at 23°C for 24 hours. In subsequent experiments, the concentration of the complexing agent was varied. Temperatures of 6°C and 60°C were also investigated. Time was varied from 1 to 72 hours. A stronger complexing agent, 5.0M KOH, was also utilized.

4.1.5 $\text{Na}_2\text{C}_6\text{H}_5\text{O}_7$ (TSC) as the Complexing Agent

The initial deposition solution for *one* PbSe thin film was prepared in a 50mL beaker as follows: 4000 μL DI, 3200 μL 0.5M $\text{Pb}(\text{CH}_3\text{COO})_2$, 1M TSC, sufficient 2.0M KOH to bring the pH of the deposition solution to 10.0, 8000 μL 0.2M Na_2SeSO_3 , sufficient 2.0M KOH to bring the pH of the deposition solution to 10.8, and finally sufficient DI to bring the final volume of the deposition solution to 18.5mL. This step was added to ensure the final concentrations of $\text{Pb}(\text{CH}_3\text{COO})_2$ and Na_2SeSO_3 in the deposition solution were the same for every deposition. A nitrogen spray gun was used to remove any potential dust from the glass substrate immediately before it was placed in the deposition solution at an angle of approximately 45 degrees. The first deposition was carried out at $60^\circ\text{C} \pm 5^\circ$ for 1 hour. The deposition solution was stirred at 50rpm using a magnetic stir bar and the lid of a petri dish was placed over the 50mL beaker to prevent evaporation of the deposition solution. Like in the work by Gorer, final concentrations of 60mM Pb^{2+} and 160-320mM TSC were used. However, the final concentration of Na_2SeSO_3 was increased from 50mM to 86mM. Upon completion of deposition, DI was used to rinse the PbSe thin film and stop the reaction from proceeding. The PbSe thin film deposited on the bottom of the substrate was used. 1.0M nitric acid was used to remove any PbSe from the top of the substrate. Subsequent depositions were carried out at temperature of 60-85°C, for times of between 1-5hrs. Additionally, the concentration of TSC added to the deposition solution was varied from 0.4-1.6M and the final concentration of Se in the deposition solution was varied from 50-86mM.

4.1.6 Experimental Setup

Fig. 7: CBD experimental setup utilizing a water bath for temperature control.



To control the temperature of the deposition, a water bath was used. A large beaker filled with water was placed on a hot plate with a thermometer submerged in the water serving as a feedback mechanism to the hot plate to ensure constant temperature control of the water bath. A ceramic tile was placed on the bottom of the beaker, and the 50mL beaker containing the deposition solution placed on the tile, to prevent direct heating of the bottom of the beaker. The water level of the deposition bath always exceeded that of the deposition solution level in the 50mL beaker (fig. 7).

4.2 Hall Effect Measurement

The majority carrier properties were measured by the Hall effect. An Ecopia HMS-3000 Hall Effect Measurement System was used employing the van der Pauw method. The van der Pauw method assumes an isotropic, homogeneous sample with uniform

thickness [44]. Though this method does not require a Hall Bar geometry and allows for the use of irregularly shaped samples, it requires that the contacts must be formed at the edges of the sample, that the area of the contacts should be at least one order of magnitude less than the sample area, and that no holes are present in the sample [44-45]. Samples were cut from the PbSe thin films approximately 11mmx11mm in dimension. Four Ohmic contacts were formed at each corner with Ag conductive paint (fig. 8).

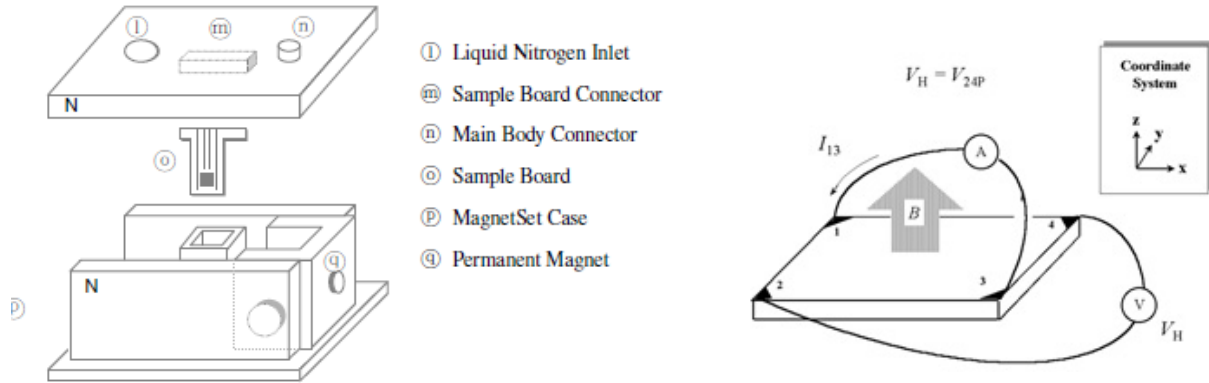
Fig. 8: Ag contact configuration on PbSe.



The sample is placed on the sample board which contains four probes, placed on each contact. The sample board is inserted into the Hall effect measurement system (fig. 9). A current is run between two of the probes perpendicular to a magnetic field of 0.55T provided by the permanent magnet. The resulting Lorentz force acts on the charge carriers in the semiconductor, sweeping electrons and holes to opposite sides of the semiconductor. This induces a potential difference across the sample called the Hall Voltage (fig. 10).

The setup works by measuring the changes in voltage and resistance due to the presence of a magnetic field. Initially, the current is run through the sample with no magnetic field present. The magnet is then inserted into the setup and the change in electrical properties is measured. Then the magnet polarity is reversed by flipping the magnet upside down and the reciprocal is measured. The instrument requires the thickness of the sample be known for calculations of the electrical properties of the majority carrier including the resistivity, mobility and carrier density. The thickness was calculated using a fringe counting technique, to be described shortly in section 4.3.1. The properties of each sample were measured across three to five trials to ensure consistency.

Fig. 9: Experimental setup for Hall effect measurement using an Ecopia HMS-3000 Hall Effect Measurement System (left). Fig. 10: Diagram of current and magnetic field (perpendicular to one another) used to induce Hall voltage (right); (image credit: National Institute of Standards and Technology or NIST).



The resistance of the semiconductor as measured by the van der Pauw method is defined by the following expression [44-45]

$$R_{13,24} = \frac{V_{24}}{I_{13}}$$

where the I_{13} is the current through probes 1 and 3, which induces V_{24} through probes 2 and 4 as defined by figure 10 above. The resistance through each set of probes is measured and averaged to give the resistivity

$$\rho = \frac{\pi d}{\ln(2)} RF \quad (\text{Eq. 6})$$

where d is the thickness, R is the averaged resistance and F is taken to be 1 for symmetric samples [44].

The Hall coefficient, measured by this technique, for a semiconductor is given by

$$R_H = \frac{1}{e} \frac{(p - b^2 n) + (\mu_n B)^2 (p - n)}{(p + bn)^2 + (\mu_n B)^2 (p - n)^2} \quad (\text{Eq. 7})$$

where p is the hole density, n is the electron density, B is the magnetic field strength, μ_n is the electron mobility, and μ_p is the hole mobility. This reduces to

$$R_H = \frac{1}{e} \frac{(p - b^2 n)}{(p + bn)^2} \quad (\text{Eq. 8})$$

in the presence of low magnetic field strength where $B \ll 1/\mu_n$ and where $b = |\mu_n/\mu_p|$. Equation 8 describes the case where both electrons and holes contribute to conduction, but hold true for all semiconductors measured by the Hall effect under a low magnetic field strength. A low magnetic fields strength such that $B \ll 1/\mu_n$ holds true for all the PbSe thin films in this work where the magnetic field strength is 0.55T for all cases. In the case of an extrinsic semiconductor, equation 8 can be simplified provided $p \gg n$ for the case of a p-type semiconductor, or $n \gg p$ for the case of an n-type semiconductor.

$$R_H = \frac{1}{ep} \quad (\text{Eq. 9a})$$

$$R_H = -\frac{1}{en} \quad (\text{Eq. 9b})$$

The Hall effect measurement instrument assumes that all samples are extrinsic and this simplified set of equations is used in the calculation of the majority carrier properties of all samples which the instrument outputs.

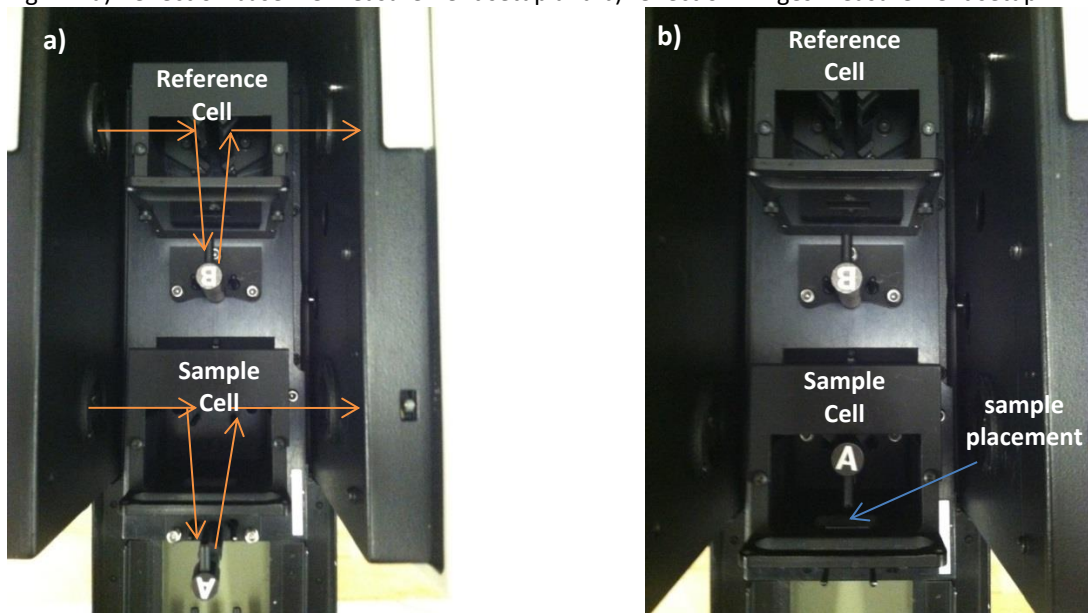
4.3 Interference Spectroscopy

A Cary 5E UV-Vis-NIR Spectrophotometer was used to obtain optical data. Two setups were used to measure the reflection and transmission fringes. Both measurements are taken for a range of 300-3000nm.

4.3.1 Reflection Fringe Measurement

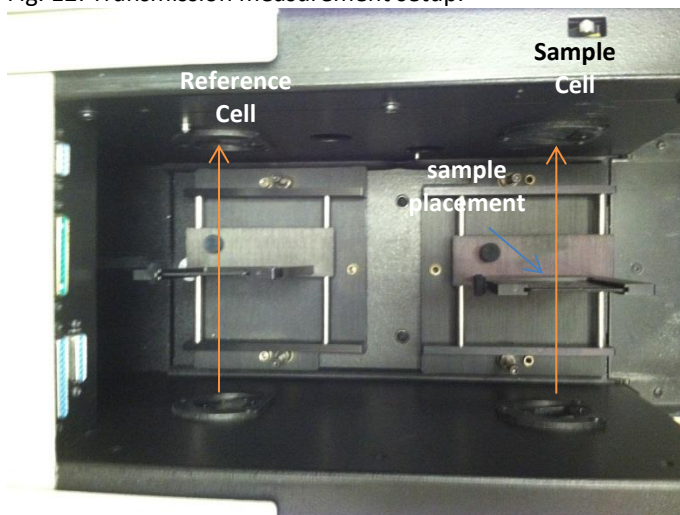
To measure the reflection fringes, first a baseline must be established. The spectrophotometer has two cells: a reference cell and a sample cell. In figure 11a below, the reference cell has the mirror labeled "B" and the sample cell has the mirror labeled "A." The mirrors are positioned as shown in the figure below to allow 100% of the incident light to be reflected and detected in each cell. The sample cell is then divided by the reference cell to establish the baseline. For identical setups, the ratio should be 1:1 or 100%. After the baseline has been established, the mirror in sample cell is repositioned so that it will not interfere with the reflected light as shown in figure 11b below, and is replaced by the sample. This light is allowed to travel along the same direction, but in this case 100% of the light will not be reflected since the sample is not a perfect mirror. Reflection will occur at each interface between the air, PbSe thin film, glass substrate, and air. The reflection at each interface occurs due to the differing refractive indices of the materials. If the reflected waves are in phase with one another, they will constructively interfere, creating a set of fringes like those the figure 13 in the following section.

Fig. 11: a) Reflection baseline measurement setup and b) reflection fringes measurement setup.



4.3.2 Transmission Fringe Pattern Measurement

Fig. 12: Transmission measurement setup.

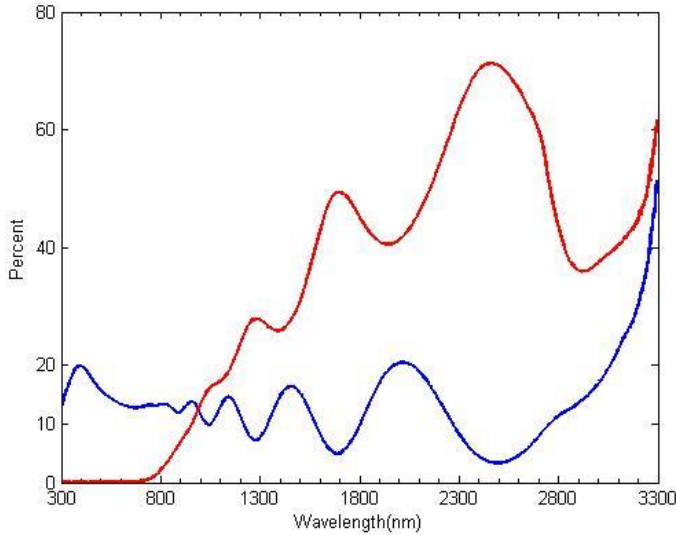


The internal setup for the measurement of the transmission fringes is different, but the method is the same. First a baseline is established. Again, the reference and sample cell are identical. In both cells, 100% of the incident light is allowed to transmit so that the ratio of the cells is 1:1, yielding a baseline of 100% (fig. 12). To obtain the transmission fringes, the sample is then placed in the sample cell as indicated in the figure 12. The direction that the thin film faces is arbitrary since transmission is not dependent on the direction of the incident light. However, the samples were always placed such that the thin film faced the

incident light. The constructive interference of the transmitted waves from each interface is measured.

4.3.3 Thickness Calculation

Fig. 13. Comparison of the reflection and transmission fringes for a PbSe thin film. Absorption does not occur between ~1000-2500nm due to the fact that the opposite extrema of the reflection and transmission fringes are aligned ($R+T=100$).



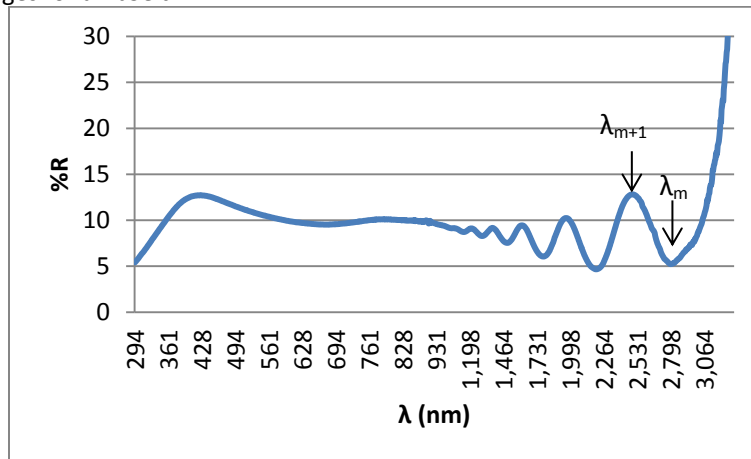
The reflection and transmission fringes measured by the spectrophotometer can be used to determine the thickness of the films based on the relationship between the thickness and the refractive index at a particular extrema of the reflection and transmission fringes. This calculation can only be performed in areas where absorption does not occur, or areas where the opposite extrema of the reflection and transmission fringes align (as shown in figure 13 where absorption does not occur between ~1000-2500nm). The reflection and

transmission fringes were compared in each case to determine where absorption was occurring. Absorption occurs in regions where the opposite extrema of the reflection and transmission are not aligned or in regions where the $R+T \neq 100$.

First the order, represented by m , of each maximum or minimum is determined by equation 10 where λ_m represents the wavelength at which the extrema of order m occurs and λ_{m+1} represents the wavelength at which the adjacent extrema of the next order ($m+1$) occurs as indicated in the figure below. The value of the order m is rounded to the nearest integer which must be even for minima and odd for maxima in the case of a reflection curve; the reverse is true for transmission interference fringes.

$$m = \frac{\lambda_{m+1}}{\lambda_m - \lambda_{m+1}} \quad (\text{Eq. 10})$$

Fig. 15: Reflection fringes for a PbSe thin film.



Using the known value of the refractive index at the wavelength of the extrema (order m) for the material investigated (in this case PbSe) [45a], the thickness can then be calculated by equation 11.

$$d = \frac{m \lambda_m}{4 n} \quad (\text{Eq. 11})$$

where d is the thickness and n is the refractive index. The reflection fringes alone were used in the determination of the thickness due to the lack of multiple fringes in the majority of the transmission data.

4.4 Heterojunction Fabrication

CBD of PbSe thin films on degenerately doped n-type Si substrates was performed as described in section 4.1.5. TSC was used as the complexing agent.

4.4.1 Contact Formation

Two device configurations were used (fig. 16-17). Au contacts were sputtered onto the heterojunction in the configuration shown below using a Denton Vacuum Desk II with an Ar plasma. The heterojunction was placed flat on a glass microslide. It was then fitted with a mask in order that two Au contacts would be sputtered on the heterojunction in the configurations shown in the figures below. The device was placed on a glass microslide so that the thickness of the Au could be estimated by the methods described in section 4.3. The Au target was placed inside the instrument. The pressure was set to 50mT and the current to 45mA. The process was allowed to take place for 15 minutes.

Fig. 16: a) Top view of heterojunction configuration (left), b) cross-section of heterojunction configuration (right).

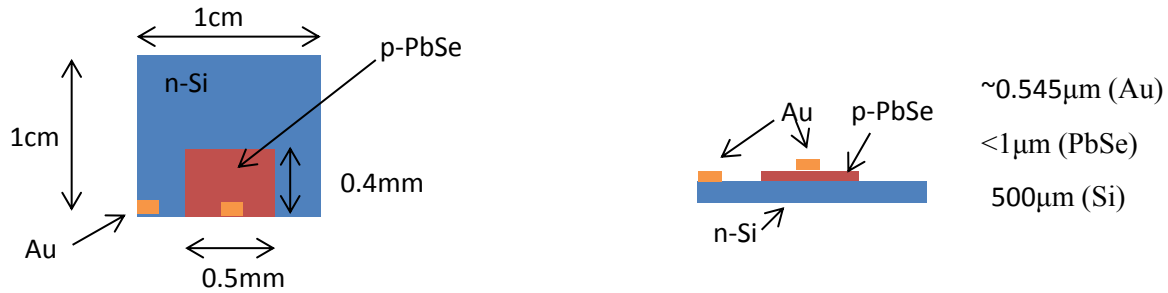
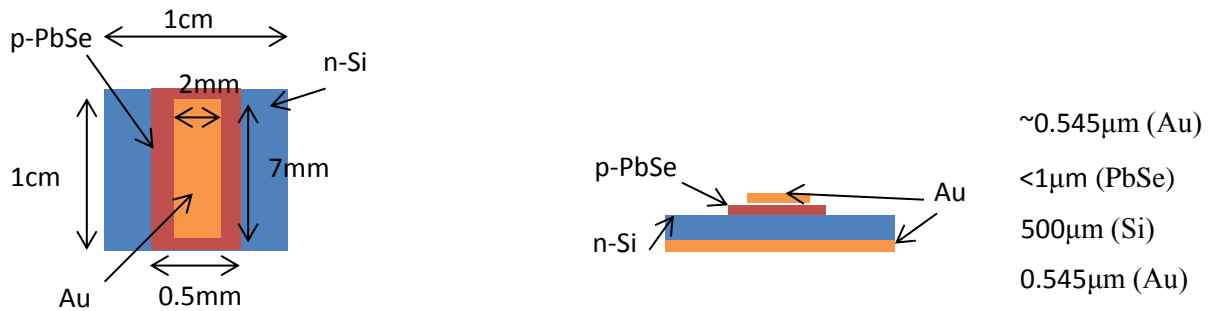


Fig. 17: a) Top view of heterojunction configuration (left), b) cross-section of heterojunction configuration (right).



4.5 Current-Voltage (I-V) Measurement

The dark I-V characteristics of each heterojunction were measured. An HP 4156B Precision SC Parameter Analyzer was used as the power source. The device was first forward biased and the voltage was swept from 0 to +5V. Then the device was reverse biased and the voltage was swept from 0 to -5V.

Additionally, the photoresponse of the heterojunctions was measured. A Keithly 2611 System Sourcemeter was used as the power source for the I-V measurement and BK Precision 1690 Solar Simulator was used to illuminate the device with about 1 sun illumination. The voltage was swept from +2V to -2V.

5. Results

5.1 PbSe on Glass

Conductive PbSe was not obtained using KOH as the complexing agent. Predominately p-type PbSe thin films were obtained using TSC as the complexing agent (described by table I in the appendix which summarizes the results for all PbSe thin films deposited with TSC as the complexing agent). While p-type PbSe thin films were obtained in many cases, there are cases for which neither p-type or n-type measurement was consistently obtained, that is the sign of the Hall coefficient was measured to be both positive and negative across several trials (table II, appendix). This occurred for PbSe thin films deposited at 60-75°C for between 1-5 hours. The deposition conditions included 1M TSC as the complexing agent and a final concentration of 86mM Se with all other conditions held constant as described in section 4.1.5.

As described in section 4.2, the Hall effect instrument measures the Hall coefficient, then calculates the majority carrier properties by assuming that the minority carrier density is negligible. Under this condition, equation 9a holds for p-type semiconductors and equation 9b holds for n-type semiconductors.

$$R_H = \frac{1}{ep} \quad (\text{Eq. 9a})$$

$$R_H = -\frac{1}{en} \quad (\text{Eq. 9b})$$

However, if the minority carrier density is not small enough to be considered negligible these equations no longer hold because both electrons *and* holes contribute to conduction. Under this case the Hall coefficient is given by

$$R_H = \frac{1}{e} \frac{(p - b^2 n)}{(p + bn)^2} \quad (\text{Eq. 8})$$

where $b = |\mu_n/\mu_p|$. It was determined which samples were extrinsic such that the minority carrier contribution is negligible and for which samples both electrons and holes contribute to conduction. Equation 8 holds true for all semiconductors while equation 9a and 9b only hold true for the simplified case where $p \gg n$ or $n \gg p$. Therefore for p-type samples, the following is true

$$R_H = \frac{1}{e} \frac{(p - b^2 n)}{(p + bn)^2} \sim \frac{1}{ep}$$

For each sample, the Hall coefficient was calculated based on the hole density output by the Hall effect measurement system using both equation 8 (assuming $b=1.5^*$) and equation 9a. If the results were within about 10% of one another, the sample is p-type and the electrical properties output by the Hall effect measurement system are therefore true. However, if the results were not within 10% of each other, clearly both electrons and holes contribute to conduction and these results need to be reexamined to determine the true electrical properties.

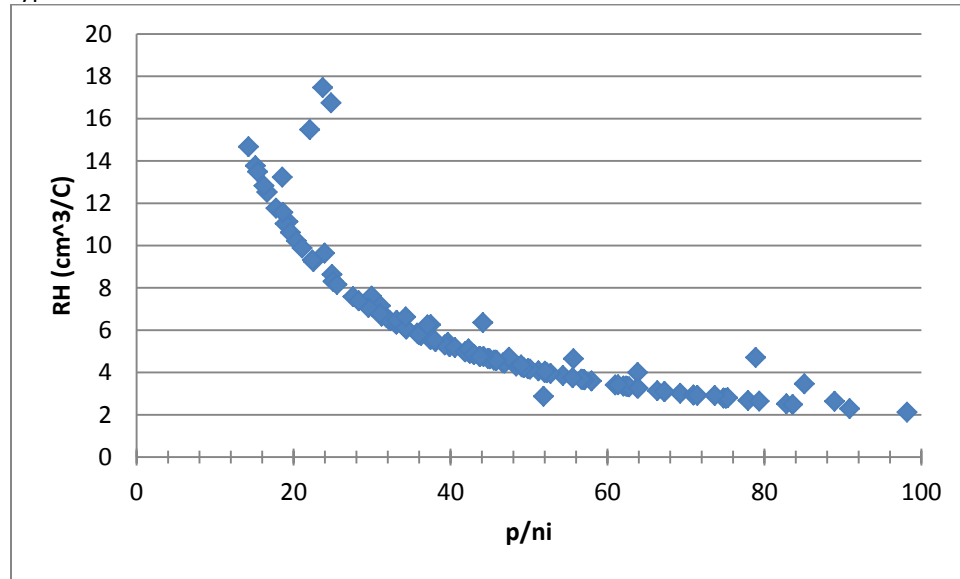
**Note: b was assumed to be 1.5 since this holds true for intrinsic PbSe [12]. The variation of b will not vary dramatically enough to impact the results of this calculation.*

From table II (located in the appendix), it is clear that for some cases of inconsistent measurement of the sign of the Hall coefficient, erroneous measurements were obtained. However, for others the sign is simply inconsistent. It is possible that a false sign was due to the non-uniformity of the thickness of the PbSe thin films, or due to low carrier densities where both electrons and holes contribute to conduction.

This is discussed in further detail in section 5.1.2.5. If the carrier densities are close to the intrinsic carrier density, it could explain the inconsistent measurement of the sign of the Hall coefficient and majority carrier density. As the ratio of the majority carrier density to the intrinsic carrier density decreases, the Hall coefficient increases exponentially for a semiconductor. However, once the majority carrier density begins to approach the intrinsic carrier density, the Hall coefficient rapidly approaches zero [12]. The Hall voltage (and Hall coefficient) for an intrinsic semiconductor is zero due to the fact that there are an equal number of holes and electrons. Thus, if the electron and hole densities are both close to intrinsic, an inconsistent measurement of the Hall coefficient could be obtained.

The Hall coefficient was plotted against the hole density for all p-type samples as shown in the figure below. Hole densities ranging from 4.28×10^{17} to $1.91 \times 10^{19} \text{ cm}^{-3}$ were achieved. We can see that the behavior follows that of what is expected from a semiconductor, where the Hall coefficient exponentially increases as the ratio of the majority carrier density to intrinsic carrier density decreases [12]. This also demonstrates that the hole density can be reproducibly varied by controlling the deposition conditions, which will be discussed in more detail in section 5.1.2. For the PbSe thin films in which the minority carrier density could not be neglected and in which the measurement of the sign of the Hall coefficient was inconsistent, the electrical properties were estimated by the approach described in the following section.

Fig. 18: Hall coefficient vs. the ratio of the hole density to the intrinsic carrier density for consistently measured p-type PbSe thin films.



5.1.1 Estimation of Electrical Properties for Two Carrier Contribution to Conduction

The true electrical properties of the PbSe thin films with electron and hole contribution to conduction and/or that exhibited inconsistent measurement of the sign of the Hall coefficient were estimated on a case by case basis by extrapolating from the consistent p-type PbSe thin film measurements by the Hall effect.

First, the hole density was extrapolated based on the hole density of the consistently measured p-type PbSe thin films. However, this suggested zero hole density. Thus, the following method was developed. Equation 8 holds true for all semiconductors provided that a low magnetic field strength is used in implementing the Hall effect measurement, where $B \ll 1/\mu_n$. As was described in section 4.2, this holds

true for all Hall effect measurements in this work. To estimate the true carrier densities of the PbSe thin films with electron and hole contribution to conduction and/or that exhibited inconsistent measurement of the sign of the Hall coefficient, a system of two equations with two unknowns was solved. Between equation 8 and equation 12, initially we have five unknowns. Only the Hall coefficient measured by the Hall effect can be trusted since it relies only on the Hall voltage and resistance of the semiconductor. The semiconductor resistivity and hole mobility were extrapolated from the consistent p-type PbSe thin film data for each condition where estimation of the electrical properties was necessary, which is described in more detail in the following sections.

Equation 8 was solved for “n”, then substituted into equation 12 and solved for “p” to yield the following expression for the hole density (Eq. 13):

$$\rho = \frac{1}{q(\mu_n n + \mu_p p)} \quad (\text{Eq. 12})$$

$$p = \frac{3\rho\mu_p + 2R_H}{5q\rho^2\mu_p^2} \quad (\text{Eq. 13})$$

$$np = n_i^2 \quad (\text{Eq. 14})$$

We now have an equation for the hole density which is described by the Hall coefficient, which was measured, and the semiconductor resistivity and hole mobility, which were extrapolated. For each PbSe thin film, the average of the p-type measurements of the Hall coefficient was used. The electron density was then found utilizing the familiar relation described by equation 14.

Case 1: 60°C

Inconsistent measurement of the sign of the Hall coefficient and consistent measurement of the sign where both electrons and holes contribute to conduction were obtained for samples deposited at 60°C for between 2-5 hours with 1M TSC as the complexing agent and a final concentration of 86mM Se. The hole mobility and semiconductor resistivity were extrapolated by examining the electrical properties of p-type PbSe thin films that exhibited consistent measurement of the sign of the Hall coefficient. For the samples which were deposited for 2.5 and 3-5 hours, the average hole mobility and semiconductor resistivity obtained for consistently p-type PbSe thin films deposited at the same conditions were used to estimate the hole mobility and semiconductor resistivity. For 2-2.833 hours, the hole mobility and semiconductor resistivity needed to be extrapolated. Trend lines were fitted to the averaged data at each time for the consistently p-type samples to extrapolate the hole mobility and semiconductor resistivity as shown in the figures below. It should be noted that fitting a trend line to the entire data set yielded zero or negative hole mobility, so only the data at 2.5 and 3 hours was used to extrapolate the hole mobility. Using these extrapolated values of hole mobility and semiconductor resistivity, the hole density was estimated employing equation 13 (table 1). Erroneous Hall coefficient measurements were obtained for the PbSe thin films deposited at 2.667 hours so the hole density could not be estimated by these means. From the table below we can see the estimated hole densities results in reasonable values of Hall coefficient, with the exception of 2 hours of deposition. The Hall coefficient was calculated using equation 8 and 9a and compared. This comparison suggests that the samples are in fact extrinsic such that the minority carrier density can in fact be neglected.

Fig. 19: Fitted average hole mobility vs. deposition time for PbSe thin films deposited at 60°C with 1M TSC and a final concentration of 86mM Se (top).

Fig. 20: Fitted average semiconductor resistivity vs. deposition time for PbSe thin films deposited at 60°C with 1M TSC and a final concentration of 86mM Se (bottom).

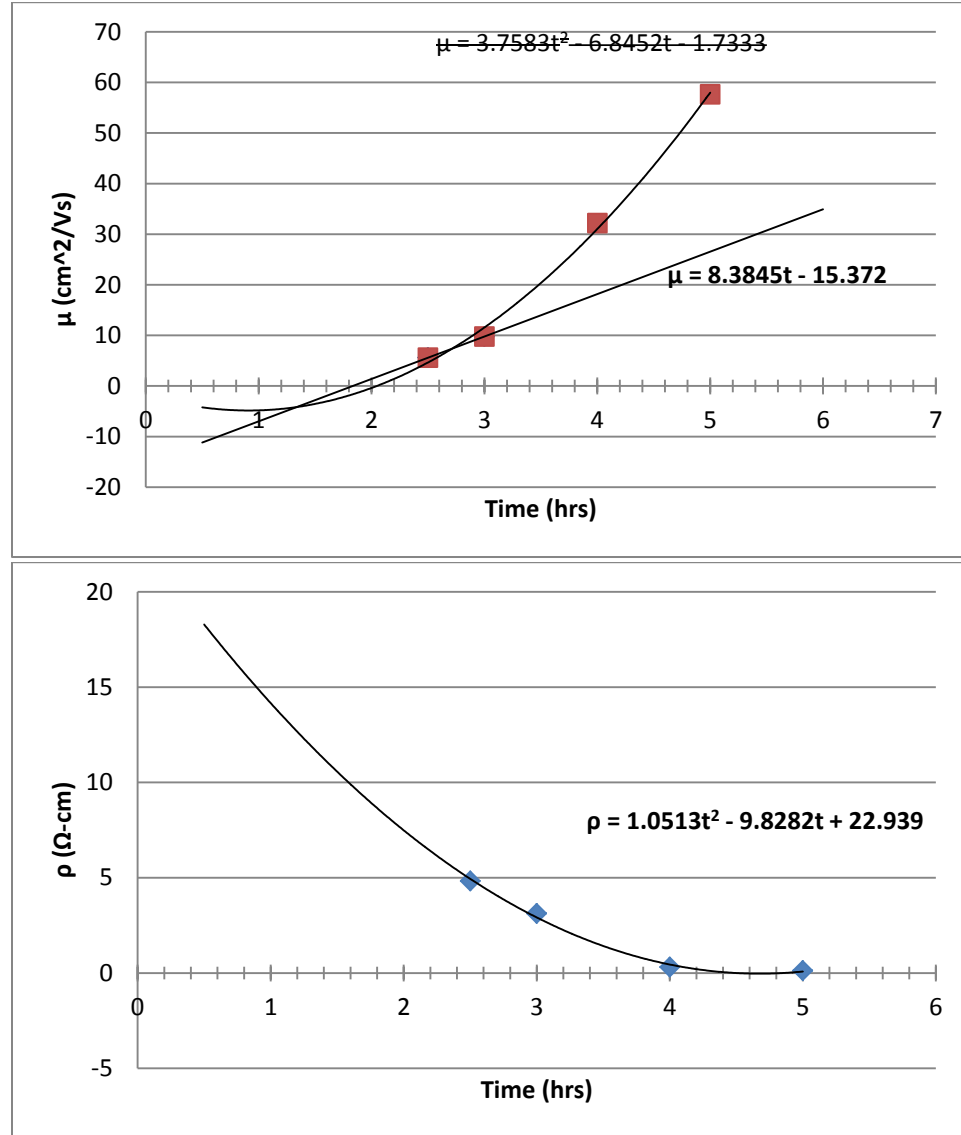


Table 1: Estimated values of hole density and semiconductor resistivity and resulting values of hole density and Hall coefficient for PbSe thin films deposited at 60°C with 1M TSC and a final concentration of 86mM Se.

| Time (hrs) | $\sim\mu_p$ (cm ² /Vs) | $\sim\rho$ (Ω-cm) | $\sim p$ (cm ⁻³) | % Standard Deviation of hole density | $\sim RH_{eq.8}$ (cm ³ /C) | $\sim RH_{eq. 9a}$ (cm ³ /C) |
|------------|-----------------------------------|-------------------|------------------------------|--------------------------------------|---------------------------------------|---|
| 2* | 1.397 | 7.488 | 6.55E+18 | 135 | 0.953 | 0.953 |
| 2.5** | 5.589 | 4.828 | 3.64E+17 | 87 | 16.548 | 17.149 |
| 2.667* | 6.989 | 4.205 | -- | -- | -- | -- |
| 2.883* | 8.801 | 3.342 | 2.17E+17 | -- | 26.016 | 28.766 |

| | | | | | | |
|-----|--------|-------|----------|----|--------|--------|
| 3** | 9.782 | 3.126 | 1.64E+17 | 20 | 31.912 | 38.062 |
| 4** | 32.202 | 0.308 | 6.65E+17 | 20 | 9.287 | 9.387 |
| 5** | 57.643 | 0.123 | 9.26E+17 | -- | 6.704 | 6.741 |

*Extrapolated from p-type data.

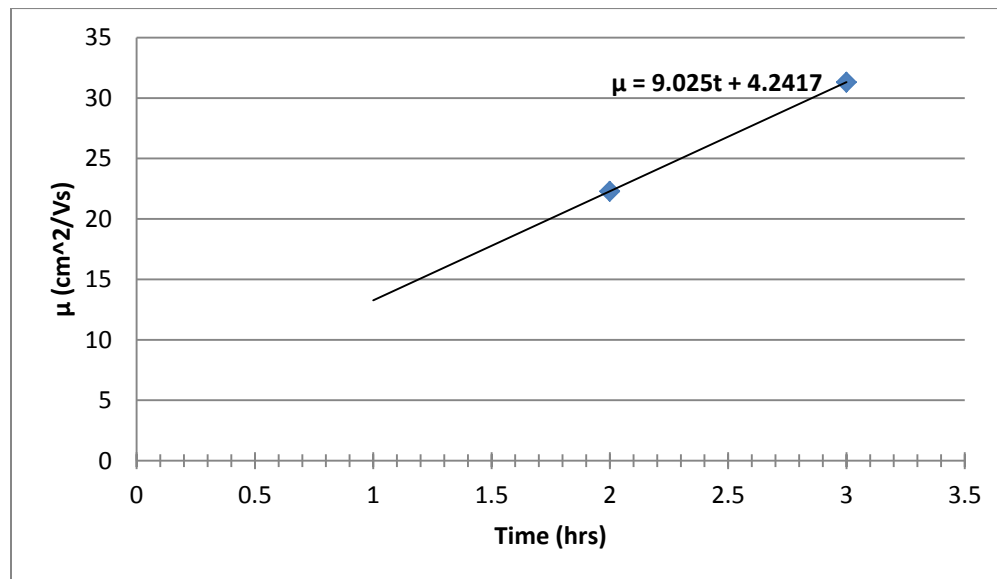
**Averaged values from p-type data.

Case 2: 70°C

Inconsistent measurement of the sign of the Hall coefficient were obtained for samples deposited at 70°C for 1 hour with 1M TSC as the complexing agent and a final concentration of 86mM Se. Using the averaged values of hole mobility and semiconductor resistivity obtained at longer periods of deposition at the same conditions, the hole mobility and semiconductor resistivity at 1 hour of deposition were extrapolated as shown in the figures and table below. These values were used to estimate the hole density utilizing equation 13. The Hall coefficient was calculated using equations 8 and 9a and compared. This comparison suggests that the samples are in fact extrinsic such that the minority carrier density can in fact be neglected (table 2).

Fig. 21: Fitted average hole mobility vs. deposition time for PbSe thin films deposited at 70°C with 1M TSC and a final concentration of 86mM Se (top)

Fig. 22: Fitted average semiconductor resistivity vs. deposition time for PbSe thin films deposited at 70°C with 1M TSC and a final concentration of 86mM Se (bottom).



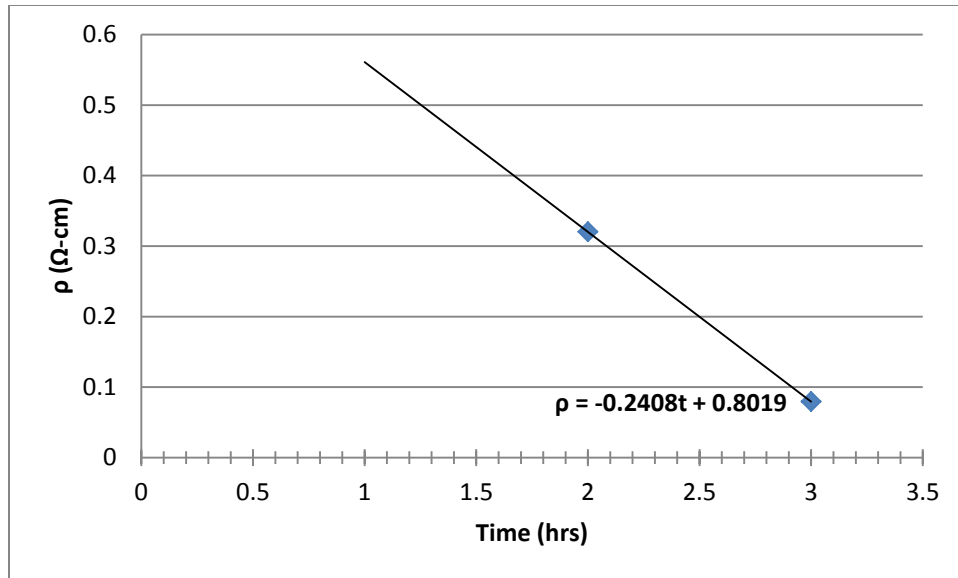


Table 2: Estimated values of hole density and semiconductor resistivity and resulting values of hole density and Hall coefficient for PbSe thin films deposited at 70°C for 1 hour with 1M TSC and a final concentration of 86mM Se.

| Time (hrs) | $\sim\mu_p$ (cm ² /Vs) | $\sim\rho$ (Ω-cm) | $\sim p$ (cm ⁻³) | $\sim RH_{eq.8}$ (cm ³ /C) | $\sim RH_{eq. 9a}$ (cm ³ /C) |
|------------|-----------------------------------|-------------------|------------------------------|---------------------------------------|---|
| 1* | 13.2667 | 0.5611 | 7.87E+18 | 0.793 | 0.793 |

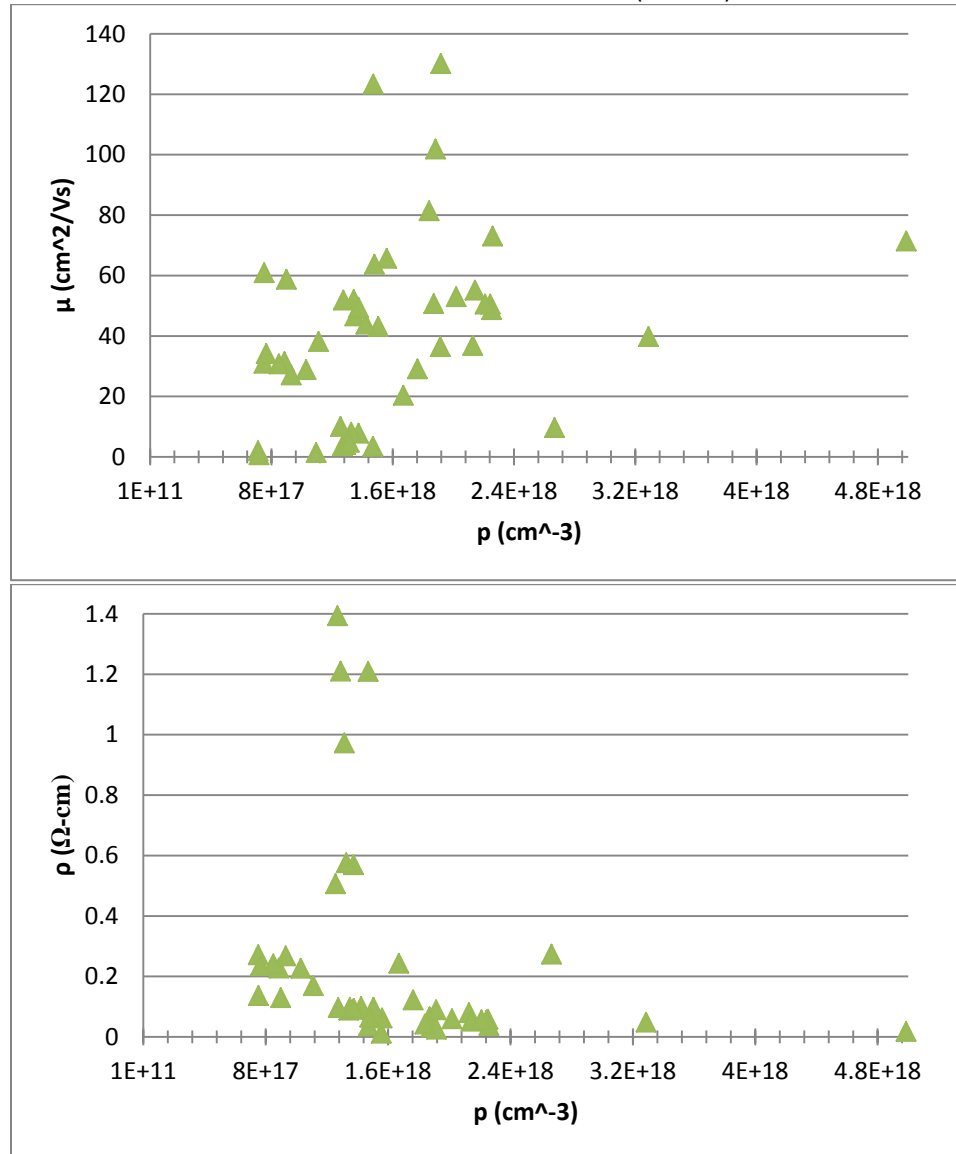
*Extrapolated from p-type data.

Case 3: 75°C

Inconsistent measurement of the sign of the Hall coefficient and consistent measurement of the sign where both electrons and holes contribute to conduction were obtained for samples deposited at 75°C for 3 hours with 1M TSC as the complexing agent and a final concentration of 86mM Se. The semiconductor resistivity and hole mobility for consistently p-type PbSe thin films deposited at 75°C for 3 hours were used for estimation. From the figures below we can see that neither the semiconductor resistivity nor the hole mobility vary significantly with hole density. The average hole mobility is 46 cm²/Vs while the semiconductor resistivity varies somewhat, but is more often than not approximately 0.1 Ω-cm with some exceptions. Using these values of semiconductor resistivity and hole mobility, the hole density was estimated utilizing equation 13. The estimated values of hole density range from 8.85x10¹⁶ cm⁻³ to 6.63x10¹⁸ cm⁻³ with a standard deviation of 136%. The calculated Hall coefficient from these values are much too high compared to that of the consistently measured Hall coefficient, indicating that the estimation method was not accurate at these conditions.

Fig. 23: Hole mobility vs. hole density for consistently p-type PbSe thin films deposited at 75°C for 3 hours with 1M TSC and a final concentration of 86mM Se (top).

Fig. 24: Semiconductor resistivity vs. hole density for consistently p-type PbSe thin films deposited at 75°C for 3 hours with 1M TSC and a final concentration of 86mM Se (bottom).



5.1.2 Analysis of Results

The following section will demonstrate that the electrical properties of the consistently p-type PbSe thin films can be controlled by variation of the deposition conditions. Only temperature, time, concentration of the complexing agent added to the deposition solution, and the final concentration of Se in the deposition solution were varied. All other parameters remain constant at the conditions described in section 4.1.5.

5.1.2.1 Variation of Time

5.1.2.1.1 60°C, 1MTSC, 86mMSe: Variation of Time

All PbSe thin films to be described in this section were deposited at 60°C with 1M TSC as the complexing agent and a final concentration of 86mM Se. The deposition time was varied from 1-5 hours.

Conductivity is not achieved at 1 or 1.5 hours of deposition. At 2 hours, conductivity is achieved. However, at this deposition time the sign of the Hall coefficient measured was inconsistent in every case. As the deposition time was increased up until 5 hours, cases of inconsistent and consistent measurement of the sign of the Hall coefficient are both present.

Analysis of the PbSe thin films for which consistently measured p-type semiconductors were achieved reveals that in general the hole mobility increases as the deposition time is increased (fig. 26). At each temperature, the hole mobility is directly dependent on the hole density. The semiconductor resistivity on the other hand, decreases as the deposition time is increased in general (fig. 27); it does not seem to be dependent on the hole density. The hole density gradually increases with deposition time in general, indicating that there are an increasing number of defects present in the thin films (fig. 28).

The crystal structure was investigated by scanning electron microscopy. It was observed that bimodal growth occurred at every temperature. Bimodal growth occurs when two distinct sizes of crystals grow simultaneously. Both microcrystals and nanocrystals are present. From the scanning electron micrographs (SEMs) below, it is apparent that the density of microcrystals and the stage of development of the nanocrystals vary with time. The increase in hole mobility with increasing time coincides with the development of the nanocrystals. It is possible that the number of defects present within the nanocrystals is reduced allowing for greater mobility, or that there is less scattering at the boundaries between nanocrystals. The fact that hole density gradually increases with time indicates that the number of defects present in the nanocrystals must be gradually increasing with time as well. Thus, it is logical to conclude that the increase in hole mobility as deposition time is increased is due to reduced scattering at the boundaries between nanocrystals caused by the development of the nanocrystalline structure.



Fig. 25: PbSe thin film deposited for 5 hours exhibiting holes in thin film.

As the deposition time is increased, the density of microcrystals decreases. This indicates that for longer periods of deposition, the microcrystals are redissolving in solution. The redissolution of the microcrystals points to ion-by-ion growth as the deposition mechanism. As described in section 2.2.1, ion-by-ion growth is an equilibrium reaction, meaning it is reversible. Redissolution can occur if the ionic product of PbSe is lower than that of the solubility product of PbSe. Though initially the concentrations of ions in the deposition solution were such that precipitation could occur, as the deposition continued for longer periods of time

the concentrations of ions in solution may have shifted to the point where the ionic product was lower than the solubility product. Hydroxide cluster growth can be ruled out for the microcrystals since it is not a reversible process. Observing the PbSe thin films deposit for 4 and 5 hours with the naked eye also points to redissolution; small holes were observed in the thin films (fig. 25). Additionally, larger crystals are expected from ion-by-ion growth.

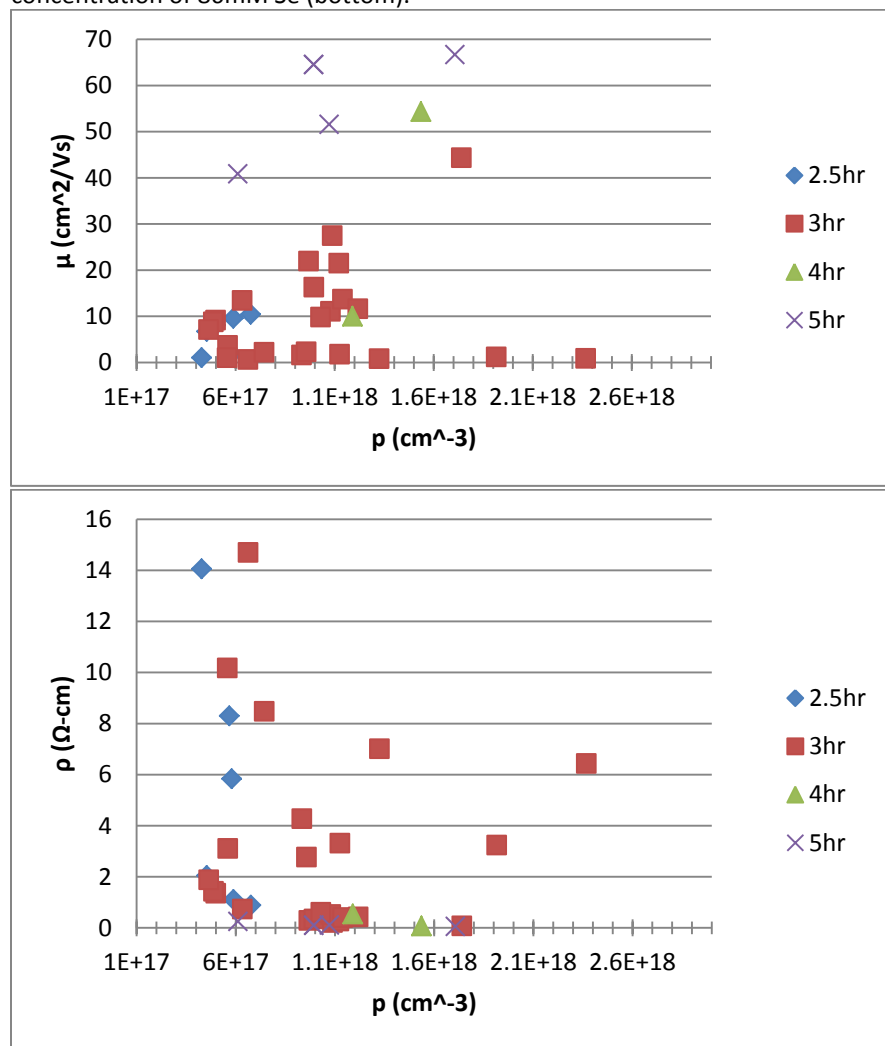
The nanocrystals, on the other hand, become more developed as deposition time increases. Since they do not seem to redissolve, and due to the fact that some clusters of nanocrystals are present in the thin films, it is reasonable to conclude that the nanocrystals form from the hydroxide cluster deposition

mechanism, which typically results in smaller crystals. Thus, the presence of bimodal growth in the PbSe thin films is the result of two separate deposition mechanisms occurring simultaneously.

Fig. 26: Hole mobility vs. hole density for PbSe thin films deposited at 60°C with 1M TSC and a final concentration of 86mM Se (top).

Fig. 27: Semiconductor resistivity vs. hole density for PbSe thin films deposited at 60°C with 1M TSC and a final concentration of 86mM Se (middle).

Fig. 28: Hole density vs. deposition time for PbSe thin films deposited at 60°C with 1M TSC and a final concentration of 86mM Se (bottom).



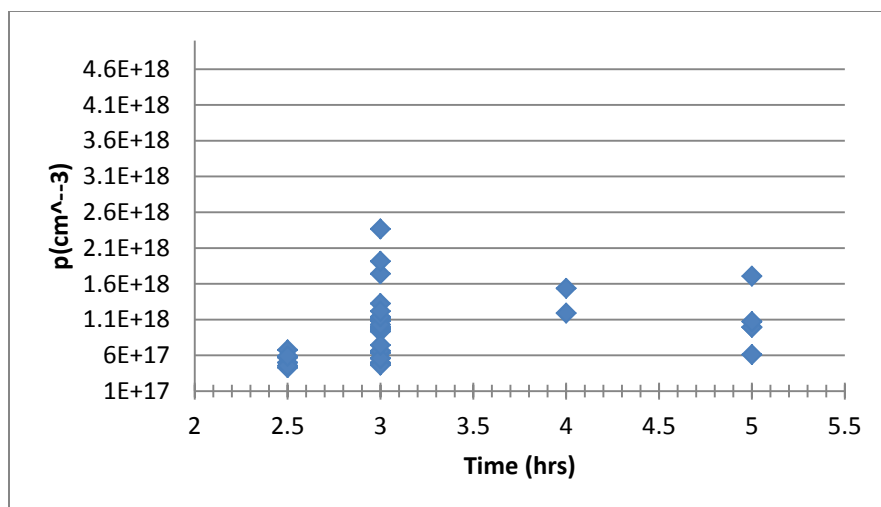
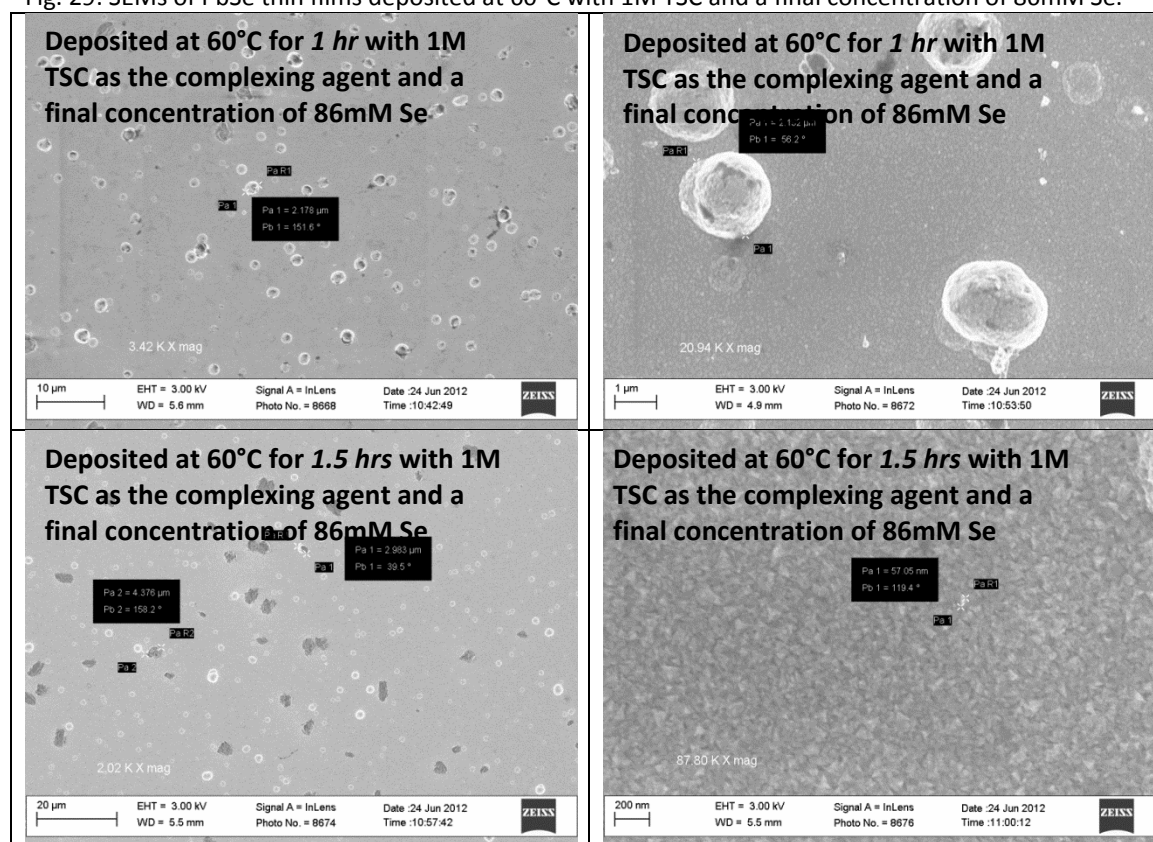
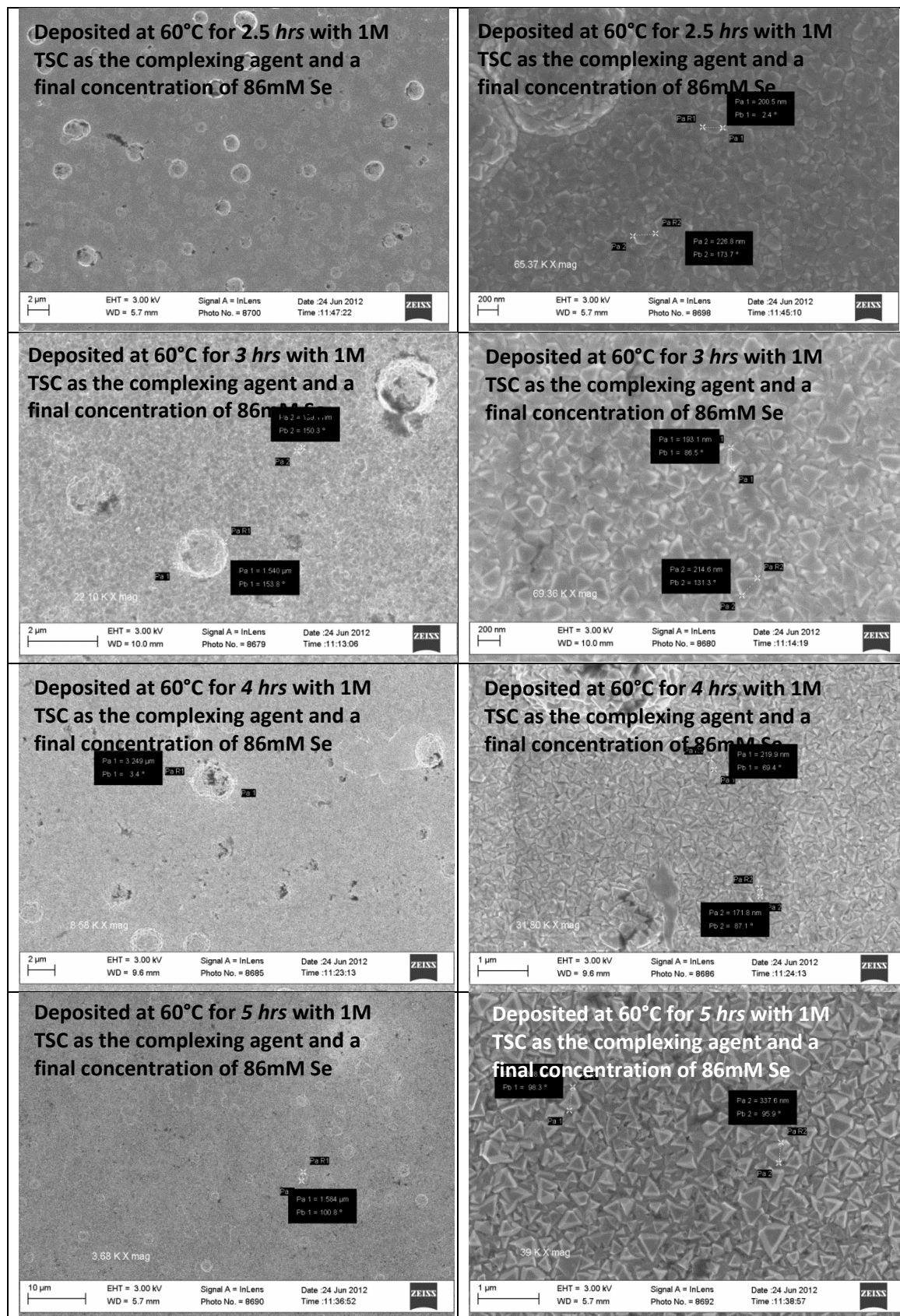


Fig. 29: SEMs of PbSe thin films deposited at 60°C with 1M TSC and a final concentration of 86mM Se.





5.1.2.1.2 75°C, 1.0M TSC, 86mM Se: Variation of Time

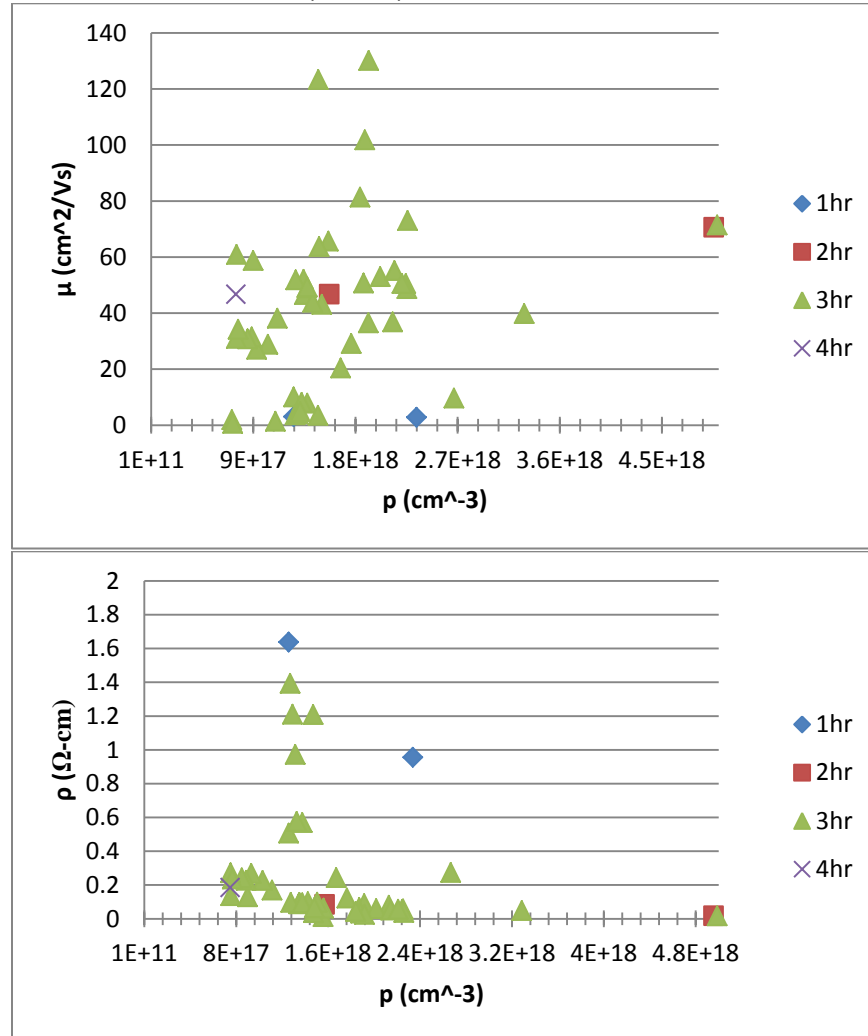
All PbSe thin films to be described in this section were deposited at 75°C with 1M TSC as the complexing agent and a final concentration of 86mM Se. The time of deposition was varied from 1-4 hours. From figure 30 below we can see the hole mobility dramatically increases as time is increased from 1 to 2 hours. However, a continued increase in time does not have a measurable effect on the magnitude of the hole mobility, which is on average $46\text{cm}^2/\text{Vs}$ for all PbSe thin films within this time range. There is a distribution present at 3 hours of deposition due to the fact that multiple samples were deposited at these conditions. Some distribution is expected due to the nature of CBD. Though on average $46\text{cm}^2/\text{Vs}$ was achieved, we can see that at lower hole densities the hole mobility tends towards lower values and at higher hole densities the hole mobility tends toward higher values. The variation in hole mobility is due to the fact that there is some variation in the structure of each PbSe thin film deposited at these conditions since the PbSe thin films appear to be polycrystalline. The reproducibility at these conditions will be discussed further in section 5.1.2.5. The semiconductor resistivity dramatically decreases as the time is increased from 1 to 2 hours, but does not change measurable as the time is increased from 2 to 4 hours (fig. 31). The majority of PbSe thin films have a semiconductor resistivity at or below $0.2\ \Omega\text{-cm}$, but again some distribution is present at 3 hours of deposition, though less than in the case of the hole mobility. The hole density is fairly constant with an increase in time, though a fair deal of distribution is present at 3 hours of deposition due to multiple depositions (fig. 32).

SEMs were taken for PbSe thin films deposited at 1 and 3 hours (fig. 33). It is apparent that bimodal growth has occurred at 3 hours of deposition. It is likely that bimodal growth has also occurred at 1 hour of deposition since this occurred for PbSe thin films deposited with an identical deposition bath at 60°C. Like at 60°C, the nanocrystals present in the thin films become more defined as time is increased. It is likely that a dramatic improvement in the structure of the nanocrystalline structure occurs from 1 to 2 hours, explaining the dramatic improvement in hole mobility and semiconductor conductivity. Clusters of nanocrystals are again observed supporting the conclusion that nanocrystals are forming by hydroxide cluster growth. It is likely that the crystal structure does not vary dramatically from 2 to 4 hours of deposition since the hole mobility and hole density are fairly constant across this time range.

Fig. 30: Hole mobility vs. hole density for PbSe thin films deposited at 75°C with 1M TSC and a final concentration of 86mM Se (top).

Fig. 31: Semiconductor resistivity vs. hole density for PbSe thin films deposited at 75°C with 1M TSC and a final concentration of 86mM Se (middle).

Fig. 32: Hole density vs. deposition time for PbSe thin films deposited at 75°C with 1M TSC and a final concentration of 86mM Se (bottom).



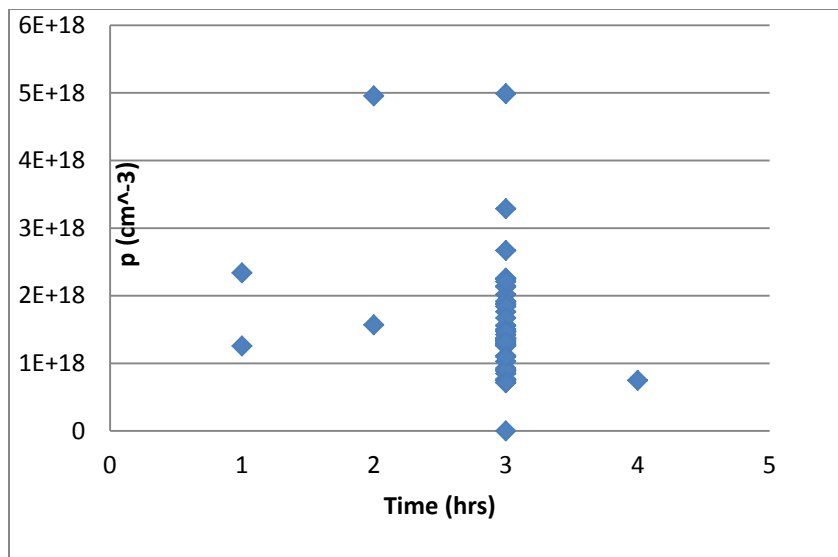
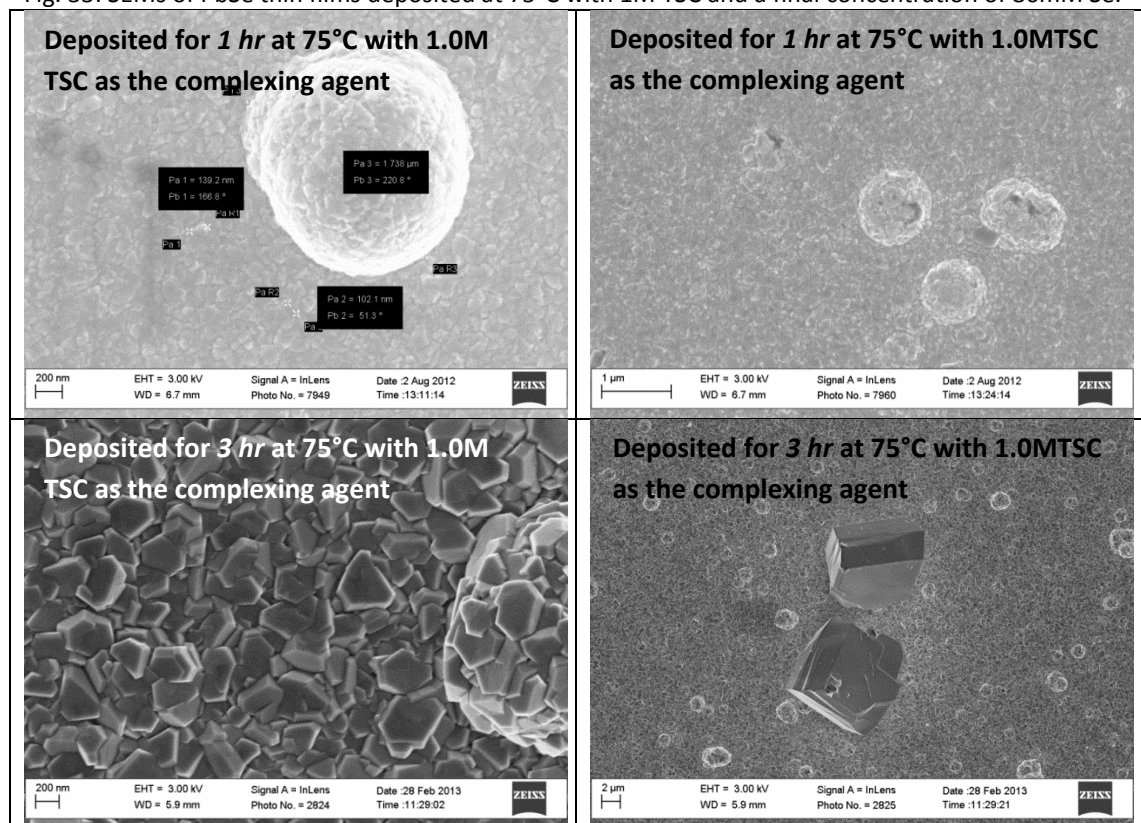


Fig. 33: SEMs of PbSe thin films deposited at 75°C with 1M TSC and a final concentration of 86mM Se.



5.1.2.2 Variation of Temperature

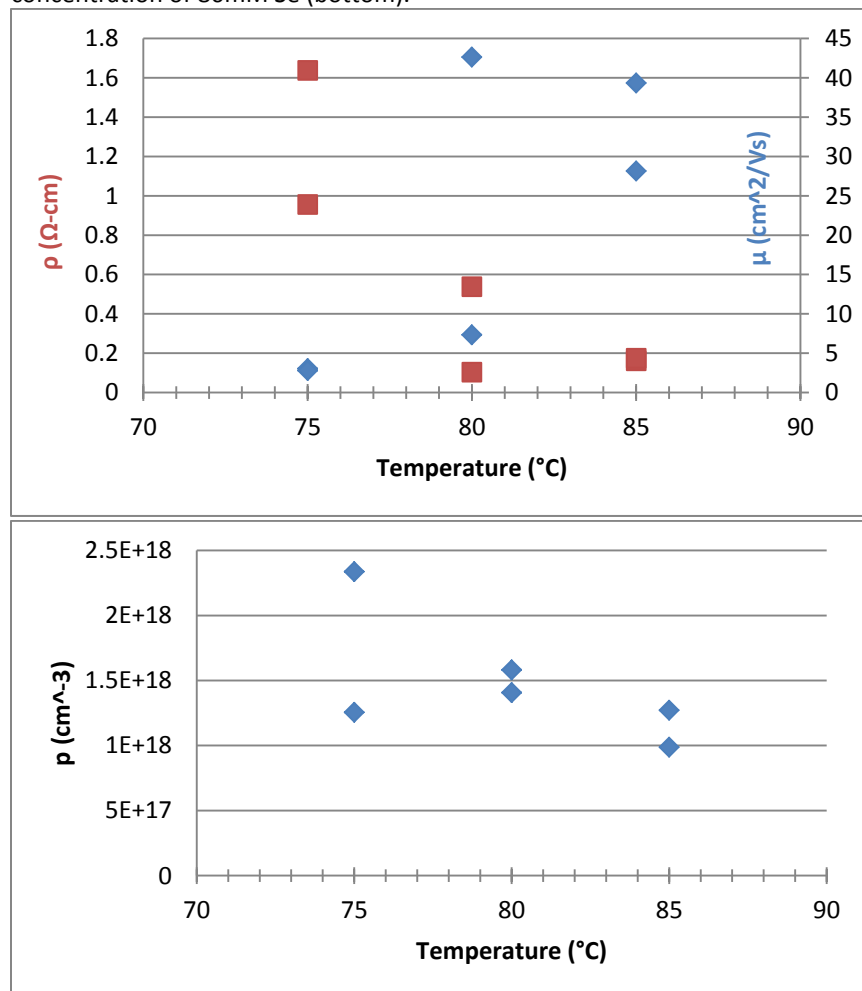
For the following descriptions of variation of temperature at various deposition times, similar trends are observed at each set of conditions. For instance, as temperature is increased at 1, 2 and 3 hours of deposition, we see an increase in hole mobility for all instances while the hole density remains fairly constant. This indicates less scattering at the boundaries between crystals as temperature is increased. Additionally, this indicates that the same deposition mechanisms are likely present in each case and the time and temperature are affecting only the deposition rate, not the deposition mechanisms.

5.1.2.2.1 1hr, 1M TSC, 86mM Se: Variation of Temperature

All PbSe thin films to be described in this section were deposited for 1 hour with 1M TSC as the complexing agent and a final concentration of 86mM Se. The temperature at which the deposition was carried out was varied from 60-85°C in steps of 5°C. An increase in semiconductor conductivity is observed as the temperature is increased. At 60°C and 65°C, there is no conductivity at only 1 hour of deposition. At 70-85°C, conductivity is achieved, but at 70°C the sign of the Hall coefficient was inconsistent. From 75-85°C conductivity increases as temperature is increased (fig. 34). A direct relationship is also observed between the hole mobility and temperature (fig. 34). It should be noted that this trend is observed in general, but there is some distribution of results present at conditions for which multiple samples were prepared. Hole density is fairly constant as temperature is increased from 75-85°C (fig. 35).

Fig. 34: Hole mobility vs. temperature and semiconductor resistivity vs. temperature for PbSe thin films deposited for 1 hour with 1M TSC and a final concentration of 86mM Se (top).

Fig. 35: Hole density vs. temperature for PbSe thin films deposited for 1 hour with 1M TSC and a final concentration of 86mM Se (bottom).

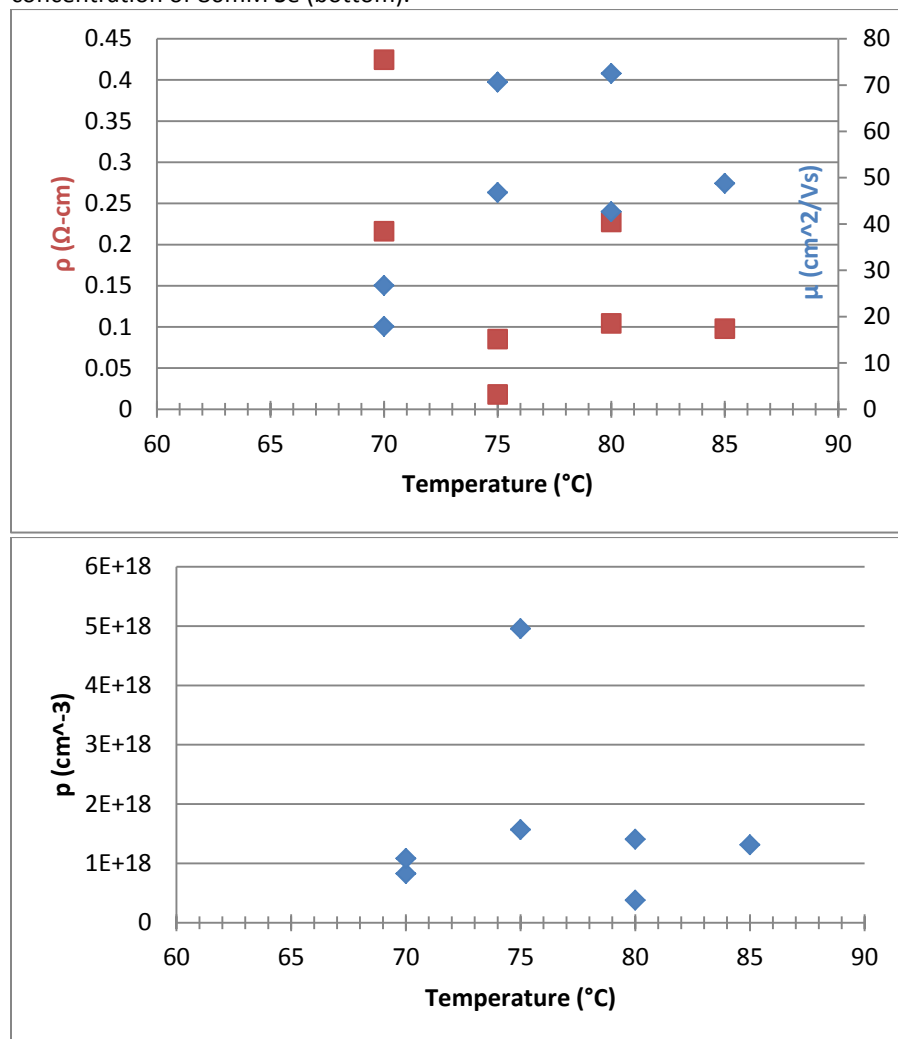


5.1.2.2.2 2hr, 1M TSC, 86mM Se: Variation of Temperature

All PbSe thin films to be described in this section were deposited for 2 hours with 1M TSC as the complexing agent and a final concentration of 86mM Se. The temperature at which the deposition was carried out was varied from 60-85°C in steps of 5°C. When taking into account the previous section as well where samples were prepared at the same conditions for only 1 hour, semiconductor conductivity can be achieved at lower temperatures provided the deposition time is increased. We see conductivity achieved at 60 and 70°C for 2 hours of deposition. However at 60-65°C the PbSe thin films are not yet extrinsic. For all other temperatures p-type thin films are obtained. Again we see that the conductivity and hole mobility are both directly proportional to the temperature. Like in the case of 1 hour of deposition, the hole density remains fairly constant across the temperature range of 70-85°C (fig. 37).

Fig. 36: Hole mobility vs. temperature and semiconductor resistivity vs. temperature for PbSe thin films deposited for 2 hours with 1M TSC and a final concentration of 86mM Se (top).

Fig. 37: Hole density vs. temperature for PbSe thin films deposited for 2 hours with 1M TSC and a final concentration of 86mM Se (bottom).



5.1.2.2.3 3hr, 1M TSC, 86mM Se: Variation of Temperature

All PbSe thin films to be described in this section were deposited for 3 hours with 1M TSC as the complexing agent and a final concentration of 86mM Se. The temperature at which the deposition was

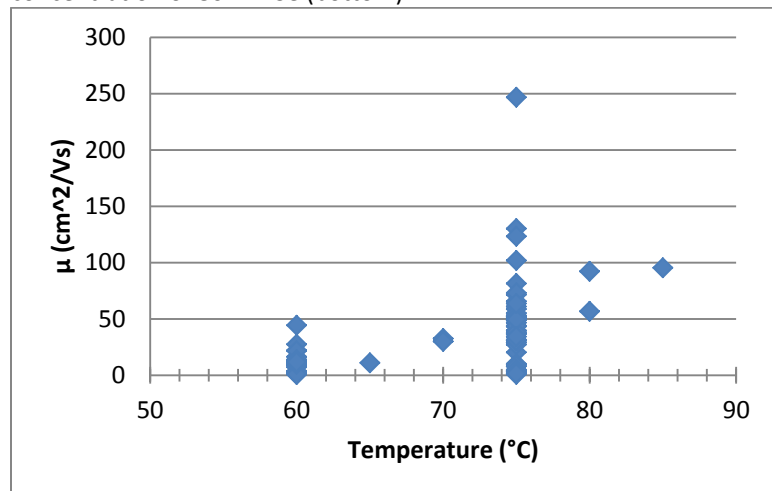
carried out was varied from 60-85°C in steps of 5°C. Consistently p-type PbSe thin films are achieved across the entire temperature range at 3 hours of deposition. However it should be noted that at 60°C and 75°C, some samples did not exhibit consistent measurement of the sign of the Hall coefficient.

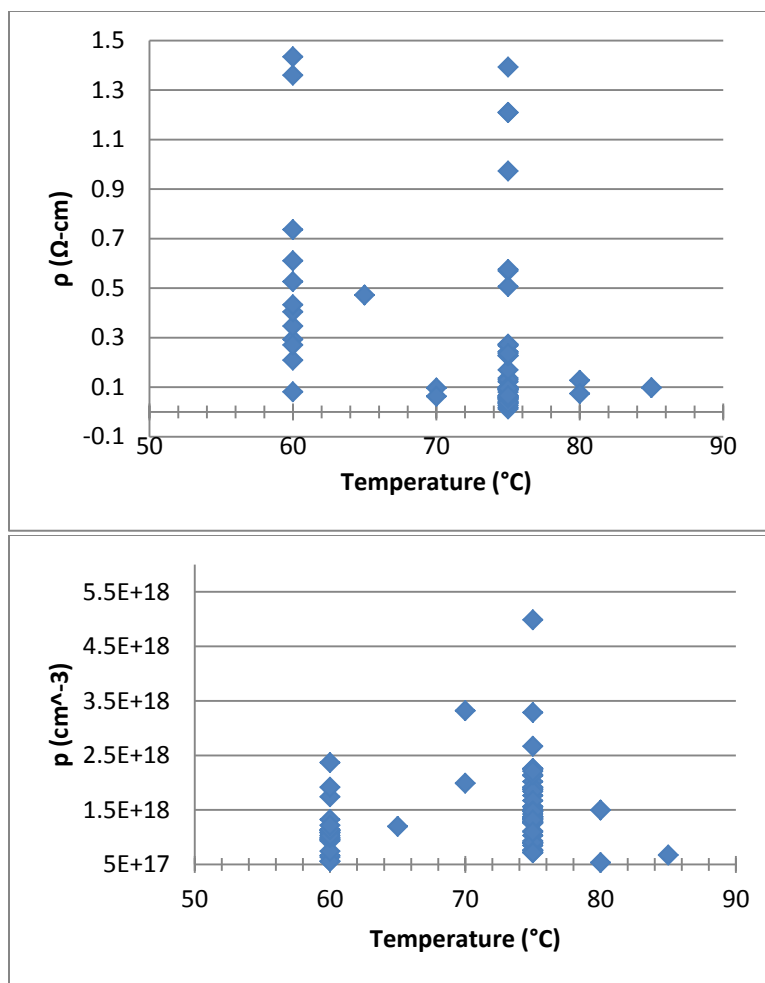
Again, a direct relationship is observed between the hole mobility and the temperature in general (fig. 38). Semiconductor resistivity remains fairly constant for samples deposited at 70-85°C, at an average of 0.2 Ω -cm in general. However, for 60°C there is some distribution present in the results, varying from 0.2-to 20 Ω -cm, due to the nature of chemical bath deposition previously discussed. We see some distribution present again at 60°C when looking at semiconductor resistivity vs. the hole density, but an average of approximately 3 Ω -cm is achieved across all hole densities, with higher resistivity present at lower hole densities. At the higher temperatures, the semiconductor resistivity does not vary greatly with hole density. At 75°C, an average of 0.1 Ω -cm is achieved and at 80-85°C an average of about 1 Ω -cm is achieved. In contrast to 1 and 2 hours of deposition, at 3 hours the semiconductor conductivity decreases in general from 60-75°C. The hole density increases with increasing temperature at 3 hours of deposition (fig. 39), in contrast to 1 and 2 hours of deposition where the hole density remained fairly constant with temperature variation.

Fig. 38: Hole mobility vs. temperature for PbSe thin films deposited for 3 hours with 1M TSC and a final concentration of 86mM Se (top).

Fig. 39: Semiconductor resistivity vs. temperature for PbSe thin films deposited for 3 hours with 1M TSC and a final concentration of 86mM Se (middle).

Fig. 40: Hole density vs. temperature for PbSe thin films deposited for 3 hours with 1M TSC and a final concentration of 86mM Se (bottom).





5.1.1.3 Variation of the Concentration of the Complexing Agent, TSC

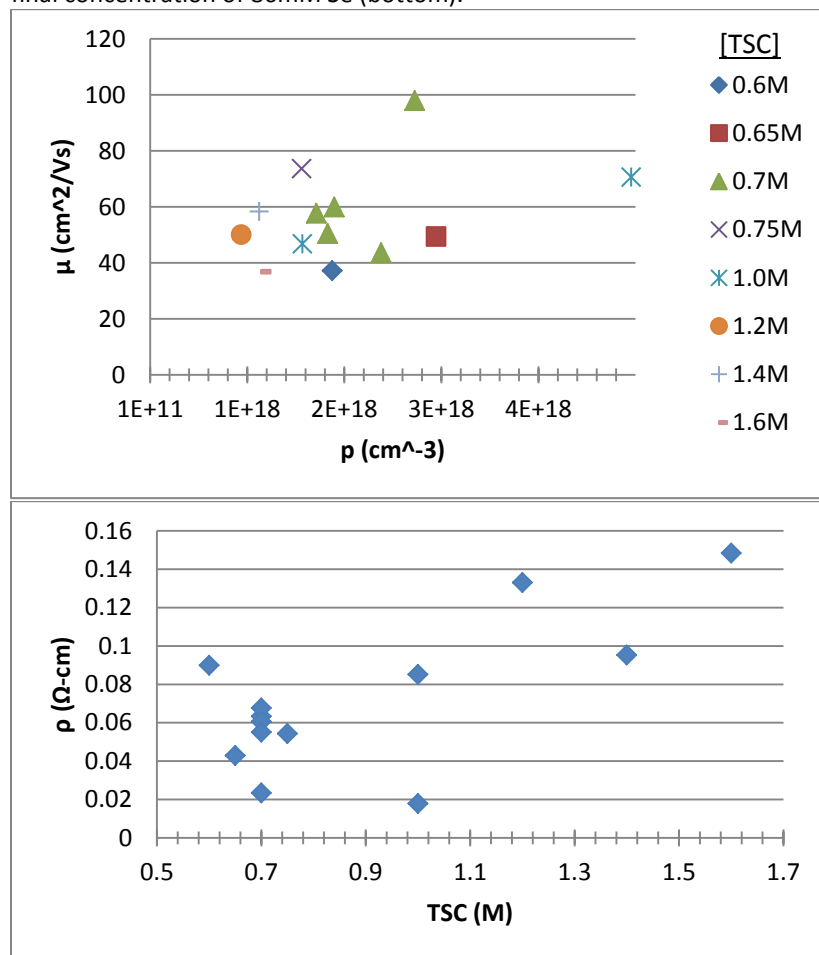
2hr, 75 $^{\circ}\text{C}$, 86mM Se: Variation of TSC

All PbSe thin films to be described in this section were deposited for 2 hours at 75 $^{\circ}\text{C}$ with a final concentration of 86mM Se. The concentration of the complexing agent, TSC, added to the deposition solution was varied from 0.40-1.60M. From the figures below we can see that high hole densities were produced at these conditions; the hole density does not vary greatly with the concentration of TSC indicating that the variation was not dramatic enough to greatly change the number of defects present within the nanocrystals. The hole mobility does not vary greatly with hole density or the concentration of TSC, validating the conclusion that the number of defects within the crystals is fairly constant with the change in TSC. At these conditions, the hole mobility is on average approximately 50 cm^2/Vs (fig. 41).

There is a noticeable change in the semiconductor resistivity of the PbSe thin films (fig.42). Conductive PbSe thin films were not achieved below 0.6M TSC. Since the TSC acts to form a complex with the $\text{Pb}(\text{CH}_3\text{CHOO})_2$ in the deposition solution to provide the Pb^{2+} ions (as described in section 2.2), it can be concluded that the concentration of TSC was not high enough to provide the necessary concentration of Pb^{2+} ions to achieve conductivity by either deposition mechanism. As the concentration of TSC is increased from 0.6-1.7M, we see an increase in semiconductor resistivity. The semiconductor resistivity is fairly constant regardless of the hole density.

Fig. 41: Hole mobility vs. hole density for PbSe thin films deposited for 2 hours at 75°C with a final concentration of 86mM Se (top).

Fig. 42: Semiconductor resistivity vs. concentration of TSC for PbSe thin films deposited for 2 hours at 75°C with a final concentration of 86mM Se (bottom).

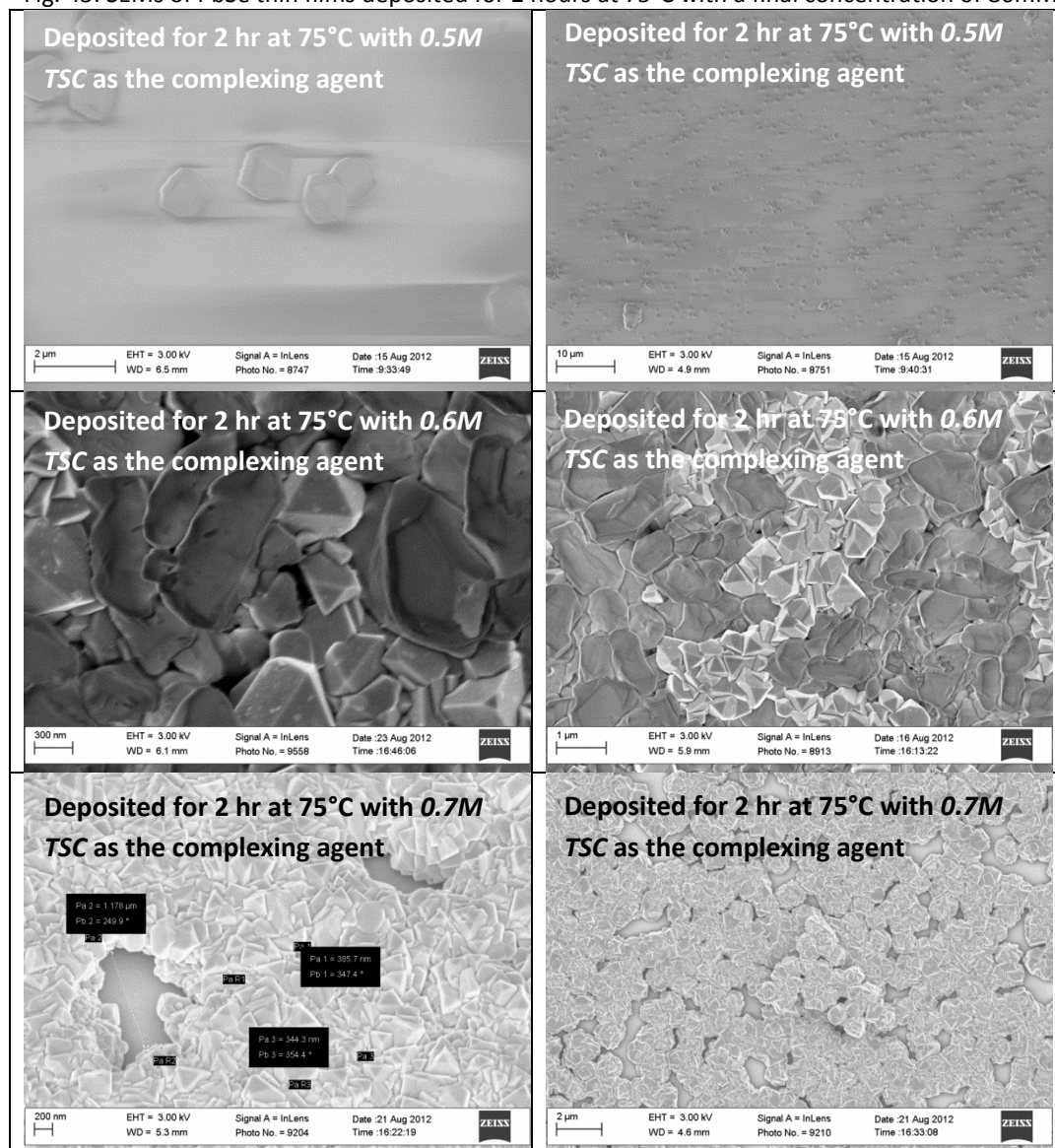


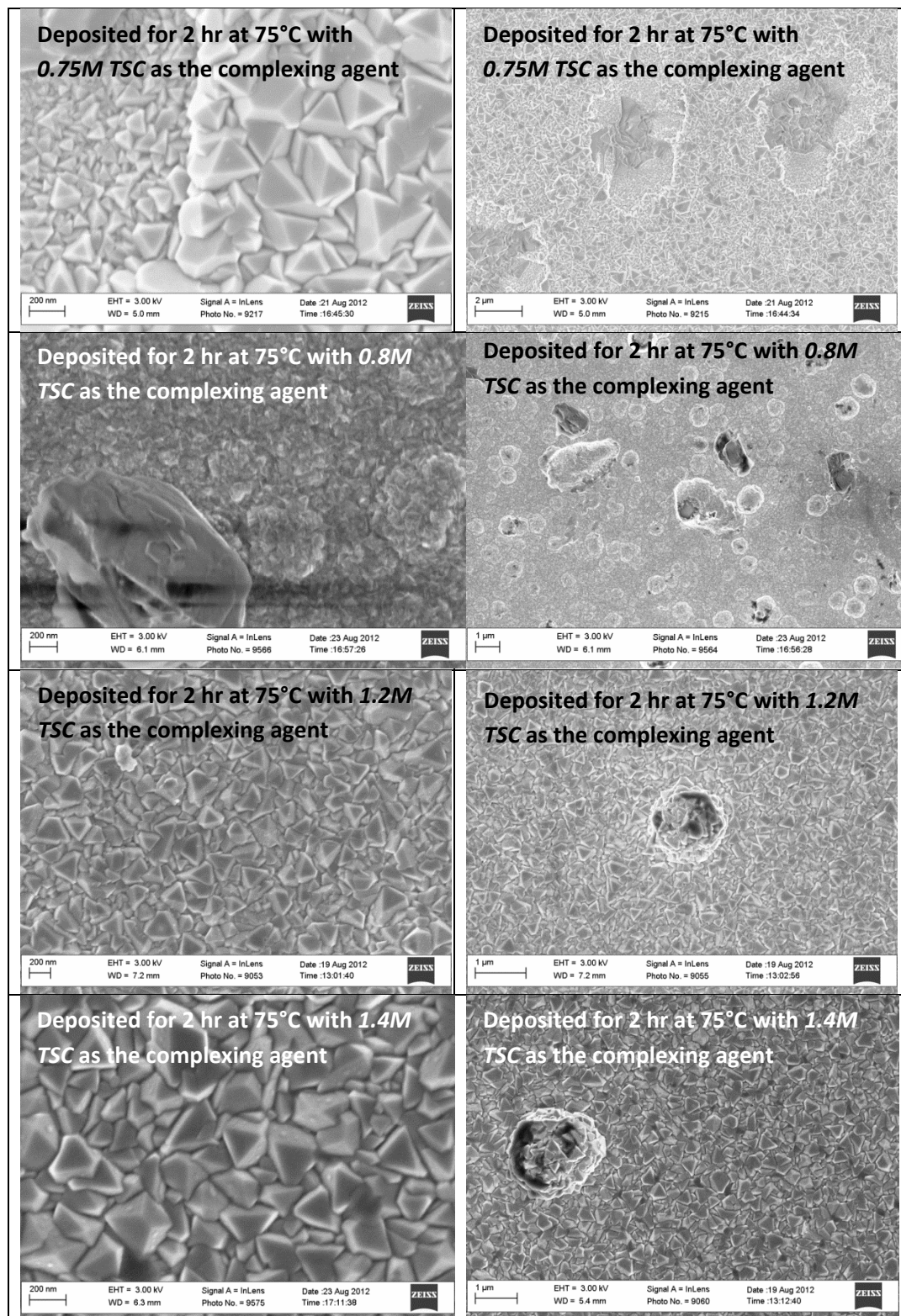
From an examination of the SEMs below (fig. 43), we can see that the concentration of the complexing agent clearly has an important influence on the kinetics of deposition, which ultimately control the shape and size of the PbSe crystals. At very low concentrations of TSC, such as 0.5M TSC, there appear to be only microcrystals present. These microcrystals are spaced very far apart explaining why the thin film is not conductive. At 0.8M TSC, bimodal growth has occurred but the microcrystals are again very far apart. The nanocrystals are not yet fully developed. This provides the charge carriers with many barriers to overcome at the boundaries between crystals, explaining why the thin film was not conductive.

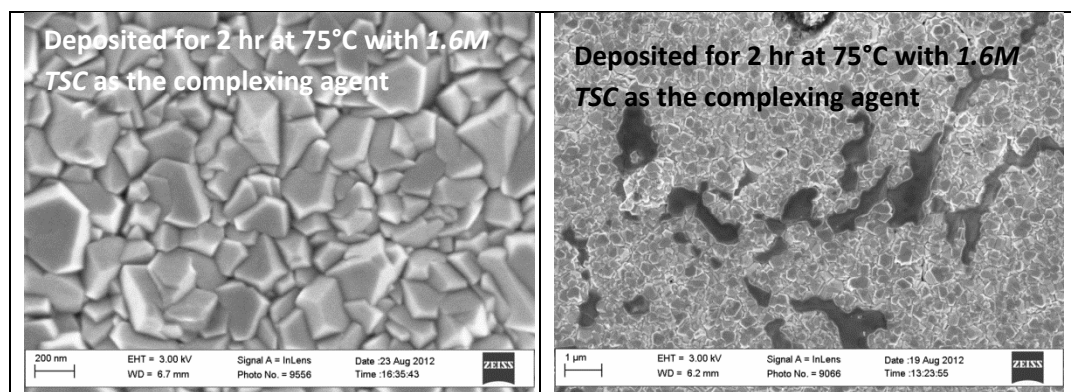
It was previously described that for other sets of conditions, bimodal growth occurred resulting in both microcrystals and nanocrystals. For almost all of the conditions described here, bimodal growth also occurred with several notable exceptions. At 0.60M and 0.65M TSC, bimodal growth still occurs, but there are areas of the PbSe thin films in which no microcrystals are present. At 0.7M TSC, the microcrystals are almost entirely eliminated and the size of nanocrystals is uniform. At 0.75M TSC, there are almost no microcrystals; however, there are two sizes of nanocrystals present. The smaller nanocrystals are less than 100nm in size. Typically the nanocrystals in the PbSe thin films deposited thus far are several hundred nanometers in size.

Over the range of 0.6-0.75M TSC, ion-by-ion growth is limited and even eliminated meaning the concentrations of the deposition solution are such that only hydroxide cluster growth occurs. As a result primarily nanocrystals are produced. At higher concentrations of TSC, bimodal growth is again present, though in general the nanocrystals are well developed allowing for conductive thin films. This indicates that in general, $\text{Pb}(\text{OH})_2$ is present and primarily hydroxide cluster growth is occurring by substitution of the Se^{2-} ions for the hydroxide. However, some free Pb^{2+} ions are generally present in the deposition solution as well, allowing for ion-by-ion growth to occur. The correct concentration of TSC creates a situation in which almost all Pb^{2+} ions are utilized for the formation of metal hydroxide and ion-by-ion growth is presented. It should be noted that the shape of the nanocrystals is notably different at 1.6M TSC when compared to the other thin films with lower concentrations of TSC. However, this does not seem to have any dramatic effects on the electrical properties.

Fig. 43: SEMs of PbSe thin films deposited for 2 hours at 75°C with a final concentration of 86mM Se.







5.1.2.4 Variation of Concentration of Se

5.1.2.4.1 2hr, 75°C, 0.7M TSC: Variation of Se

All PbSe thin films to be described in this section were deposited for 2 hours at 75°C with 0.7M TSC as the complexing agent. The final concentration of the Se in the deposition solution was varied from 50-86mM Se. Conductivity was not achieved at 50mM Se. As the concentration of Se is increased, semiconductor conductivity is achieved at 60mM Se and continues to increase with an increase in concentration of Se (fig. 45). From the figure below we can see that the hole mobility also increases with an increase in the concentration of Se (fig. 44). However, the hole mobility decreases with an increase in the hole density in general. We expect this because as the hole density increases, the number of defects present in the PbSe thin film increases. This will cause scattering and decrease the hole mobility. The conductivity also decreases with an increase in the hole density. Again, we should also expect a decrease in the conductivity for larger hole densities due to the fact that more defects are present. Hole density decreases with an increase in the concentration of Se.

From the SEMs below (fig. 46), we can see that bimodal growth has occurred under all conditions. As the concentration of Se increases, the nanocrystals become more developed. At 50mM Se, the nanocrystals are quite amorphous. They become more defined as the concentration of Se is increased. This is likely due to the fact that the number of Se^{2-} ions available is what controls the deposition rate. If more Se^{2-} ions are available, the deposition rate should be faster and we expect that the nanocrystals will be more developed. The increase in conductivity and hole mobility coincides with the increased development of the nanocrystals. This indicates that less defects are present in the nanocrystals since the hole density was observed to decrease with an increase in the concentration of Se, explaining the increase in hole mobility with an increasing concentration of Se. It is likely that the less scattering at the boundaries between nanocrystals also contributes to the increase in hole mobility with an increase in the concentration of Se based on the improved nanocrystalline structure.

Fig. 44: Hole mobility vs. the concentration of Se for PbSe thin films deposited for 2 hours at 75°C with 0.7M TSC as the complex agent (top).

Fig. 45: Semiconductor resistivity vs. the concentration of Se for PbSe thin films deposited for 2 hours at 75°C with 0.7M TSC as the complex agent (bottom).

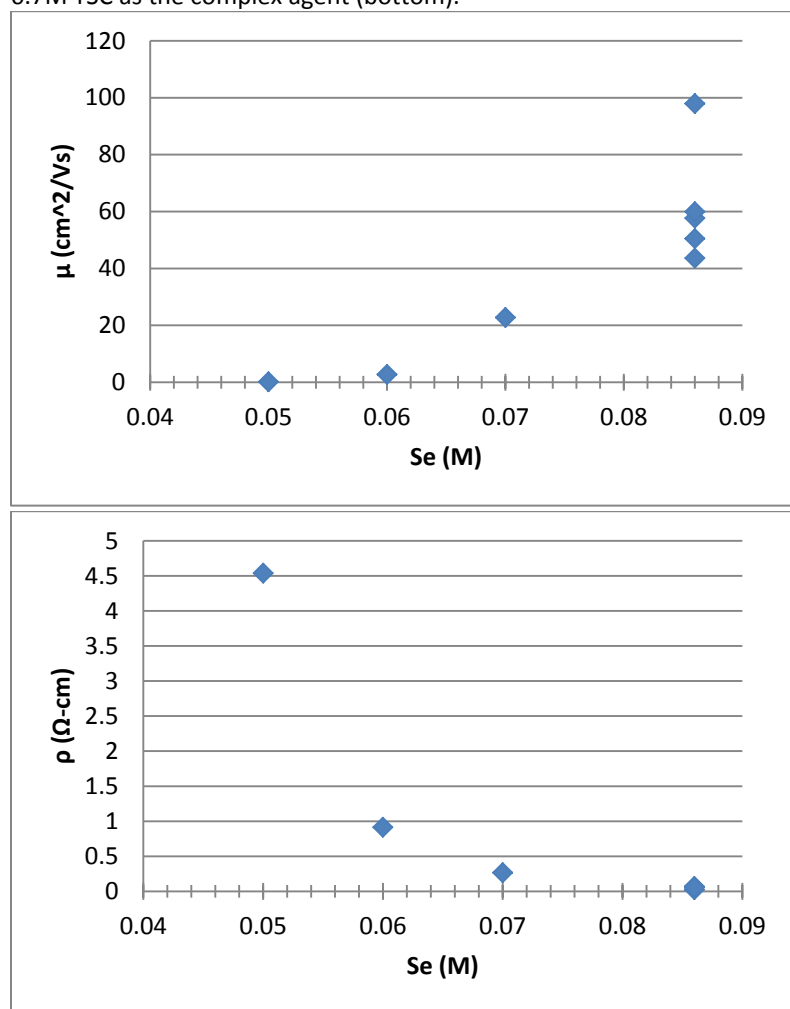
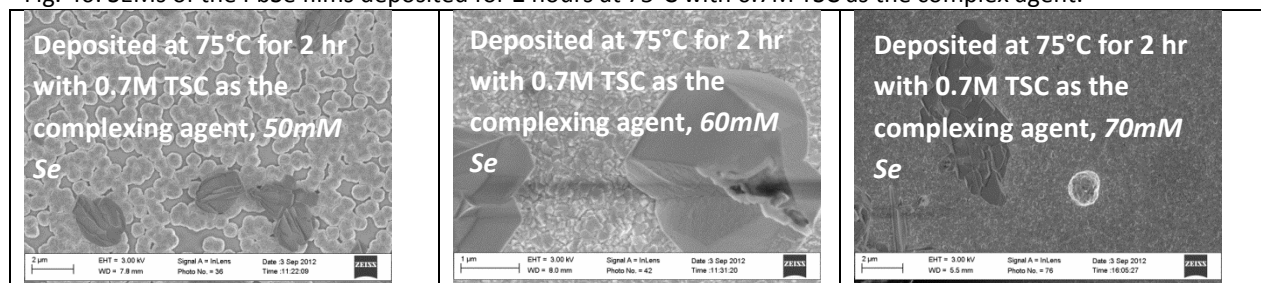


Fig. 46: SEMs of the PbSe films deposited for 2 hours at 75°C with 0.7M TSC as the complex agent.



5.1.2.4.2 2hr, 75°C, 0.75M TSC: Variation of Se

All PbSe thin films to be described in this section were deposited for 2 hours at 75°C with 0.75M TSC as the complexing agent. The final concentration of the Se in the deposition bath was varied from 50-86mM Se. Like in the previous case, conductivity is not achieved at 50mM Se. Again we see that as the concentration of Se is increased, the semiconductor conductivity increases (fig. 48). The hole mobility

also increases with an increase in the concentration of Se, though not dramatically (fig. 47). Again, the hole mobility decreases with an increase in the hole density. This is expected because as the hole density increases, the number of defects present in the PbSe thin film increases. This will cause scattering and decrease the mobility. Hole density remains fairly constant as the concentration of Se is varied.

From the SEMs below (fig. 49), we can see that bimodal growth has occurred under all conditions. As the concentration of Se increases, the nanocrystals become more developed. At 50mM Se, the nanocrystals are quite amorphous. They become more defined as the concentration of Se is increased. This is likely due to the fact that the number of Se^{2-} ions available is what controls the deposition rate. If more Se^{2-} ions are available, the deposition rate should be faster and we expect that the nanocrystals will be more developed. The increase in conductivity and hole mobility coincides with the increased development of the nanocrystals. This likely indicates that less scattering occurs at the boundaries between nanocrystals. Though the hole density remains fairly constant, all other trends follow that of those observed for the case of 0.7M TSC above.

Fig. 47: Hole mobility vs. concentration of Se for PbSe thin films deposited for 2 hours at 75°C with 0.75M TSC as the complex agent (top).

Fig. 48: Semiconductor resistivity vs. concentration of Se for PbSe thin films deposited for 2 hours at 75°C with 0.75M TSC as the complex agent (bottom).

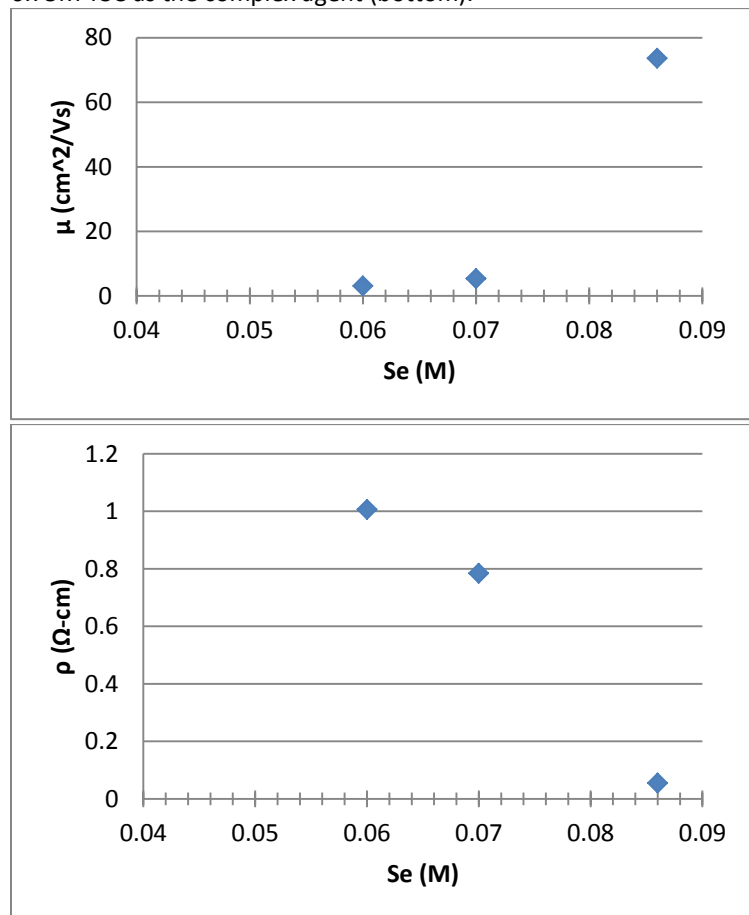
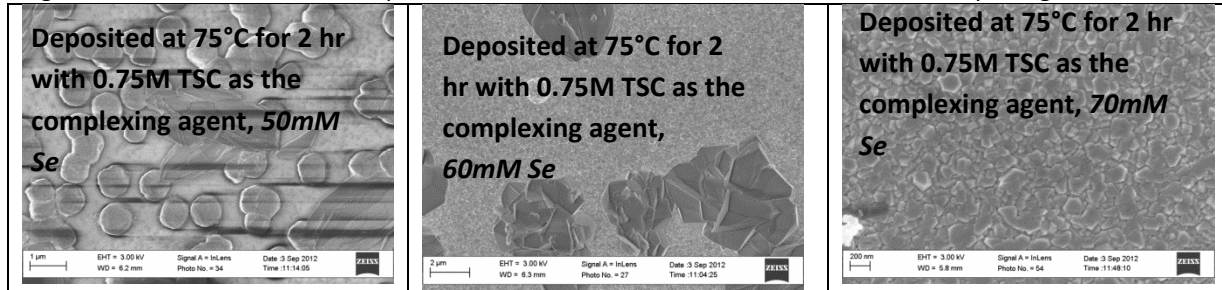


Fig. 49: SEMs of the PbSe films deposited for 2 hours at 75°C with 0.75M TSC as the complex agent.



5.1.2.5 Reproducibility

The average electrical properties and percent standard deviation were calculated for conditions at which at least 5 or more PbSe thin films were deposited (table 3). Clearly, there is a larger degree of distribution associated with these results. Some variation in electrical properties will always be present due to the nature of CBD. However, more controllable electrical properties are desired to allow for scalable technology.

Table 3: Average electrical properties, and the corresponding percent deviation, for conditions at which 5 or more PbSe thin films were deposited.

| Temp. (°C) | Time (hrs) | Se (M) | TSC (M) | ρ (Ω -cm) | % dev_ ρ | μ (cm^2/Vs) | % dev_ μ | p (cm^{-3}) | % dev_ p |
|------------|------------|--------|---------|------------------------|---------------|-----------------------------------|--------------|--------------------------|------------|
| 60 | 2.5 | 0.086 | 1 | 4.828 | 102.25 | 5.589 | 72.63 | 5.42E+17 | 15.93 |
| 60 | 3 | 0.086 | 1 | 3.126 | 119.89 | 9.782 | 109.14 | 1.78E+18 | 209.20 |
| 60 | 4 | 0.086 | 1 | 0.308 | 106.99 | 32.202 | 97.36 | 1.36E+18 | 17.94 |
| 60 | 5 | 0.086 | 1 | 0.123 | 60.66 | 57.643 | 19.28 | 1.08E+18 | 36.85 |
| 75 | 3 | 0.086 | 1 | 1.224 | 347.74 | 45.651 | 89.90 | 1.61E+18 | 55.56 |
| 75 | 2 | 0.086 | 0.7 | 0.054 | 32.80 | 61.916 | 34.14 | 2.11E+18 | 20.32 |

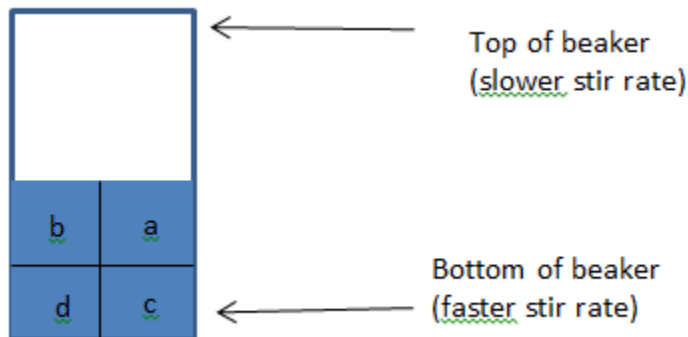


Fig. 50: Depiction of how samples were cut from PbSe thin films.

Additionally, many PbSe thin films were cut into four samples as described by figure 50. Each sample was measured and the electrical properties of each compared. For PbSe thin films where consistent measurement of the sign of the Hall coefficient was obtained for all four samples it was generally found that the percent standard deviation between the samples was below 35% for the semiconductor

resistivity and on average around 6% for the hole density. There is a great degree of distribution present for the hole mobility, likely due to the polycrystalline structure of the PbSe. The effect of stir rate due to the positioning of the glass substrate at an angle of about 45 degrees can be ruled out as playing a role in the variation of hole mobility since the stir rate does not have an effect on deposition [46].

For some PbSe thin films, consistent measurement of the sign of the Hall coefficient was obtained for some samples, but not for others. There is no consistent trend between which samples exhibit consistency or inconsistency of this measurement. One possibility is that the non-uniformity of the film

thickness is causing a false measurement of the sign of the Hall coefficient. This was observed in ZnO thin films [47]. This seems likely to be the case for many of the samples with inconsistent measurement of the sign since the magnitude of the Hall coefficient is not greatly changed. In other instances the Hall coefficient magnitude is erroneous, possibly due to a bad contact. Finally, as previously discussed low carrier densities near the intrinsic concentration may be causing the inconsistent measurement of the sign of the Hall coefficient.

5.2 PbSe-Si Heterojunction

5.2.1 Highly Doped p-type PbSe and Degenerately Doped n-type Si

P-type PbSe was deposited by chemical bath deposition as described in section 4.1.5 at 75°C for 3 hours with 1M TSC as the complexing agent and a final concentration of 86mM Se. The device geometry is described by the figure 16 in section 4.4.1. The average hole density of the PbSe thin film deposited at these conditions is $1.61 \times 10^{18} \text{ cm}^{-3}$ with a standard deviation of 56%. The average mobility is $46 \text{ cm}^2/\text{Vs}$ with a standard deviation of 90%.

A band diagram of the heterojunction was developed to facilitate understanding of the I-V characteristics. The Fermi level of a p-type semiconductor is given by

$$E_i - E_F = kT \ln \left(\frac{N_A}{n_i} \right) \quad (\text{Eq. 15})$$

where E_i is the intrinsic energy level, E_F is the Fermi level, k is the Boltzmann constant, T is the temperature, N_A is the number of acceptors assuming complete ionization and n_i is the intrinsic carrier density. For complete ionization

$$p \sim N_A \gg N_D$$

where p is the hole density and N_D is the number of donors. The Fermi level of PbSe for this set of conditions was estimated using equation 15 utilizing the knowledge that the band gap of PbSe is 0.27eV for bulk material and that the hole density is $1.61 \times 10^{18} \text{ cm}^{-3}$ at these conditions used to form heterojunction #165. Taking into account these assumptions, the Fermi level for the p-type PbSe is 0.03145eV, indicating that the doping is non-degenerate. The electron density of the n-type Si was looked up utilizing the known relationship between resistivity and electron density for monocrystalline Si at room temperature [47a]. Given a resistivity of $0.001 \Omega\text{-cm}$, the electron density for Si is $9 \times 10^{19} \text{ cm}^{-3}$. Doping above 10^{18} cm^{-3} is generally considering to be degenerately doped for Si. To verify this, the Fermi level was first calculated utilizing equation 15. The Fermi level comes to be 1.14eV for a band gap of 1.11eV and an intrinsic carrier density of $1.45 \times 10^{10} \text{ cm}^{-3}$. This verifies that the Si is degenerately doped, but does not give the correct position of the Fermi level since equation 15 does not hold true for degenerately doped semiconductors. The true Fermi level of the Si was then estimated using the Joyce-Dixon approximation

$$\frac{E_i - E_F}{kT} = \ln \left(\frac{n}{N_c} \right) + \sum_{m=1} \left[A_m \left(\frac{n}{N_c} \right)^m \right] \quad (\text{Eq. 16})$$

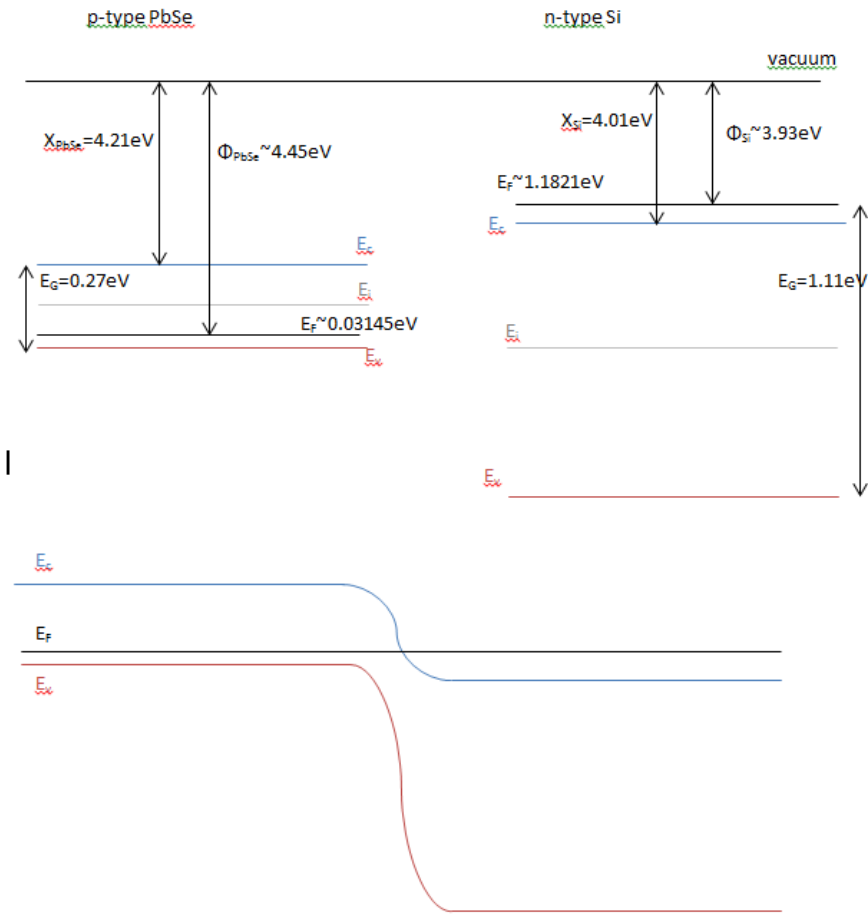
where the first four coefficients A_m are $A_1=0.353553$, $A_2=-4.95007 \times 10^{-3}$, $A_3=4.48386 \times 10^{-3}$, and $A_4=-4.42563 \times 10^{-6}$ for parabolic bands [48]. The Fermi level of the degenerately doped n-type Si was found to be approximately 1.1821eV. Utilizing the approximated positions of the Fermi levels, the band diagram of the PbSe-Si heterojunction was drawn to understand the degree of band bending that will be present in the heterojunction (fig. 52). The values of electron affinities were taken from the literature [49-51] and the work functions were calculated based on the estimated Fermi levels. The Anderson model was used to predict the band offsets [51a]. While this does seem to agree with the band diagram that the valence band offset will be larger than the conduction band offset, it should be noted that this model is usually inaccurate.

$$\Delta E_C = \chi_{\text{PbSe}} - \chi_{\text{Si}} = 0.2 \text{ eV} \quad (\text{Eq. 17})$$

$$\Delta E_V = E_{G_Si} - E_{G_PbSe} - \Delta E_C = 0.63eV \quad (\text{Eq. 18})$$

From the band diagram, we can see that under forward bias the holes in the valence band of PbSe will not be able to overcome the barrier in the depletion region to travel to the valence band of Si due to thermal excitation at room temperature. The same is true of the electrons in the conduction band in Si. Thus, under forward bias we do not expect any current. Under reverse bias, there is no barrier for the holes in the valence band of Si to overcome nor for the electrons in the conduction band of PbSe to overcome in order to travel across the depletion region. However, there are very few holes or electrons available to contribute to conduction in the valence band of Si and conduction band of PbSe, so we expect a small current under reverse bias. Lower doping in both materials is desirable to reduce the barrier in the depletion region to charge carriers.

Fig. 52: Band diagram of a heterojunction between highly doped p-type PbSe and degenerately doped n-type Si (not drawn to scale).



Two Au contacts were sputtered onto PbSe and Si separately to determine the nature of this contact on each semiconductor. Figure 55 below demonstrates that Au forms an Ohmic contact with PbSe due to the linear and symmetric I-V characteristics. Figure 56 demonstrates that Au forms a rectifying contact with the n-type Si due to its non-linear and asymmetric I-V characteristics. The ideality factor of this Schottky diode is 15.185 under forward bias. The forward bias current of a heterojunction is given by

$$I \propto \exp\left(\frac{qV_A}{\eta kT}\right) \quad (\text{Eq. 19})$$

where q is an elementary charge, V_A is the applied voltage, η is an ideality factor, k is the Boltzmann constant and T is the temperature [52]. By fitting a trend line to the exponential forward current, the ideality factor can be determined.

$$\frac{qV_A}{\eta kT} = cV_A \quad (\text{Eq. 20})$$

where c is a constant dependent on the fitted curve. Factoring out the applied voltage, V_A , from both terms and solving for the identity factor yields

$$\eta = \frac{q}{ckT} \quad (\text{Eq. 21})$$

where kT is 26meV at room temperature. Values of 1.3-2 and 4-5.5 have been obtained for pN PbSe-Si heterojunctions where p denotes the small band gap p-type semiconductor and N denotes the larger band gap n-type semiconductor. It should also be noted that breakdown and soft breakdown was observed in these works at 30V and 20V respectively [52].

The equation fitted to the data also suggests that the saturation current is $3 \times 10^{-6} \text{A}$ or $3 \mu\text{A}$ since the equation for an ideal diode is given by

$$I = I_0 \exp\left(\frac{qV_A}{\eta kT} - 1\right) \quad (\text{Eq. 22})$$

where I_0 is the saturation current, which reduces to the following in the case of a forward bias.

$$I = I_0 \exp\left(\frac{qV_A}{\eta kT}\right) \quad (\text{Eq. 23})$$

The I-V characteristics of the heterojunction were also measured and compared to that of the Au-Si-Au contact to determine whether a successful heterojunction was made between PbSe and Si. From figure 56, we can see that the Au-Si-Au contact configuration allows current to flow in two directions. Thus, the Au-Si-Au contact can be modeled as two diodes in series with one another, oriented in reverse directions as shown below where each Au contact forms a Schottky barrier with Si. If a heterojunction was not present between the PbSe and Si, we would expect current to flow only in one direction due to the presence of only one diode formed from the contact between Au and Si. From the I-V characteristics of the heterojunction, we can see that current is able to flow in two directions (fig. 57). Thus, a heterojunction between the PbSe and Si is present and can be modeled as a variable resistor in series with two diodes. The variable resistor represents the spread resistance contribution of the PbSe and Si layers, where the resistance due to the PbSe is much larger than the Si, a diode from the heterojunction between PbSe and Si, and a diode from the Au contact on Si. As was predicted by the band diagram, the reverse bias current is larger than the forward bias current. An exponential fit cannot be made to the forward bias current to estimate the ideality factor. Furthermore, it was determined that there was no photoresponse under approximately 1 sun illumination.

Fig. 53: Circuit model of Au-Si-Au contact.

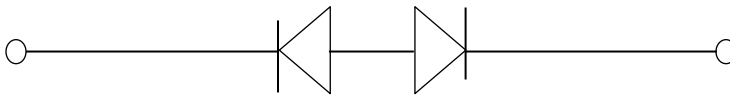


Fig. 54: Circuit model of heterojunction #165 (Au-PbSe-Si-Au).

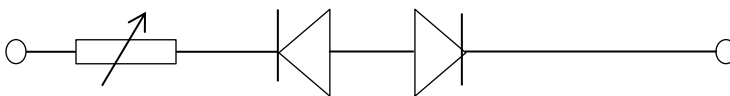
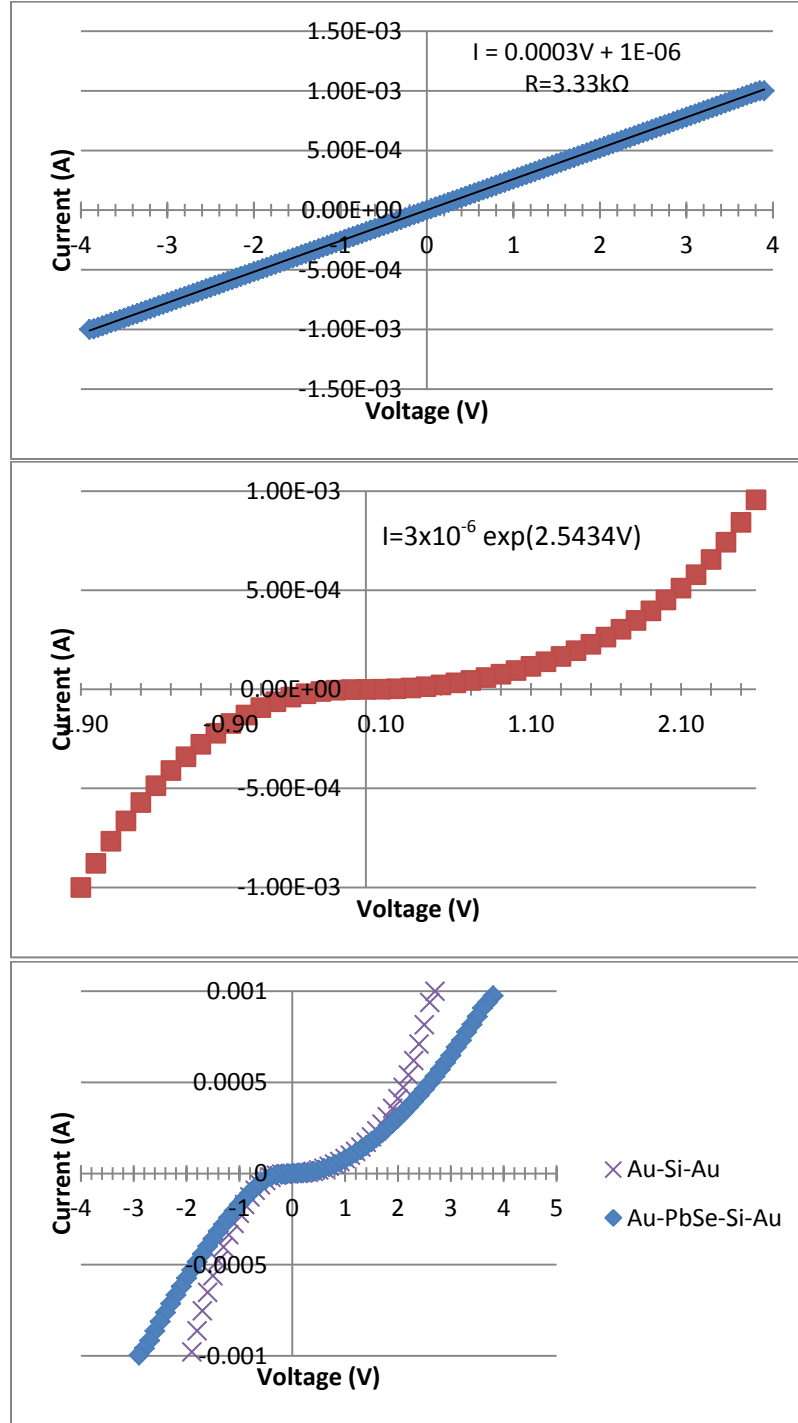


Fig. 55: I-V characteristics of Au-PbSe-Au (top).

Fig. 56: I-V characteristics of and Au-Si-Au (middle).

Fig. 57: Comparison of dark I-V characteristics of heterojunction #165 and the Au-Si-Au contact (bottom).

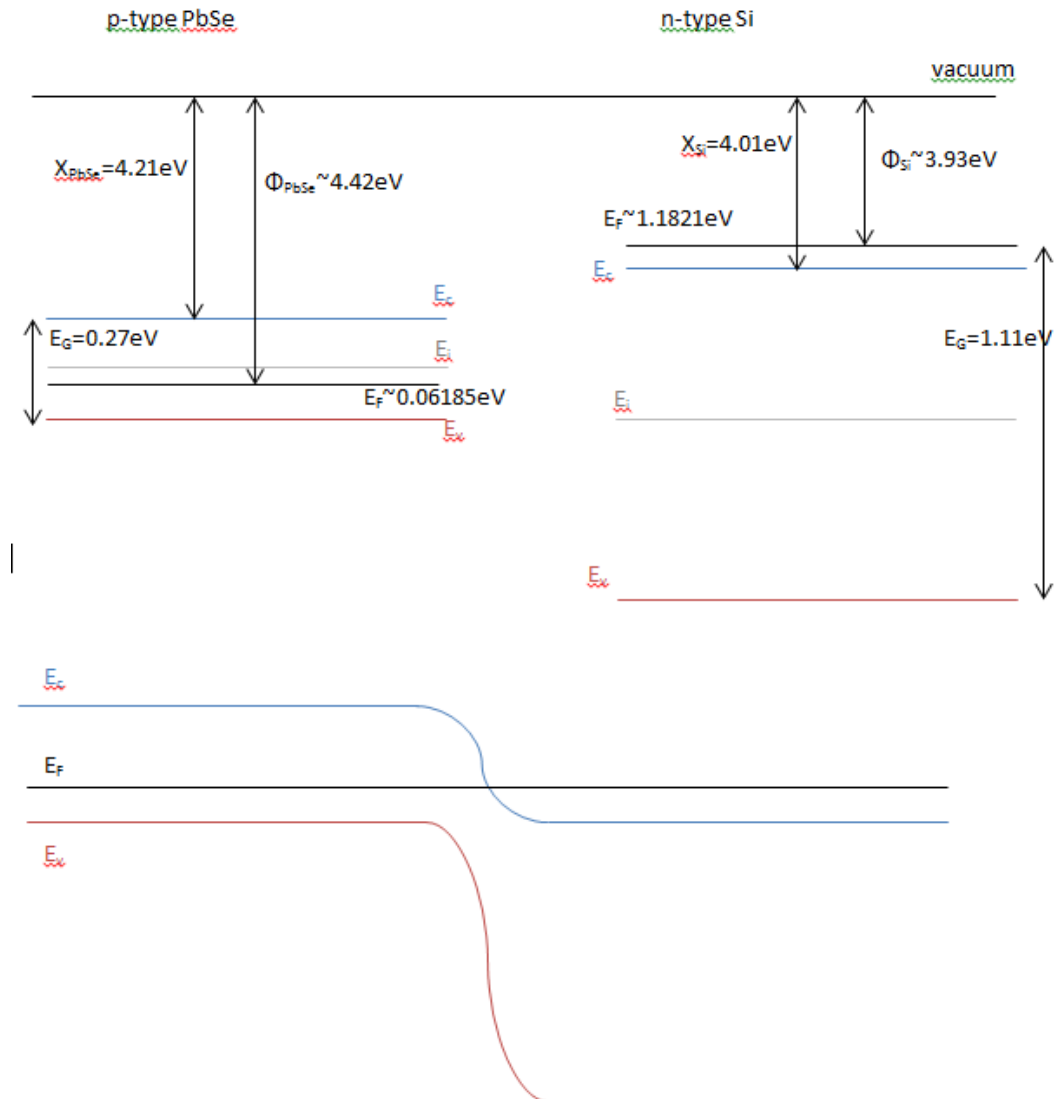


5.2.2 Lightly Doped p-type PbSe and Degenerately Doped n-type Si

P-type PbSe was deposited by chemical bath deposition onto degenerately doped n-type Si as described in section 4.1.5. The deposition was carried out at 60°C for 3 hours with 1M TSC as the complexing agent and a final concentration of 86mM Se. The device geometry is described by fig. 17 in section 4.4.1. For

the depositions carried out at 60°C for 3 hours the hole density ranges from 4.63×10^{17} to $1.91 \times 10^{19} \text{ cm}^{-3}$ and is on average $1.78 \times 10^{18} \text{ cm}^{-3}$, but there is a huge standard deviation of 209%. The hole mobility is on average $9.78 \text{ cm}^2/\text{Vs}$ with a standard deviation of 109%. The Fermi level of the p-type PbSe was calculated utilizing equation 15 and assuming the hole density to be $5 \times 10^{17} \text{ cm}^{-3}$; it was found to be 0.06185eV. Drawing a band diagram of the heterojunction with the lightly doped p-type PbSe reveals that the barrier to carriers to move across the depletion region is smaller than in the case of the highly doped PbSe (fig. 58). This is expected and should allow current to flow more easily in this heterojunction than in heterojunction #165 under reverse bias. Under forward bias, the barrier in the depletion region should still be too larger and restrict any current flow due to thermal excitation.

Fig. 58: Band diagram of a heterojunction between lightly doped p-type PbSe and degenerately doped n-type Si (not drawn to scale).

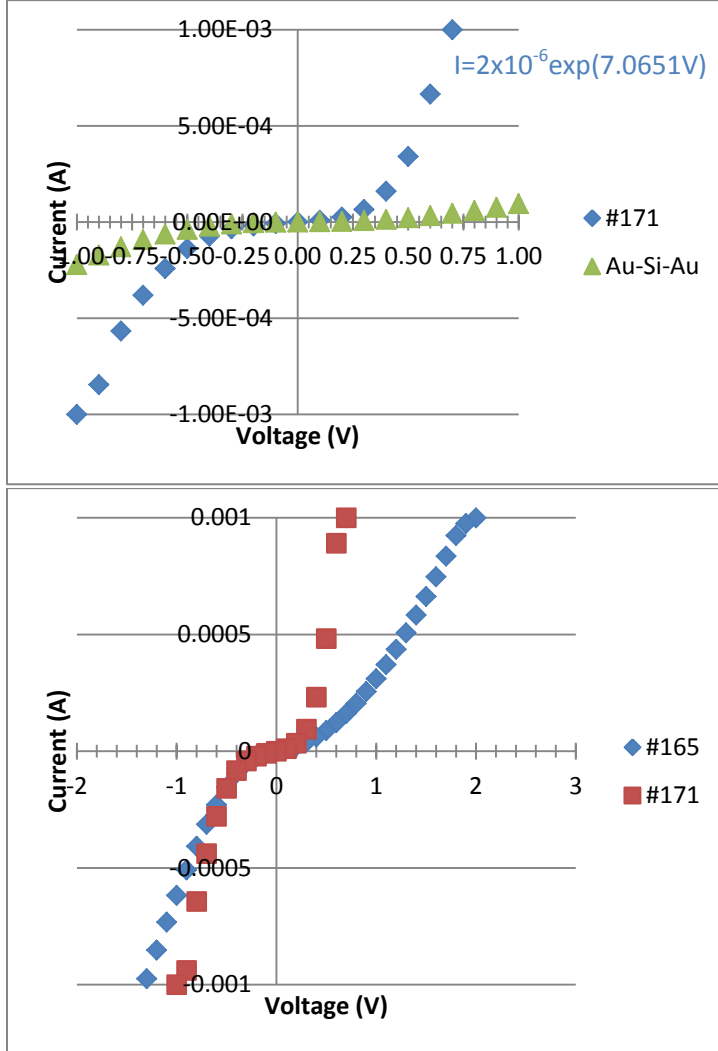


The I-V characteristics of heterojunction #171 show behavior of a diode (fig. 59). Since current is again flowing in two directions, we can conclude that there is a successful heterojunction between the PbSe and Si. The ideality factor of the forward bias current was calculated to be 5.44 by fitting the data below. This fit suggests a saturation current of $2 \mu\text{A}$, but with the presence of the Au-Si diode, it is impossible to tell what the saturation current truly is. By comparing the I-V of heterojunction #171 to #165, we see

that the #171 is much less resistive than #165, as expected. In the case of heterojunction #171, the forward bias current is larger than the reverse bias current. The dramatic increase in current flow for heterojunction #171 suggests that the more lightly doped PbSe dramatically decreased the built in voltage in the depletion region.

Fig. 59: Comparison of dark I-V characteristics of heterojunction #171 and the Au-Si-Au contact (top).

Fig. 60: Comparison of dark I-V characteristics of heterojunction #171 and #165 (bottom).



6. Conclusions

The goal of this work was to fabricate nanocrystalline PbSe thin films by chemical bath deposition, which have the potential to exhibit carrier multiplication and form a successful heterojunction with Si. Some, but not all, of these goals were achieved. Polycrystalline p-type PbSe thin films were successfully deposited by chemical bath deposition. All thin films were less than $1\mu\text{m}$ in thickness, a condition necessary for reducing the overall cost of a solar cell. The hole density of the p-type PbSe thin films can be reproducibly varied by altering the deposition conditions; hole densities between 4.28×10^{17} to $1.91 \times 10^{19} \text{ cm}^{-3}$ have been achieved. Additionally, the results suggest that for some PbSe thin films fabricated, both electrons and holes contribute to conduction. It has also been shown that bimodal

growth occurs as a result of two separate deposition mechanisms occurring simultaneously. Ion-by-ion growth produces microcrystals while hydroxide cluster growth produces nanocrystals. The bimodal growth can be greatly reduced and even eliminated by varying the concentration of the complexing agent, TSC, between 0.60 and 0.75M for 2 hours of deposition at 75°C with a final concentration of 86mM Se (with all other conditions constant as described in section 4.1.5). High mobility can be obtained provided that the nanocrystalline structure of the PbSe thin films is developed to the point where scattering at the boundaries between the nanocrystals is reduced and/or the development of defects reaches stability as deposition conditions are varied. In general this requires either longer deposition time or higher temperature. Photoconductivity measurements were not able to be conducted in this work. Finally, PbSe quantum dot size nanocrystals were not achieved at any of the deposition conditions in this work thereby excluding the potential for carrier multiplication.

A heterojunction between p-type PbSe and n-type Si was successfully fabricated. This heterojunction exhibits rectifying characteristics; the rectifying contact between the Si and Au makes it difficult to determine the exact characteristics of this heterojunction. Additionally, no photoresponse was observed for the heterojunctions produced in this work. This is of course a necessary condition for solar cell application.

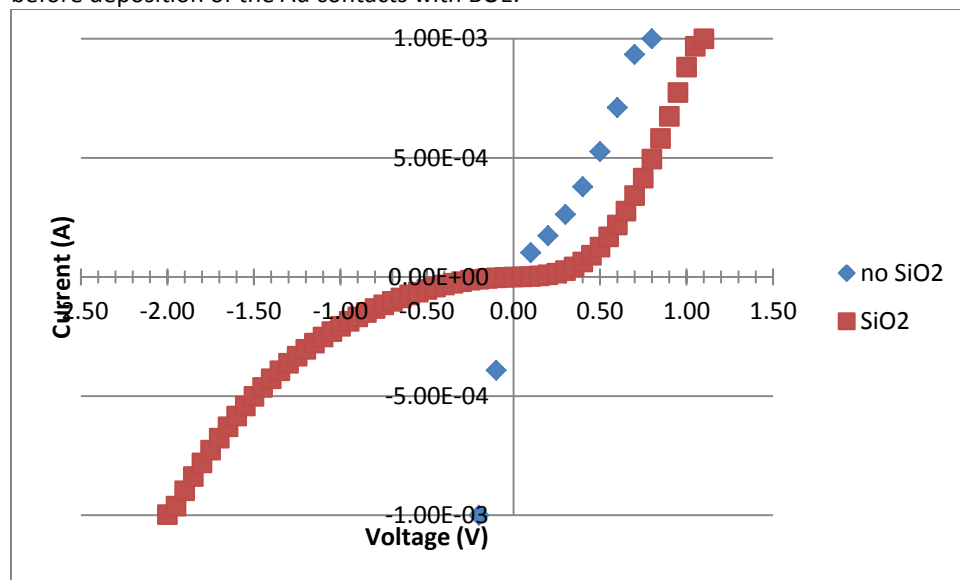
It can be concluded from this initial investigation that PbSe does have the potential to be incorporated into a thin film solar cell. While it is possible that the lower doping of the PbSe and Si may create a better heterojunction between PbSe and Si, it is the recommendation of this author that other chemical bath deposition procedures be investigated so that quantum dot size PbSe nanocrystals can be achieved and provide the potential of carrier multiplication.

7. Future Work

In order to realize the long term goals of this research, several recommendations can be made. Alternative procedures for chemical bath deposition of PbSe should be investigated to achieve quantum dot size nanocrystals. If carrier multiplication is to be realized within the heterojunction, PbSe quantum dots must first be produced. Also, an investigation of photoconductivity of the PbSe thin films should be conducted to help understand the recombination mechanisms in PbSe and why no photoreponse was exhibited by the PbSe-Si heterojunctions.

To improve the PbSe-Si heterojunction, several recommendations can be made. The n-type Si used in this work was degenerately doped. This contributed to a very large barrier for charge carriers to overcome within the depletion region. Investigation of a heterojunction between lightly doped PbSe and non-degenerately (and preferably lightly) doped n-type Si, should be conducted. Also, an effort should be made to generate an Ohmic contact with Si. The removal of the native oxide layer present on the Si will improve the situation (fig. 61). The native oxide layer (SiO₂) was removed from the degenerately doped n-type Si following the procedure described in section 4.1.2 immediately prior to deposition of the Au contacts by sputtering. The I-V characteristics of the metal-semiconductor contact were measured employing the procedure described in section 4.5. From the figure below we can see that the removal of the SiO₂ vastly improved the contact between the Au and Si. The I-V curve is more linear in forward and reverse bias. The I-V characteristics are not symmetric, in part due to the fact that the size of the contacts are not identical. Alternatively, other materials could be employed for the contact with Si. While Al is commonly used, TiSi₂ is more likely to form an Ohmic contact with Si and should be investigated [53].

Fig. 61: Comparison of the I-V characteristics of Au-Si-Au in which the native oxide layer was and wasn't removed before deposition of the Au contacts with BOE.



8. References

1. N. M. Gabor, Z. Zhong, K. Bosnick, J. Park, P. K. McEuen, *Science* 325, 2009, pp. 1367-1371.
2. R. Ellingson, M. C. Beard, J. C. Johnson, P. Yu, O. I. Micic, A. J. Nozik, A. Shabaev, A. L. Efros, *Nano Lett.* 5, 2005, pp. 865.
3. R. D. Schaller, V. I. Klimov, *Phys. Rev. Lett.* 92, 2004, pp. 1.
4. R. D. Schaller, M. Sykora, J. M. Pietryga, and V. I. Klimov, *Nano Letters*, 6, 2006, pp. 424-429.
5. S. Gorer, A. Albu-Yaron, G. Hodes, *J. Phys. Chem.* 99, 1995, pp. 16442-16448.
6. A. Bhardwaj, J. P. Kar, O.P. Thakur, P. Srivastava, H. K. Sehgal. *J. Nanoscience and Nanotechnology* 9, pp. 5953-5957, 2009.
7. A. Bhardwaj, V. R. Balakrishnam, P. Srivastava, H. K. Sehgal. *Semicond. Sci. Technol* 23, 2008, pp. 1-6.
8. Yu. I. Ravich, B. A. Efimova, I. A. Smirnov. *Semiconducting Lead Chalcogenides*. New York, Plenum Press, 1970.
9. K. S. Syed Alie, R. Saravanan, S. Israel, R. K. Rajaram. *Bull. Mater. Sci.* 29, 2006, pp. 107-114.
11. Collaboration: Authors and editors of the volumes III/17E-17F-41C: *Lead selenide (PbSe) energy gap and band structure*. Madelung, O., Rössler, U., Schulz, M. (ed.). SpringerMaterials - The Landolt-Börnstein Database (<http://www.springermaterials.com>). DOI: 10.1007/10681727_890
12. G. Căruntu, C. Panait, *IEEE International Workshop on Intelligent Data Acquisition and Advanced Computing Systems: Technology and Applications* 21-23 September 2009, Rende (Cosenza), Italy, pp. 323-326.
13. P.R. Norton, "Infrared Image Sensors", *Optical Engineering*, Nov. 1991.
14. H. Du, C. Chen, R. Krishan, T.D. Krauss, J.M. Harbold, F.W. Wise, M.G. Thomas, J. Silcox, *Nano Lett.* 2 (2002), pp. 1321.
15. J.M. Pietryga, R.D. Schaller, D. Weder, M.H. Stewart, V.I. Klimov, , J.A. Hollingsworth, *J. Am. Chem. Soc.* 126 (2004) 11752
16. EIA. "How much carbon dioxide (CO₂) is produced per kilowatt-hour when generating electricity with fossil fuels?," [Online]. Available: <http://www.eia.gov/tools/faqs/faq.cfm?id=74&t=11>
17. EIA. "Electric Power Monthly," [Online]. Available: <http://www.eia.gov/electricity/monthly/>

18. M. A. Green, K. Emery, Y. Hishikawa, W. Warta, E. Dunlop. *Prog. Photovolt: Res. Appl.* 20, 2012, pp. 12-20.
19. A. Bhardwaj, J. P. Kar, O.P. Thakur, P. Srivastava, H. K. Sehgal. *J. Nanoscience and Nanotechnology* 9, 2009, pp. 5953-5957
20. D. A. Kiewit. *Phys. Stat. Sol. (a)* 1, 1970, pp. 725-728.
21. U. M. Nayef. *Eng. & Technology* 25, no. 5, 2007, pp. 690-695
22. A. Bhardwaj, V. R. Balakrishnam, P. Srivastava, H. K. Sehgal. *Semicond. Sci. Technol.* 23 2008, pp. 1-6.
23. A. V. Shah, H. Schade, M. Vanecek, J. Meier, E. Vallat-Sauvain, N. Wyrsh, U. Kroll, C. Droz, J. Bailat. *Prog. Photovolt: Res. Appl.* 12, 2004, pp. 113-142.
24. P. Jayarama Reddy. *Solar Power Generation*. CRC Press: Boca Raton, 2012, section 2.8.
25. A. Kolodziej, *Opto-Electronics Review* 12 (1), 2004, pp. 21-32.
26. M. A. Green, K. Emery, Y. Hishikawa, W. Warta, E. Dunlop. *Prog. Photovolt: Res. Appl.* 20, 2012, pp. 12-20.
27. P. Jayarama Reddy. *Solar Power Generation*. CRC Press: Boca Raton, 2012, section 3.4.
28. T. L. Chu, S. S. Chu, C. Ferekides, C. Q. Wu, J. Britt et al. *J. Appl. Phys.* 70 (12), 1991, pp. 7608-7612.
29. G. Hodes. *Chemical Solution Deposition of Semiconductor Films*. CRC Press, 2002, chapter 9.
31. I. Repins, M. A. Contreras, B. Egass, C. DeHart, J. Scharf, C. L. Perkins, B. To, R. Noufi. *Prog. Photovolt: Res. Appl.* 16, 2008, pp. 235-239.
32. P. Jayarama Reddy. *Solar Power Generation*. CRC Press: Boca Raton, 2012, section 3.3.
33. I. Grozdanov, M. Najdoski, S. K. Dey. *Material Letters* 38 1999, pp. 28-32.
34. G. Hodes. *Chemical Solution Deposition of Semiconductor Films*. CRC Press, 2002.
35. G. Hodes. *Chemical Solution Deposition of Semiconductor Films*. CRC Press, 2002, section 1.1.3.
36. G. Hodes. *Chemical Solution Deposition of Semiconductor Films*. CRC Press, 2002, section 2.6.1, 3.3.1.
37. G. Hodes. *Chemical Solution Deposition of Semiconductor Films*. CRC Press, 2002, Section 2.6.2, 3.3.2.
38. P.P. Hankare et. al. *Materials Chemistry and Physics*, 82, 2003, pp. 505-508.
39. G. Hodes. *Chemical Solution Deposition of Semiconductor Films*. CRC Press, 2002, Section 3.2.2.1
40. G. Hodes. *Chemical Solution Deposition of Semiconductor Films*. CRC Press, 2002.
41. G. Hodes. *Chemical Solution Deposition of Semiconductor Films*. CRC Press, 2002, Section 1.2.
42. G. Hodes. *Chemical Solution Deposition of Semiconductor Films*. CRC Press, 2002, Section 3.2.2.4.
44. D. K. Schroder. *Semiconductor Material and Device Characterization*. John Wiley & Sons, Inc.: New York, 1998, chapter 1, section 1.2.2
45. "Van der Pauw method," [Online]. Available: http://en.wikipedia.org/wiki/Van_der_Pauw_method
- 45a. E. D. Palik. *Handbook of Optical Constants*, San Diego: Academic Press, 1998, pg 520-521.
46. G. Hodes. *Chemical Solution Deposition of Semiconductor Films*. CRC Press, 2002, Section 3.7.
47. T. Ohgaki, N. Ohashi, S. Sugimura, H. Ryoken, I. Sakaguchi, Y. Adachi, H. Haneda. *J. Mater. Res.*, 23, 2008, pp. 2293-2295.
- 47a. B. J. Van Zeghbroeck, (1996, 1997) "2.9.2 Resistivity" [Online]. Available: <http://ecee.colorado.edu/~bart/book/mobility.htm#resistivity>
48. H. Kroemer. *J. Appl. Phys.* 52, 1981, pp. 873-876.
49. G. Bi, F. Zhao, J. Ma, S. Mukerjee, D. Li, Z. Shi. *PIERS ONLINE* 5, 2009, pp. 61-64.
50. B. L. Sharma, R. K. Puohit. *Semiconductor Heterojunctions*. Pergamon Press: Oxford, 1974, Ch 2, pg. 24.
51. A. G. Milnes, D. L. Feucht. *Heterojunctions and Metal-Semiconductor Heterojunctions*. Academic Press: New York, 1972, section 1.3, pg.8.
- 51a. A. G. Milnes, D. L. Feucht. *Heterojunctions and Metal-Semiconductor Heterojunctions*. Academic Press: New York, 1972, Ch. 2, section 2.1, pg.24.

52. B. L. Sharma, R. K. Purohit. *Semiconductor Heterojunctions*. Pergamon Press: Oxford, 1974, Ch. 5, section, 5.2.1 pg. 87-95.
53. R. F. Pierret. *Semiconductor Device Fundamentals*. Bangladesh, India, Pearson, 1996, Ch. 14, section 14.3.2, pp. 498-501.

Table I: Average electrical properties of consistently measured p-type PbSe thin films. Boxes highlighted in red indicate no conductivity. Boxes highlighted in yellow indicate an inconsistent measurement of the sign of the Hall coefficient.

| Sample # | Date Deposited | Date Measured | Time (hrs) | Temp. (°C) | TSC_i (M) | Se_f (M) | Optical Thickness (μm) | ρ (Ω-cm) | μ (cm ² /Vs) | p (cm ⁻³) | RH (cm ³ /C) |
|----------|----------------|---------------|------------|------------|-----------|----------|------------------------|---------------|-----------------------------|-----------------------|-------------------------|
| i | 5/11/12 | 5/11/12 | 2 | 60 | 1 | 0.086 | 0.601 | 90.880 | 0.563 | 2.12E+17 | 51.179 |
| ii | 5/11/12 | 5/11/12 | 2.5 | 60 | 1 | 0.086 | 0.752 | 14.063 | 1.044 | 4.28E+17 | 14.670 |
| iii | 5/23/12 | 5/23/12 | 2 | 60 | 1 | 0.086 | 0.63 | | | | |
| iv | 5/23/12 | 5/23/12 | 2.5 | 60 | 1 | 0.086 | 0.696 | | | | |
| v | 5/23/12 | 5/23/12 | 5 | 60 | 1 | 0.086 | 1.18 | 0.097 | 64.533 | 9.93E+17 | 6.285 |
| vi | 6/4/12 | 6/5/12 | 3 | 60 | 1 | 0.086 | 0.716 | 1.360 | 9.209 | 4.98E+17 | 12.527 |
| vii | 6/4/12 | 6/5/12 | 4 | 60 | 1 | 0.086 | 0.783 | 0.540 | 10.033 | 1.19E+18 | 5.420 |
| viii | 6/4/12 | 6/5/12 | 5 | 60 | 1 | 0.086 | 0.788 | 0.113 | 51.593 | 1.07E+18 | 5.855 |
| ix | 6/8/12 | 6/8/12 | 2.5 | 60 | 1 | 0.086 | 0.517 | 5.837 | 1.907 | 5.79E+17 | 11.131 |
| x | 6/11/12 | 6/12/12 | 2.5 | 60 | 1 | 0.086 | 0.468 | | | | |
| xi | 6/11/12 | 6/12/12 | 2.5 | 60 | 1 | 0.086 | 0.452 | 8.300 | 1.367 | 5.68E+17 | 11.033 |
| xii | 6/11/12 | 6/12/12 | 2.5 | 60 | 1 | 0.086 | 0.471 | | | | |
| xiii | 6/18/12 | 6/18/12 | 2.5 | 60 | 1 | 0.086 | NA | | | | |
| 1 | 6/8/12 | 6/8/12 | 2.5 | 60 | 1 | 0.086 | 0.595 | 8.516 | 2.584 | 3.77E+17 | 16.812 |
| 2 | 6/8/12 | 6/8/12 | 2.5 | 60 | 1 | 0.086 | 0.547 | 2.599 | 5.262 | 3.49E+17 | 17.895 |
| 3 | 6/13/12 | 6/13/12 | 2.5 | 60 | 1 | 0.086 | 0.582 | 1.552 | 8.066 | 4.99E+17 | 12.520 |
| 4 | 6/13/12 | 6/13/12 | 2.5 | 60 | 1 | 0.086 | 0.547 | 0.886 | 10.433 | 6.76E+17 | 9.239 |
| 5 | 6/18/12 | 6/18/12 | 2.5 | 60 | 1 | 0.086 | 0.63 | 2.048 | 6.725 | 4.54E+17 | 13.771 |
| 6 | 6/19/12 | 6/20/12 | 2.5 | 60 | 1 | 0.086 | 0.569 | 1.108 | 9.584 | 5.88E+17 | 10.620 |
| 7 | 6/19/12 | 6/20/12 | 5 | 60 | 1 | 0.086 | 0.712 | 0.055 | 66.677 | 1.71E+18 | 3.673 |
| 8 | 6/20/12 | 6/21/12 | 3 | 60 | 1 | 0.086 | 0.64 | 0.293 | 21.990 | 9.68E+17 | 6.450 |
| 9 | 6/20/12 | 6/21/12 | 4 | 60 | 1 | 0.086 | 0.737 | 0.075 | 54.370 | 1.54E+18 | 4.072 |
| 10 | 6/26/12 | 6/27/12 | 0.5 | 60 | 1 | 0.086 | 0.329 | | | | |
| 11 | 6/26/12 | 6/27/12 | 3 | 60 | 1 | 0.086 | 0.562 | | | | |
| 12 | 6/26/12 | 6/27/12 | 4 | 60 | 1 | 0.086 | 0.565 | 1.690 | 7.658 | 6.32E+17 | 12.920 |

| | | | | | | | | | | | |
|----|---------|---------|-----|----|-----|-------|-------|-------|--------|----------|--------|
| 13 | 6/26/12 | 6/27/12 | 5 | 60 | 1 | 0.086 | 0.569 | 0.528 | 15.103 | 7.84E+17 | 7.970 |
| 14 | 7/4/12 | 7/4/12 | 0.5 | 60 | 1 | 0.086 | 0.321 | | | | |
| 15 | 7/4/12 | 7/4/12 | 1 | 60 | 1 | 0.086 | 0.57 | | | | |
| 16 | 7/4/12 | 7/4/12 | 2 | 60 | 1 | 0.086 | 0.449 | | | | |
| 17 | 7/4/12 | 7/4/12 | 3 | 60 | 1 | 0.086 | 0.632 | 4.517 | 3.919 | 3.53E+17 | 17.701 |
| 18 | 7/4/12 | 7/4/12 | 4 | 60 | 1 | 0.086 | 0.556 | 1.008 | 15.213 | 4.08E+17 | 15.328 |
| 19 | 7/4/12 | 7/4/12 | 5 | 60 | 1 | 0.086 | 0.607 | 0.250 | 40.880 | 6.11E+17 | 10.221 |
| 20 | 7/23/12 | 7/24/12 | 4 | 60 | 1 | 0.086 | 0.486 | 0.345 | 16.053 | 1.13E+18 | 5.534 |
| 21 | 7/24/12 | 7/24/12 | 1 | 65 | 1 | 0.086 | 0.582 | | | | |
| 22 | 7/24/12 | 7/24/12 | 2 | 65 | 1 | 0.086 | 0.404 | 2.830 | 2.536 | 3.18E+17 | 2.176 |
| 23 | 7/24/12 | 7/24/12 | 3 | 65 | 1 | 0.086 | NA | 0.472 | 10.893 | 1.20E+18 | 5.219 |
| 24 | 7/26/12 | 7/26/12 | 1 | 70 | 1 | 0.086 | 0.882 | | | | |
| 25 | 7/26/12 | 7/26/12 | 2 | 70 | 1 | 0.086 | 0.951 | 0.424 | 17.857 | 8.27E+17 | 7.581 |
| 26 | 7/26/12 | 7/26/12 | 3 | 70 | 1 | 0.086 | 0.445 | 0.063 | 30.040 | 3.32E+18 | 1.881 |
| 27 | 7/27/12 | 7/27/12 | 0.5 | 75 | 1 | 0.086 | 0.153 | | | | |
| 28 | 7/27/12 | 7/27/12 | 1 | 75 | 1 | 0.086 | 0.184 | 0.956 | 2.799 | 2.34E+18 | 2.675 |
| 29 | 7/27/12 | 7/27/12 | 2 | 75 | 1 | 0.086 | 0.154 | 0.018 | 70.623 | 4.96E+18 | 1.260 |
| 30 | 7/27/12 | 7/27/12 | 3 | 75 | 1 | 0.086 | 0.261 | 0.018 | 71.430 | 4.99E+18 | 1.252 |
| 31 | 7/31/12 | 7/31/12 | 1 | 85 | 1 | 0.086 | 0.67 | 0.161 | 39.337 | 9.88E+17 | 6.345 |
| 32 | 8/1/12 | 8/1/12 | 1 | 80 | 1 | 0.086 | 0.61 | 0.166 | 29.130 | 1.29E+18 | 4.844 |
| 33 | 8/1/12 | 8/1/12 | 2 | 80 | 1 | 0.086 | 2.47 | 0.227 | 72.487 | 3.79E+17 | 16.490 |
| 34 | 8/1/12 | 8/1/12 | 3 | 80 | 1 | 0.086 | 2.19 | 0.128 | 92.270 | 5.33E+17 | 11.767 |
| 35 | 8/15/12 | 8/16/12 | 1 | 60 | 1 | 0.05 | 0.46 | | | | |
| 36 | 8/15/12 | 8/16/12 | 2 | 60 | 1 | 0.05 | 0.86 | | | | |
| 37 | 8/15/12 | 8/16/12 | 3 | 60 | 1 | 0.05 | 0.47 | 0.081 | 44.373 | 1.74E+18 | 3.597 |
| 38 | 8/15/12 | 8/16/12 | 2 | 75 | 0.8 | 0.086 | 0.44 | | | | |
| 39 | 8/15/12 | 8/16/12 | 2 | 75 | 0.6 | 0.086 | 0.88 | 0.090 | 37.173 | 1.88E+18 | 3.342 |
| 40 | 8/19/12 | 8/20/12 | 2 | 75 | 1.2 | 0.086 | 0.644 | 0.133 | 50.080 | 9.37E+17 | 6.663 |
| 41 | 8/19/12 | 8/20/12 | 2 | 75 | 1.4 | 0.086 | 0.705 | 0.095 | 58.290 | 1.12E+18 | 5.553 |
| 42 | 8/19/12 | 8/20/12 | 2 | 75 | 1.6 | 0.086 | 0.611 | 0.148 | 36.790 | 1.14E+18 | 5.459 |

| | | | | | | | | | | | |
|----|---------|---------|-----|----|------|-------|-------|-------|--------|----------|-------|
| 43 | 8/15/12 | 8/16/12 | 2 | 75 | 0.4 | 0.086 | < 0.5 | | | | |
| 44 | 8/21/12 | 8/22/12 | 2 | 75 | 0.55 | 0.086 | < 0.6 | | | | |
| 45 | 8/21/12 | 8/22/12 | 2 | 75 | 0.65 | 0.086 | 0.537 | 0.043 | 49.380 | 2.95E+18 | 2.119 |
| 46 | 8/21/12 | 8/22/12 | 2 | 75 | 0.7 | 0.086 | 0.688 | 0.023 | 97.940 | 2.73E+18 | 2.290 |
| 47 | 8/21/12 | 8/22/12 | 2 | 75 | 0.75 | 0.086 | 0.737 | 0.054 | 73.630 | 1.56E+18 | 4.001 |
| 48 | 8/24/12 | 8/24/12 | 1.5 | 75 | 0.7 | 0.086 | * | | | | |
| 49 | 8/24/12 | 8/24/12 | 2.5 | 75 | 0.7 | 0.086 | * | | | | |
| 50 | 8/24/12 | 8/24/12 | 1.5 | 75 | 0.75 | 0.086 | * | | | | |
| 51 | 8/24/12 | 8/24/12 | 2.5 | 75 | 0.75 | 0.086 | * | | | | |
| 52 | 8/27/12 | 8/28/12 | 2 | 75 | 0.7 | 0.05 | 0.434 | 4.539 | 0.152 | 9.04E+18 | 0.690 |
| 53 | 8/27/12 | 8/28/12 | 2 | 75 | 0.7 | 0.06 | 0.418 | 0.914 | 2.749 | 2.48E+18 | 2.513 |
| 54 | 8/27/12 | 8/28/12 | 2 | 75 | 0.7 | 0.07 | 0.514 | 0.266 | 22.750 | 1.03E+18 | 6.053 |
| 55 | 8/28/12 | 8/28/12 | 2 | 75 | 0.75 | 0.05 | 0.26 | | | | |
| 56 | 8/28/12 | 8/28/12 | 2 | 75 | 0.75 | 0.06 | 0.573 | 1.006 | 3.075 | 2.02E+18 | 3.093 |
| 57 | 8/28/12 | 8/28/12 | 2 | 75 | 0.75 | 0.07 | 0.337 | 0.784 | 5.322 | 1.50E+18 | 4.172 |
| 58 | 8/31/12 | 8/31/12 | 2 | 70 | 0.7 | 0.06 | 0.414 | 1.315 | 4.031 | 1.18E+18 | 5.301 |
| 59 | 8/31/12 | 8/31/12 | 2 | 70 | 0.75 | 0.07 | 0.416 | 2.607 | 1.650 | 1.45E+18 | 4.303 |
| 60 | 9/2/12 | 9/3/12 | 2 | 80 | 0.7 | 0.06 | 0.502 | 0.529 | 8.427 | 1.40E+18 | 4.455 |
| 61 | 9/2/12 | 9/3/12 | 2 | 80 | 0.75 | 0.07 | 0.504 | 0.484 | 5.138 | 2.51E+18 | 2.489 |
| 62 | 9/4/12 | 9/4/12 | 2 | 75 | 1.4 | 0.07 | 0.539 | 0.358 | 16.910 | 1.03E+18 | 6.052 |
| 63 | 9/6/12 | 9/6/12 | 3 | 60 | 1 | 0.086 | * | | | | |
| 64 | 9/6/12 | 9/6/12 | 2 | 60 | 1 | 0.086 | * | | | | |
| 65 | 9/6/12 | 9/6/12 | 1 | 60 | 1 | 0.086 | * | | | | |
| 67 | 9/7/12 | 9/7/12 | 2 | 75 | 1 | 0.086 | * | | | | |
| 68 | 9/12/12 | 9/12/12 | 2 | 75 | 0.7 | 0.086 | 0.645 | 0.063 | 57.690 | 1.71E+18 | 3.652 |
| 69 | 9/12/12 | 9/12/12 | 2 | 75 | 0.7 | 0.086 | 0.731 | 0.068 | 50.450 | 1.83E+18 | 3.412 |
| 70 | 9/12/12 | 9/12/12 | 2 | 75 | 0.7 | 0.086 | 0.622 | 0.061 | 43.583 | 2.38E+18 | 2.642 |
| 71 | 9/12/12 | 9/12/12 | 2 | 75 | 0.7 | 0.086 | 0.733 | 0.055 | 59.917 | 1.90E+18 | 3.301 |
| 72 | 9/19/12 | 9/19/12 | 2 | 70 | 0.7 | 0.086 | 0.741 | 0.863 | 3.317 | 2.55E+18 | 3.457 |
| 73 | 9/19/12 | 9/19/12 | 2 | 70 | 0.75 | 0.086 | 0.592 | 0.080 | 46.130 | 1.70E+18 | 3.684 |

| | | | | | | | | | | | |
|-------|----------|----------|-----|----|------|-------|----------|--------|---------|----------|--------|
| 74 | 9/19/12 | 9/19/12 | 2 | 80 | 0.7 | 0.086 | 0.648 | 0.061 | 62.880 | 1.63E+18 | 3.856 |
| 75 | 9/19/12 | 9/19/12 | 2 | 80 | 0.75 | 0.086 | 0.565 | 0.043 | 69.460 | 2.08E+18 | 3.018 |
| 76 | 9/23/12 | 9/24/12 | 2.5 | 80 | 0.75 | 0.086 | 1.03 | 0.056 | 66.487 | 1.67E+18 | 3.750 |
| 77 | 9/23/12 | 9/24/12 | 3 | 80 | 0.75 | 0.086 | 1.29 | 0.075 | 60.983 | 1.37E+18 | 4.581 |
| 78 | 9/23/12 | 9/24/12 | 3.5 | 80 | 0.75 | 0.086 | 0.573 | 0.072 | 46.893 | 1.86E+18 | 3.359 |
| 79 | 9/24/12 | 9/25/12 | 1 | 75 | 1 | 0.086 | 0.623 | 1.638 | 3.037 | 1.26E+18 | 4.973 |
| 80 | 9/24/12 | 9/25/12 | 2 | 75 | 1 | 0.086 | 0.793 | 0.085 | 46.797 | 1.57E+18 | 3.984 |
| 81 | 9/24/12 | 9/25/12 | 3 | 75 | 1 | 0.086 | 1.41 | 0.136 | 60.923 | 7.52E+17 | 8.311 |
| 82 | 9/25/12 | 9/26/12 | 1 | 80 | 1 | 0.086 | 0.752 | 0.539 | 7.336 | 1.58E+18 | 3.951 |
| 83 | 9/25/12 | 9/26/12 | 2 | 80 | 1 | 0.086 | 0.928 | 0.104 | 42.633 | 1.41E+18 | 4.445 |
| 84 | 9/25/12 | 9/26/12 | 3 | 80 | 1 | 0.086 | 1.14 | 0.074 | 56.713 | 1.50E+18 | 4.182 |
| 85 | 9/30/12 | 9/30/12 | 4 | 75 | 1 | 0.086 | 0.982 | 0.185 | 46.720 | 7.47E+17 | 8.636 |
| 86 | 10/1/12 | 10/1/12 | 1 | 85 | 1 | 0.086 | 0.782 | 0.175 | 28.150 | 1.27E+18 | 4.928 |
| 87 | 10/1/12 | 10/1/12 | 2 | 85 | 1 | 0.086 | 0.805 | 0.098 | 48.750 | 1.31E+18 | 4.766 |
| 88 | 10/1/12 | 10/1/12 | 3 | 85 | 1 | 0.086 | 1.84 | 0.098 | 95.353 | 6.72E+17 | 9.319 |
| 89 | 10/2/03 | 10/3/12 | 20 | 25 | 1 | 0.05 | 0.161 | | | | |
| 90 | 10/3/12 | 10/4/12 | 3 | 75 | 1 | 0.086 | 0.748 | 0.012 | 246.767 | 1.56E+18 | 2.868 |
| 91 | 10/3/12 | 10/4/12 | 3 | 75 | 1 | 0.086 | 0.6 | 0.048 | 39.780 | 3.29E+18 | 1.926 |
| 92 | 10/3/12 | 10/4/12 | 3 | 75 | 1 | 0.086 | 0.65 | 0.080 | 36.823 | 2.13E+18 | 2.933 |
| 93 | 10/10/12 | 10/11/12 | 1 | 70 | 1 | 0.086 | 0.59 | | | | |
| 94 | 10/10/12 | 10/11/12 | 2 | 70 | 1 | 0.086 | 0.762 | 0.216 | 26.727 | 1.08E+18 | 5.775 |
| 95 | 10/10/12 | 10/11/12 | 3 | 70 | 1 | 0.086 | 0.702 | 0.096 | 32.593 | 1.99E+18 | 3.138 |
| 96 | 10/17/12 | 10/17/12 | 3 | 75 | 1 | 0.086 | 0.711 | 0.066 | 50.720 | 1.87E+18 | 3.359 |
| 99 | 11/5/12 | 11/29/12 | 3 | 75 | 1 | 0.086 | 0.689 | 0.055 | 50.520 | 2.24E+18 | 2.785 |
| 98 | 11/5/12 | 12/3/12 | 3 | 75 | 1 | 0.086 | NA | | | | |
| 100 | 11/5/12 | 12/3/12 | 3 | 75 | 1 | 0.086 | 0.926447 | 0.130 | 58.740 | 8.99E+17 | 7.610 |
| 101 | 11/18/12 | 12/3/12 | 3 | 75 | 1 | 0.086 | NA | | | | |
| 102 | 11/18/12 | 12/3/12 | 3 | 75 | 1 | 0.086 | 0.606633 | 0.273 | 9.654 | 2.67E+18 | 2.639 |
| 103 | 11/18/12 | 12/3/12 | 3 | 75 | 1 | 0.086 | 0.434768 | 0.089 | 36.467 | 1.91E+18 | 3.261 |
| 104-1 | 12/4/12 | 12/4/12 | 2.5 | 60 | 1 | 0.086 | 0.564 | 70.697 | 0.530 | 1.96E+17 | 37.600 |

| | | | | | | | | | | | |
|-------|----------|----------|-------|----|---|-------|-------|-----------|--------|----------|-------------|
| 104-2 | 12/4/12 | 12/4/12 | 2.5 | 60 | 1 | 0.086 | 0.564 | 115.200 | 2.878 | 2.35E+16 | 333.167 |
| 105 | 12/4/12 | 12/4/12 | 2.5 | 60 | 1 | 0.086 | 0.676 | | | | |
| 106 | 12/4/12 | 12/4/12 | 2.5 | 60 | 1 | 0.086 | 0.531 | | | | |
| 107 | 12/5/12 | 12/5/12 | 2.5 | 55 | 1 | 0.086 | 0.396 | | | | |
| 108 | 12/6/12 | 12/6/12 | 2.5 | 50 | 1 | 0.086 | 0.281 | | | | |
| 109 | 12/7/12 | 12/7/12 | 2.5 | 45 | 1 | 0.086 | 0.135 | | | | |
| 110 | 12/10/12 | 12/10/12 | 2.5 | 60 | 1 | 0.086 | 0.558 | 29.060 | 0.619 | 3.57E+17 | 17.970 |
| 111 | 12/10/12 | 12/10/12 | 2.33 | 60 | 1 | 0.086 | 0.532 | | | | |
| 112 | 12/10/12 | 12/10/12 | 2.167 | 60 | 1 | 0.086 | 0.418 | 158.133 | 0.170 | 6.24E+17 | 26.664 |
| 113 | 12/10/12 | 12/10/12 | 2 | 60 | 1 | 0.086 | 0.543 | | | | |
| 123a | 1/17/13 | 1/18/13 | 2.667 | 60 | 1 | 0.086 | 0.371 | | | | |
| 123b | 1/17/13 | 1/18/13 | 2.667 | 60 | 1 | 0.086 | 0.371 | | | | |
| 123c | 1/17/13 | 1/18/13 | 2.667 | 60 | 1 | 0.086 | 0.371 | | | | |
| 123d | 1/17/13 | 1/18/13 | 2.667 | 60 | 1 | 0.086 | 0.371 | | | | |
| 124a | 1/17/13 | 1/18/13 | 2.833 | 60 | 1 | 0.086 | 0.374 | | | | |
| 124b | 1/17/13 | 1/18/13 | 2.833 | 60 | 1 | 0.086 | 0.374 | 58792.000 | 62.124 | 2.17E+12 | 3638800.000 |
| 124c | 1/17/13 | 1/18/13 | 2.833 | 60 | 1 | 0.086 | 0.374 | | | | |
| 124d | 1/17/13 | 1/18/13 | 2.833 | 60 | 1 | 0.086 | 0.374 | | | | |
| 126a | 1/20/13 | 1/21/13 | 3 | 60 | 1 | 0.086 | 0.482 | 0.623 | 15.692 | 3.87E+17 | 5.846 |
| 126b | 1/20/13 | 1/21/13 | 3 | 60 | 1 | 0.086 | 0.482 | 0.739 | 13.386 | 6.33E+17 | 9.886 |
| 128a | 1/22/13 | 1/23/13 | 3 | 60 | 1 | 0.086 | 0.577 | | | | |
| 128b | 1/22/13 | 1/23/13 | 3 | 60 | 1 | 0.086 | 0.577 | | | | |
| 130a | 1/29/13 | 1/30/13 | 3 | 60 | 1 | 0.086 | 0.5 | 7.347 | 3.597 | 2.37E+17 | 26.436 |
| 130b | 1/29/13 | 1/30/13 | 3 | 60 | 1 | 0.086 | 0.5 | 7.712 | 5.468 | 3.69E+17 | 42.462 |
| 130c | 1/29/13 | 1/30/13 | 3 | 60 | 1 | 0.086 | 0.5 | 4.684 | 4.068 | 3.28E+17 | 19.050 |
| 130d | 1/29/13 | 1/30/13 | 3 | 60 | 1 | 0.086 | 0.5 | 4.046 | 5.339 | 2.92E+17 | 21.580 |
| 131a | 1/29/13 | 1/30/13 | 3 | 60 | 1 | 0.086 | 0.457 | | | | |
| 131b | 1/29/13 | 1/30/13 | 3 | 60 | 1 | 0.086 | 0.457 | 2.052 | 6.565 | 4.95E+17 | 13.432 |
| 131c | 1/29/13 | 1/30/13 | 3 | 60 | 1 | 0.086 | 0.457 | 1.452 | 8.833 | 4.87E+17 | 12.824 |
| 131d | 1/29/13 | 1/30/13 | 3 | 60 | 1 | 0.086 | 0.457 | 1.906 | 7.079 | 4.63E+17 | 13.488 |

| | | | | | | | | | | | |
|------|---------|---------|-----|----|---|-------|-------|--------|--------|----------|--------|
| 133a | 2/3/13 | 2/4/13 | 3 | 60 | 1 | 0.086 | 0.374 | | | | |
| 133b | 2/3/13 | 2/4/13 | 3 | 60 | 1 | 0.086 | 0.374 | | | | |
| 133c | 2/3/13 | 2/4/13 | 3 | 60 | 1 | 0.086 | 0.374 | | | | |
| 133d | 2/3/13 | 2/4/13 | 3 | 60 | 1 | 0.086 | 0.374 | 3.270 | 1.221 | 1.92E+18 | 3.998 |
| 135a | 2/3/13 | 2/4/13 | 3 | 60 | 1 | 0.086 | 0.562 | | | | |
| 135b | 2/3/13 | 2/4/13 | 3 | 60 | 1 | 0.086 | 0.562 | 7.040 | 0.903 | 1.32E+18 | 6.361 |
| 135c | 2/3/13 | 2/4/13 | 3 | 60 | 1 | 0.086 | 0.562 | 3.128 | 3.698 | 5.59E+17 | 11.573 |
| 135d | 2/3/13 | 2/4/13 | 3 | 60 | 1 | 0.086 | 0.562 | 4.296 | 1.665 | 9.32E+17 | 7.149 |
| 137a | 2/5/13 | 2/7/13 | 3 | 60 | 1 | 0.086 | 0.437 | 2.793 | 2.364 | 9.56E+17 | 6.603 |
| 137b | 2/5/13 | 2/7/13 | 3 | 60 | 1 | 0.086 | 0.437 | 3.342 | 1.870 | 1.12E+18 | 6.259 |
| 137c | 2/5/13 | 2/7/13 | 3 | 60 | 1 | 0.086 | 0.437 | 2.883 | 1.642 | 1.91E+19 | 4.744 |
| 137d | 2/5/13 | 2/7/13 | 3 | 60 | 1 | 0.086 | 0.437 | 2.542 | 2.237 | 2.13E+18 | 5.700 |
| 139a | 2/5/13 | 2/7/13 | 3 | 60 | 1 | 0.086 | 0.49 | 14.826 | 1.037 | 6.62E+17 | 15.480 |
| 139b | 2/5/13 | 2/7/13 | 3 | 60 | 1 | 0.086 | 0.49 | | | | |
| 139c | 2/5/13 | 2/7/13 | 3 | 60 | 1 | 0.086 | 0.49 | 10.266 | 1.284 | 5.57E+17 | 13.230 |
| 139d | 2/5/13 | 2/7/13 | 3 | 60 | 1 | 0.086 | 0.49 | | | | |
| 140a | 2/7/13 | 2/10/13 | 3 | 60 | 1 | 0.086 | 0.611 | 8.548 | 1.966 | 7.43E+17 | 16.746 |
| 140b | 2/7/13 | 2/10/13 | 3 | 60 | 1 | 0.086 | 0.611 | 7.117 | 8.515 | 2.29E+17 | 30.330 |
| 140c | 2/7/13 | 2/10/13 | 3 | 60 | 1 | 0.086 | 0.611 | 6.468 | 0.922 | 2.37E+18 | 4.712 |
| 140d | 2/7/13 | 2/10/13 | 3 | 60 | 1 | 0.086 | 0.611 | | | | |
| 141a | 2/7/13 | 2/10/13 | 3 | 60 | 1 | 0.086 | 0.623 | | | | |
| 141b | 2/7/13 | 2/10/13 | 3 | 60 | 1 | 0.086 | 0.623 | 0.347 | 18.596 | 9.94E+17 | 6.463 |
| 141c | 2/7/13 | 2/10/13 | 3 | 60 | 1 | 0.086 | 0.623 | 0.209 | 27.492 | 1.09E+18 | 5.756 |
| 141d | 2/7/13 | 2/10/13 | 3 | 60 | 1 | 0.086 | 0.623 | 0.271 | 20.646 | 1.12E+18 | 5.605 |
| 142a | 2/7/13 | 2/10/13 | 3 | 60 | 1 | 0.086 | 0.621 | 0.529 | 10.960 | 1.08E+18 | 5.795 |
| 142b | 2/7/13 | 2/10/13 | 3 | 60 | 1 | 0.086 | 0.621 | 0.614 | 9.946 | 1.03E+18 | 6.104 |
| 142c | 2/7/13 | 2/10/13 | 3 | 60 | 1 | 0.086 | 0.621 | 0.406 | 13.596 | 1.14E+18 | 5.519 |
| 142d | 2/7/13 | 2/11/13 | 3 | 60 | 1 | 0.086 | 0.621 | 0.435 | 11.904 | 1.22E+18 | 5.180 |
| 143a | 2/14/13 | 2/14/13 | 2.5 | 60 | 1 | 0.086 | 0.528 | | | | |
| 143b | 2/14/13 | 2/14/13 | 2.5 | 60 | 1 | 0.086 | 0.528 | | | | |

| | | | | | | | | | | | |
|------|---------|---------|-----|----|---|-------|-------|-------|---------|----------|-------|
| 143c | 2/14/13 | 2/14/13 | 2.5 | 60 | 1 | 0.086 | 0.528 | | | | |
| 143d | 2/14/13 | 2/14/13 | 2.5 | 60 | 1 | 0.086 | 0.528 | | | | |
| 145a | 2/17/13 | 2/18/13 | 3 | 75 | 1 | 0.086 | 0.66 | 0.059 | 52.316 | 2.02E+18 | 3.099 |
| 145b | 2/17/13 | 2/18/13 | 3 | 75 | 1 | 0.086 | 0.66 | 0.033 | 100.202 | 1.88E+18 | 3.317 |
| 145c | 2/17/13 | 2/18/13 | 3 | 75 | 1 | 0.086 | 0.66 | 0.025 | 131.920 | 1.92E+18 | 3.260 |
| 145d | 2/17/13 | 2/18/13 | 3 | 75 | 1 | 0.086 | 0.66 | 0.042 | 80.816 | 1.84E+18 | 3.415 |
| 147a | 2/17/13 | 2/18/13 | 3 | 75 | 1 | 0.086 | 0.745 | 0.097 | 47.892 | 1.35E+18 | 4.644 |
| 147b | 2/17/13 | 2/18/13 | 3 | 75 | 1 | 0.086 | 0.745 | 0.063 | 64.854 | 1.56E+18 | 4.059 |
| 147c | 2/17/13 | 2/18/13 | 3 | 75 | 1 | 0.086 | 0.745 | 0.092 | 49.826 | 1.37E+18 | 4.577 |
| 147d | 2/17/13 | 2/18/13 | 3 | 75 | 1 | 0.086 | 0.745 | 0.039 | 111.022 | 1.47E+18 | 4.264 |
| 148a | 2/19/13 | 2/20/13 | 3 | 75 | 1 | 0.086 | 0.597 | 0.058 | 47.718 | 2.25E+18 | 2.777 |
| 148b | 2/19/13 | 2/20/13 | 3 | 75 | 1 | 0.086 | 0.597 | 0.052 | 56.494 | 2.14E+18 | 2.918 |
| 148c | 2/19/13 | 2/20/13 | 3 | 75 | 1 | 0.086 | 0.597 | 0.037 | 75.356 | 2.26E+18 | 2.800 |
| 148d | 2/19/13 | 2/20/13 | 3 | 75 | 1 | 0.086 | 0.597 | 0.056 | 51.878 | 2.21E+18 | 2.906 |
| 149a | 2/19/13 | 2/20/13 | 3 | 75 | 1 | 0.086 | 0.751 | 0.088 | 52.820 | 1.34E+18 | 4.664 |
| 149b | 2/19/13 | 2/20/13 | 3 | 75 | 1 | 0.086 | 0.751 | 0.098 | 42.490 | 1.50E+18 | 4.156 |
| 149c | 2/19/13 | 2/20/13 | 3 | 75 | 1 | 0.086 | 0.751 | 0.099 | 47.624 | 1.42E+18 | 4.718 |
| 149d | 2/19/13 | 2/20/13 | 3 | 75 | 1 | 0.086 | 0.751 | | | | |
| 150a | 2/19/13 | 2/20/13 | 3 | 75 | 1 | 0.086 | 0.62 | 0.141 | 44.196 | 1.11E+18 | 6.247 |
| 150b | 2/19/13 | 2/20/13 | 3 | 75 | 1 | 0.086 | 0.62 | | | | |
| 150c | 2/19/13 | 2/20/13 | 3 | 75 | 1 | 0.086 | 0.62 | | | | |
| 150d | 2/19/13 | 2/20/13 | 3 | 75 | 1 | 0.086 | 0.62 | | | | |
| 151a | 2/19/13 | 2/20/13 | 3 | 75 | 1 | 0.086 | 0.62 | | | | |
| 151b | 2/19/13 | 2/20/13 | 3 | 75 | 1 | 0.086 | 0.62 | | | | |
| 151c | 2/19/13 | 2/20/13 | 3 | 75 | 1 | 0.086 | 0.62 | | | | |
| 151d | 2/19/13 | 2/20/13 | 3 | 75 | 1 | 0.086 | 0.62 | | | | |
| 152a | 2/26/13 | 2/27/13 | 3 | 75 | 1 | 0.086 | 0.636 | 0.244 | 19.042 | 1.67E+18 | 4.646 |
| 152b | 2/26/13 | 2/27/13 | 3 | 75 | 1 | 0.086 | 0.636 | 0.227 | 29.098 | 1.03E+18 | 6.622 |
| 152c | 2/26/13 | 2/27/13 | 3 | 75 | 1 | 0.086 | 0.636 | | | | |
| 152d | 2/26/13 | 2/27/13 | 3 | 75 | 1 | 0.086 | 0.636 | 0.269 | 25.236 | 9.31E+17 | 6.792 |

| | | | | | | | | | | | |
|------|---------|---------|---|----|---|-------|-------|------------|----------|----------|-----------|
| 153b | 2/26/13 | 2/27/13 | 3 | 75 | 1 | 0.086 | 0.636 | | | | |
| 153c | 2/26/13 | 2/27/13 | 3 | 75 | 1 | 0.086 | 0.636 | | | | |
| 153d | 2/26/13 | 2/27/13 | 3 | 75 | 1 | 0.086 | 0.636 | | | | |
| 154b | 4/7/13 | 4/8/13 | 2 | 60 | 1 | 0.086 | 0.546 | | | | |
| 154c | 4/7/13 | 4/8/13 | 2 | 60 | 1 | 0.086 | 0.546 | | | | |
| 154d | 4/7/13 | 4/8/13 | 2 | 60 | 1 | 0.086 | 0.546 | | | | |
| 158a | 4/16/13 | 4/17/13 | 2 | 60 | 1 | 0.086 | 0.56 | | | | |
| 158b | 4/16/13 | 4/17/13 | 2 | 60 | 1 | 0.086 | 0.56 | | | | |
| 158c | 4/16/13 | 4/17/13 | 2 | 60 | 1 | 0.086 | 0.56 | | | | |
| 158d | 4/16/13 | 4/17/13 | 2 | 60 | 1 | 0.086 | 0.56 | | | | |
| 159a | 4/24/13 | 4/25/13 | 3 | 75 | 1 | 0.086 | 0.765 | 0.097 | 50.700 | 1.27E+18 | 4.906 |
| 159b | 4/24/13 | 4/25/13 | 3 | 75 | 1 | 0.086 | 0.765 | 0.094 | 48.506 | 1.38E+18 | 4.571 |
| 159c | 4/24/13 | 4/25/13 | 3 | 75 | 1 | 0.086 | 0.765 | 0.065 | 64.876 | 1.48E+18 | 4.226 |
| 159d | 4/24/13 | 4/25/13 | 3 | 75 | 1 | 0.086 | 0.765 | 671140.000 | 404.156 | 2.72E+11 | 1.667E+08 |
| 160a | 4/24/13 | 4/25/13 | 3 | 75 | 1 | 0.076 | 0.831 | 0.229 | 30.908 | 8.86E+17 | 7.067 |
| 160b | 4/24/13 | 4/25/13 | 3 | 75 | 1 | 0.076 | 0.831 | 0.243 | 30.434 | 8.49E+17 | 7.386 |
| 160c | 4/24/13 | 4/25/13 | 3 | 75 | 1 | 0.076 | 0.831 | 0.273 | 30.412 | 7.52E+17 | 8.312 |
| 160d | 4/24/13 | 4/25/13 | 3 | 75 | 1 | 0.076 | 0.831 | 0.236 | 34.584 | 7.66E+17 | 8.159 |
| 161a | 4/24/13 | 4/25/13 | 3 | 75 | 1 | 0.066 | 0.603 | 0.563 | 6679.843 | 9.05E+17 | 3742.426 |
| 161b | 4/24/13 | 4/25/13 | 3 | 75 | 1 | 0.066 | 0.603 | 0.574 | 7.946 | 1.37E+18 | 4.559 |
| 161c | 4/24/13 | 4/25/13 | 3 | 75 | 1 | 0.066 | 0.603 | 0.510 | 9.759 | 1.26E+18 | 4.976 |
| 161d | 4/24/13 | 4/25/13 | 3 | 75 | 1 | 0.066 | 0.603 | 0.580 | 8.197 | 1.33E+18 | 4.756 |
| 162a | 4/24/13 | 4/25/13 | 3 | 75 | 1 | 0.056 | 0.507 | 1.400 | 3.648 | 1.27E+18 | 5.112 |
| 162b | 4/24/13 | 4/25/13 | 3 | 75 | 1 | 0.056 | 0.507 | 1.217 | 3.985 | 1.29E+18 | 4.851 |
| 162c | 4/24/13 | 4/25/13 | 3 | 75 | 1 | 0.056 | 0.507 | 1.219 | 3.571 | 1.47E+18 | 4.350 |
| 162d | 4/24/13 | 4/25/13 | 3 | 75 | 1 | 0.056 | 0.507 | 0.980 | 4.855 | 1.31E+18 | 4.757 |
| 163a | 4/26/13 | 4/26/13 | 3 | 75 | 1 | 0.044 | 0.481 | 11.122 | 1.580 | 7.12E+17 | 17.471 |
| 163c | 4/26/13 | 4/26/13 | 3 | 75 | 1 | 0.044 | 0.481 | 14.234 | 0.677 | 7.19E+17 | 9.640 |
| 164a | 4/26/13 | 4/26/13 | 3 | 75 | 1 | 0.022 | 0.239 | | | | |
| 164c | 4/26/13 | 4/26/13 | 3 | 75 | 1 | 0.022 | 0.239 | | | | |

| | | | | | | | | | | | |
|------|---------|---------|---|----|---|-------|-------|--------|-------|----------|--------|
| 164d | 4/26/13 | 4/26/13 | 3 | 75 | 1 | 0.022 | 0.239 | | | | |
| 167a | 5/9/13 | 5/13/13 | 3 | 75 | 1 | 0.035 | 0.394 | | | | |
| 167b | 5/9/13 | 5/13/13 | 3 | 75 | 1 | 0.035 | 0.394 | | | | |
| 167c | 5/9/13 | 5/13/13 | 3 | 75 | 1 | 0.035 | 0.394 | | | | |
| 167d | 5/9/13 | 5/13/13 | 3 | 75 | 1 | 0.035 | 0.394 | 26.070 | 1.630 | 1.10E+18 | 31.373 |
| 168a | 5/9/13 | 5/13/13 | 3 | 75 | 1 | 0.03 | 0.328 | | | | |
| 168b | 5/9/13 | 5/13/13 | 3 | 75 | 1 | 0.03 | 0.328 | | | | |
| 168c | 5/9/13 | 5/13/13 | 3 | 75 | 1 | 0.03 | 0.328 | | | | |
| 168d | 5/9/13 | 5/13/13 | 3 | 75 | 1 | 0.03 | 0.328 | | | | |
| 169a | 5/13/13 | 5/14/13 | 3 | 60 | 1 | 0.086 | 0.557 | | | | |
| 169b | 5/13/13 | 5/14/13 | 3 | 60 | 1 | 0.086 | 0.557 | | | | |
| 169c | 5/13/13 | 5/14/13 | 3 | 60 | 1 | 0.086 | 0.557 | | | | |
| 169d | 5/13/13 | 5/14/13 | 3 | 60 | 1 | 0.086 | 0.557 | | | | |

*Note: No film growth occurred under these conditions.

Table II: PbSe thin films for which the measurement of the sign of the Hall coefficient and majority carrier density was inconsistent across three to five trials of measurement or for which both electrons and holes contribute to conduction.

| | | ρ (Ω -cm) | | | | | μ (cm ² /Vs) | | | | | Majority Carrier Density (cm ⁻³) | | | | | RH (cm ³ /C) | | | | |
|----------|------------------------------|------------------------|-----------|-----------|-------------|--------|-----------------------------|----------|----------|----------|----------|--|-----------|-----------|-----------|-----------|-------------------------|------------|------------|------------|------------|
| Sample # | Optical Thickness (μ m) | Trial # 1 | 2 | 3 | 4 | 5 | Trial # 1 | 2 | 3 | 4 | 5 | Trial # 1 | 2 | 3 | 4 | 5 | Trial # 1 | 2 | 3 | 4 | 5 |
| iv | 0.696 | 5.304 | 115.573 | 57.603 | | | 28.510 | 5.040 | 9.367 | | | 4.13E+16 | -1.07E+16 | -1.16E+16 | | | 1.513E+02 | -5.824E+02 | -5.396E+02 | | |
| x | 0.468 | 13.073 | 13.591 | 13.709 | | | 0.499 | 0.282 | 0.537 | | | 1.24E+18 | 1.76E+18 | 4.68E+17 | | | 5.031E+00 | 3.542E+00 | 1.335E+01 | | |
| xii | 0.471 | 6.436 | 6.587 | 6.686 | | | 4.565 | 2.931 | 5.817 | | | -5.72E+18 | 4.18E+18 | 2.14E+17 | | | -1.091E+00 | 1.492E+00 | 2.912E+01 | | |
| xiii | NA | 86.891 | 88.169 | 88.947 | | | 1.867 | 0.623 | 0.367 | | | -3.85E+16 | 1.14E+17 | 1.91E+17 | | | -1.622E+02 | 5.492E+01 | 3.263E+01 | | |
| 11 | 0.562 | 42.122 | 44.286 | 44.820 | | | 1.168 | 0.000 | 2.025 | | | -1.27E+17 | 4.86E+20 | -6.88E+16 | | | -4.920E+01 | 1.285E-02 | -9.076E+01 | | |
| 93 | 0.59 | 165.100 | 169.100 | 171.000 | | | 0.991 | 0.278 | 0.910 | | | 3.82E+16 | -1.33E+17 | -4.01E+16 | | | 1.636E+02 | -4.695E+01 | -1.556E+02 | | |
| 105 | 0.676 | 63.100 | 64.920 | 66.140 | | | 89.160 | 0.819 | 0.562 | | | -1.11E+15 | -1.17E+17 | -1.68E+17 | | | -5.626E+03 | -5.316E+01 | -3.718E+01 | | |
| 106 | 0.531 | 159.000 | 164.300 | 167.500 | | | 0.137 | 7.407 | 0.260 | | | 2.88E+17 | -5.13E+15 | -1.43E+17 | | | 2.171E+01 | -1.217E+03 | -4.353E+01 | | |
| 107 | 0.396 | 69760.000 | 37130.000 | 35430.000 | | | 83.980 | 46.560 | 534.000 | | | -1.07E+12 | -3.61E+12 | 3.30E+11 | | | -5.859E+06 | -1.729E+06 | 1.892E+07 | | |
| 108 | 0.281 | 64530.000 | 42800.000 | 53710.000 | | | 75.600 | 177.600 | 39.710 | | | 1.28E+12 | 8.21E+11 | -2.93E+12 | | | 4.879E+06 | 7.599E+06 | -2.132E+06 | | |
| 109 | 0.135 | 86350.000 | 66710.000 | 76270.000 | | | 37.750 | 606.400 | 831.900 | | | -1.92E+12 | -1.54E+11 | -9.84E+10 | | | -3.260E+06 | -4.045E+07 | -6.345E+07 | | |
| 111 | 0.532 | 39.650 | 40.190 | 40.600 | | | 0.769 | 0.114 | 0.062 | | | 2.05E+17 | 1.36E+18 | -2.46E+18 | | | 3.047E+01 | 4.591E+00 | -2.537E+00 | | |
| 113 | 0.543 | 535000.000 | 1695.000 | 1458.000 | | | 0.043 | 31.800 | 5.374 | | | -2.69E+14 | 1.16E+14 | 7.96E+14 | | | -2.320E+04 | 5.389E+04 | 7.838E+03 | | |
| 123a | 0.371 | 873.500 | 1405.000 | 1392.000 | 974.600 | 300.6 | 721.800 | 3759.000 | 1185.000 | 700.600 | 3829.000 | -9.90E+12 | 1.18E+12 | -3.79E+12 | -9.14E+12 | 5.43E+12 | -6.305E+05 | 5.282E+06 | -1.649E+06 | -6.828E+05 | 1.151E+06 |
| 123b | 0.371 | 2089.000 | 2472.000 | 2577.000 | 2678.000 | 2650 | 1614.000 | 665.700 | 396.700 | 401.500 | 1693.000 | -1.85E+12 | 3.79E+12 | 6.11E+12 | 5.81E+12 | -1.39E+12 | -3.372E+06 | 1.646E+06 | 1.022E+06 | 1.075E+06 | -4.487E+06 |
| 123c | 0.371 | 193800.000 | 14460.000 | 836.000 | 3500.000 | 13330 | 11.620 | 345.500 | 8436.000 | 255.500 | 292.800 | 2.77E+12 | 1.25E+12 | -8.85E+11 | -6.98E+12 | -1.60E+12 | 2.252E+06 | 4.995E+06 | -7.053E+06 | -8.943E+05 | -3.904E+06 |
| 123d | 0.371 | 1585.000 | 1357.000 | 1384.000 | 1531.000 | 528.8 | 140.300 | 2506.000 | 4385.000 | 6291.000 | 1201.000 | -2.81E+13 | 1.84E+12 | 1.03E+12 | -6.48E+11 | 9.83E+12 | -2.223E+05 | 3.400E+06 | 6.069E+06 | -9.632E+06 | 6.350E+05 |
| 124a | 0.374 | 26.450 | 27.550 | 28.080 | 28.590 | 28.9 | 4.402 | 1.543 | 0.381 | 1.805 | 1.812 | -5.36E+16 | -1.47E+17 | 5.83E+17 | 1.21E+17 | -1.19E+17 | -1.164E+02 | -4.250E+01 | 1.071E+01 | 5.159E+01 | -5.236E+01 |
| 124c | 0.374 | 33.770 | 44.520 | 41.830 | 42.500 | 47.59 | 67.660 | 320.400 | 307.500 | 170.400 | 1046.000 | -2.73E+15 | 4.38E+14 | -4.85E+14 | 8.62E+14 | -1.25E+14 | -2.285E+03 | 1.426E+04 | -1.286E+04 | 7.243E+03 | -4.978E+04 |
| 124d | 0.374 | 18.200 | 14.180 | 622.700 | 4209000.000 | 430700 | 18630.000 | 8399.000 | 2.366 | 0.003 | 0.380 | -1.84E+13 | -5.24E+13 | 4.24E+15 | 4.46E+14 | 3.82E+13 | -3.392E+05 | -1.191E+05 | 1.473E+03 | 1.400E+04 | 1.636E+05 |
| 126a | 0.482 | 0.617 | 0.623 | 0.624 | 0.625 | 0.6273 | 17.680 | 15.040 | 15.740 | 15.160 | 14.840 | 5.72E+17 | 6.67E+17 | -6.36E+17 | 6.59E+17 | 6.71E+17 | 1.091E+01 | 9.360E+00 | -9.820E+00 | 9.473E+00 | 9.307E+00 |
| 128a | 0.577 | 18.280 | 0.863 | 0.868 | 0.870 | 0.8712 | 6580.000 | 14.310 | 17.310 | 14.550 | 17.180 | -5.19E+13 | 5.05E+17 | 4.15E+17 | 4.93E+17 | 4.17E+17 | -1.203E+05 | 1.235E+01 | 1.503E+01 | 1.266E+01 | 1.496E+01 |
| 131a | 0.457 | 34.430 | 19.180 | 18.790 | 17.630 | 24.79 | 112.800 | 371.900 | 4869.000 | 2346.000 | 648.200 | -1.61E+15 | 8.75E+14 | -6.82E+13 | -1.51E+14 | 3.89E+14 | -3.883E+03 | 7.135E+03 | -9.148E+04 | -4.136E+04 | 1.607E+04 |

| | | | | | | | | | | | | | | | | | | | | | |
|------|-------|-----------|-----------|--------------|--------------|-----------|------------|------------|----------|-----------|-----------|-----------|-----------|-----------|-----------|-----------|------------|------------|------------|------------|------------|
| 132 | 0.374 | 0.246 | 0.060 | 0.098 | 1.158 | 0.8627 | 490.200 | 254.500 | 289.600 | 3.377 | 14.820 | -5.18E+16 | 4.08E+17 | 2.19E+17 | -1.60E+18 | 4.88E+17 | -1.204E+02 | 1.528E+01 | 2.851E+01 | -3.910E+00 | 1.278E+01 |
| 133a | 0.374 | 8.101 | 8.132 | 8.170 | 8.192 | 8.211 | 0.661 | 4.076 | 4.141 | 4.659 | 1.522 | 1.17E+18 | 1.88E+17 | 1.85E+17 | -1.64E+17 | -5.00E+17 | 5.355E+00 | 3.315E+01 | 3.383E+01 | -3.817E+01 | -1.249E+01 |
| 133b | 0.374 | 4.365 | 4.361 | 4.379 | 4.390 | 4.402 | 7.146 | 0.166 | 2.615 | 4.360 | 3.615 | -2.00E+17 | 8.64E+18 | -5.45E+17 | 3.26E+17 | 3.92E+17 | -3.120E+01 | 7.226E-01 | -1.145E+01 | 1.914E+01 | 1.591E+01 |
| 133c | 0.374 | 12.000 | 11.890 | 11.910 | 11.940 | 11.96 | 0.602 | 9.427 | 0.307 | 0.292 | 0.689 | 8.64E+17 | -5.57E+16 | 1.71E+18 | 1.79E+18 | 7.57E+17 | 7.225E+00 | -1.121E+02 | 3.655E+00 | 3.486E+00 | 8.243E+00 |
| 134 | 0.562 | 1.269 | 1.749 | 1.950 | 1.903 | 1.718 | 108.600 | 61.060 | 188.700 | 28.330 | 43.750 | -4.53E+16 | 5.85E+16 | 1.70E+16 | 1.16E+17 | 8.31E+16 | -1.378E+02 | 1.068E+02 | 3.680E+02 | 5.390E+01 | 7.514E+01 |
| 135a | 0.562 | 11.400 | 11.450 | 11.480 | 11.510 | 11.53 | 1.467 | 2.420 | 0.550 | 0.712 | 1.202 | 3.73E+17 | 2.25E+17 | 9.88E+17 | -7.62E+17 | 4.50E+17 | 1.673E+01 | 2.771E+01 | 6.316E+00 | -8.196E+00 | 1.387E+01 |
| 139b | 0.49 | 11.850 | 11.990 | 12.100 | 12.190 | 12.26 | 1.334 | 1.445 | 1.633 | 0.536 | 0.183 | 3.95E+17 | 3.60E+17 | 3.16E+17 | 9.55E+17 | -2.79E+18 | 1.580E+01 | 1.733E+01 | 1.976E+01 | 6.537E+00 | -2.239E+00 |
| 139d | 0.49 | 9.881 | 9.971 | 10.040 | 10.100 | 10.14 | 6.004 | 0.960 | 1.215 | 3.591 | 0.940 | -1.05E+17 | -6.53E+17 | 5.12E+17 | 1.72E+17 | -6.55E+17 | -5.932E+01 | -9.567E+00 | 1.219E+01 | 3.626E+01 | -9.531E+00 |
| 140d | 0.611 | 48.670 | 5.365 | 5.383 | 5.396 | 5.409 | 0.947 | 1.835 | 1.081 | 2.705 | 0.798 | 5.67E+17 | 4.62E+17 | 3.97E+17 | 8.45E+17 | -9.24E+17 | 1.101E+01 | 1.352E+01 | 1.574E+01 | 7.389E+00 | -6.753E+00 |
| 141a | 0.623 | 0.315 | 0.315 | 0.316 | 0.316 | 0.3169 | 20.800 | 20.130 | 4413.000 | 14.900 | 13.060 | 1.36E+17 | 6.34E+17 | 1.07E+18 | 4.28E+17 | 1.45E+18 | 6.542E+00 | 6.344E+00 | -1.393E+03 | 4.713E+00 | 4.140E+00 |
| 143a | 0.528 | 54.440 | 56.490 | 57.290 | 57.650 | 57.89 | 11.160 | 0.271 | 0.252 | 0.525 | 0.075 | 1.03E+16 | -4.07E+17 | -4.33E+17 | 2.06E+17 | -1.44E+18 | 6.078E+02 | -1.532E+01 | -1.441E+01 | 3.026E+01 | -4.344E+00 |
| 143b | 0.528 | 46.170 | 47.540 | 48.410 | 49.050 | 49.62 | 2.779 | 0.073 | 1.408 | 0.215 | 0.626 | -4.87E+16 | 1.80E+18 | 9.16E+16 | -5.91E+17 | 2.01E+17 | -1.283E+02 | 3.478E+00 | 6.816E+01 | -1.056E+01 | 3.108E+01 |
| 143c | 0.528 | 37.950 | 38.940 | 39.580 | 40.120 | 40.52 | 2.188 | 5.226 | 9.140 | 3.495 | 0.724 | -7.52E+16 | 3.07E+16 | -1.73E+16 | 4.45E+16 | -2.13E+17 | -8.303E+01 | 2.035E+02 | -3.618E+02 | 1.402E+02 | -2.932E+01 |
| 143d | 0.528 | 35.040 | 35.990 | 36.570 | 36.960 | 37.27 | 2.233 | 0.047 | 0.663 | 0.578 | 1.217 | -7.98E+16 | -3.71E+18 | -2.58E+17 | 2.92E+17 | -1.38E+17 | -7.824E+01 | -1.681E+00 | -2.424E+01 | 2.136E+01 | -4.536E+01 |
| 149d | 0.751 | 13510.000 | 0.098 | 0.098 | 0.099 | 0.09873 | 1.117 | 34.340 | 52.870 | 53.110 | 53.290 | -4.14E+14 | 1.85E+18 | 1.20E+18 | 1.19E+18 | 1.19E+18 | -1.508E+04 | 3.367E+00 | 5.201E+00 | 5.233E+00 | 5.261E+00 |
| 150b | 0.62 | 0.224 | 0.227 | 0.222 | 0.364 | 0.2314 | 20.330 | 467.000 | 6939.000 | 5292.000 | 11750.000 | 1.37E+18 | -5.89E+16 | -4.05E+15 | -3.24E+15 | -2.30E+15 | 4.553E+00 | -1.060E+02 | -1.541E+03 | -1.928E+03 | -2.719E+03 |
| 150c | 0.62 | 0.240 | 0.323 | 0.209 | 0.242 | 0.2436 | 298.000 | 315.000 | 35.640 | 31.220 | 38.840 | -8.72E+16 | -6.14E+16 | 8.37E+17 | 8.26E+17 | 6.60E+17 | -7.158E+01 | -1.016E+02 | 7.458E+00 | 7.561E+00 | 9.462E+00 |
| 150d | 0.62 | 0.203 | 0.206 | 0.208 | 0.204 | 0.2017 | 115.800 | 13930.000 | 188.100 | 1.265 | 3.290 | -2.65E+17 | 2.18E+15 | 1.60E+17 | -2.42E+19 | 9.41E+18 | -2.354E+01 | 2.866E+03 | 3.904E+01 | -2.579E-01 | 6.637E-01 |
| 151a | 0.62 | 21.340 | 190.400 | 63270000.000 | 12320000.000 | 264600000 | 173300.000 | 152000.000 | 0.076 | 0.343 | 0.135 | -1.69E+12 | -2.16E+11 | 1.30E+12 | 1.48E+12 | 1.74E+11 | -3.698E+06 | -2.894E+07 | 4.812E+06 | 4.223E+06 | 3.581E+07 |
| 151b | 0.62 | 72.230 | 73.180 | 73.730 | 74.230 | 74.59 | 7.389 | 10.450 | 1.753 | 2.293 | 1.334 | -1.17E+16 | -8.16E+15 | 4.83E+16 | -3.67E+16 | 6.28E+16 | -5.338E+02 | -7.646E+02 | 1.292E+02 | -1.702E+02 | 9.948E+01 |
| 151c | 0.62 | 93.270 | 121.100 | 100.000 | 100.400 | 100.9 | 33.160 | 8.657 | 3.577 | 0.822 | 0.256 | 2.02E+15 | -5.95E+15 | 1.75E+16 | 7.56E+16 | 2.42E+17 | 3.092E+03 | -1.049E+03 | 3.578E+02 | 8.257E+01 | 2.579E+01 |
| 151d | 0.62 | 70.390 | 71.400 | 72.030 | 72.720 | 73.25 | 1.091 | 10.680 | 11.170 | 0.901 | 2.657 | -8.13E+16 | 8.18E+15 | 7.76E+15 | 9.53E+16 | 3.21E+16 | -7.680E+01 | 7.627E+02 | 8.049E+02 | 6.552E+01 | 1.946E+02 |
| 152c | 0.636 | 0.816 | 0.818 | 0.819 | 0.821 | 0.8221 | 2.932 | 3.352 | 1.005 | 12.830 | 3.968 | 2.61E+18 | -2.28E+18 | -7.58E+18 | 5.93E+17 | 1.91E+18 | 2.392E+00 | -2.741E+00 | -8.233E-01 | 1.053E+01 | 3.262E+00 |
| 152 | 0.636 | 162.300 | 162.900 | 163.200 | 163.400 | 163.5 | 2.282 | 3.844 | 0.302 | 1.962 | 0.293 | 1.69E+16 | 9.97E+15 | 1.27E+17 | 1.95E+16 | -1.30E+17 | 0.000E+00 | 0.000E+00 | 0.000E+00 | 0.000E+00 | 0.000E+00 |
| 153b | 0.636 | 162.300 | 162.900 | 163.200 | 163.400 | 163.5 | 2.282 | 3.844 | 0.302 | 1.962 | 0.293 | 1.69E+16 | 9.97E+15 | 1.27E+17 | 1.95E+16 | -1.30E+17 | 3.705E+02 | 6.262E+02 | 4.929E+01 | 3.205E+02 | -4.786E+01 |
| 153c | 0.636 | 314.400 | 382.600 | 385.300 | 357.000 | 333.3 | 2195.000 | 225.800 | 23.660 | 451.200 | 1916.000 | -9.04E+12 | 7.23E+13 | 6.85E+14 | 3.88E+13 | 9.77E+12 | -6.903E+05 | 8.639E+04 | 9.118E+03 | 1.611E+05 | 6.388E+05 |
| 153d | 0.636 | 144.300 | 407.600 | 95.640 | 98.660 | 103.1 | 97.790 | 304.300 | 2280.000 | 18760.000 | 500.800 | 4.42E+14 | 5.03E+13 | 2.86E+13 | -3.37E+12 | 1.21E+14 | 1.411E+04 | 1.240E+05 | 2.180E+05 | -1.850E+06 | 5.161E+04 |
| 153 | 0.636 | 171.600 | 172.600 | 174.000 | 174.400 | 174.7 | 2.535 | 0.237 | 0.351 | 1.516 | 0.535 | -1.44E+16 | 1.53E+17 | -1.02E+17 | 2.36E+16 | 6.69E+16 | -4.351E+02 | 4.092E+01 | -6.100E+01 | 2.644E+02 | 9.337E+01 |
| 154b | 0.546 | 63030.000 | 44440.000 | 32180.000 | 28920.000 | 8710 | 61.470 | 99.230 | 202.200 | 657.700 | 1144.000 | -1.61E+12 | 1.42E+12 | 5.95E+10 | -3.28E+11 | -6.26E+11 | -3.875E+06 | 4.410E+06 | 6.505E+06 | -1.902E+07 | -9.968E+06 |
| 154c | 0.546 | 1078.000 | 1215.000 | 1158.000 | 1159.000 | 1185 | 410.400 | 482.100 | 27.500 | 462.100 | 172.200 | 1.41E+13 | 1.07E+13 | 1.96E+14 | -1.17E+13 | 3.06E+13 | 4.423E+05 | 5.860E+05 | 3.184E+04 | -5.356E+05 | 2.040E+05 |

| | | | | | | | | | | | | | | | | | | | | | |
|------|-------|----------|-----------|----------|-----------|-------|-----------|-----------|-----------|----------|----------|-----------|-----------|-----------|-----------|-----------|------------|------------|------------|------------|------------|
| 154d | 0.546 | 651.800 | 81850.000 | 490.400 | 10980.000 | 430.9 | 22750.000 | 121.400 | 44830.000 | 2063.000 | 4606.000 | 4.21E+11 | 6.28E+11 | 2.84E+11 | 2.76E+11 | -3.15E+12 | 1.483E+07 | 9.937E+06 | 2.199E+07 | 2.264E+07 | -1.985E+06 |
| 158a | 0.56 | 347.900 | 455.300 | 443.900 | 448.400 | 412.9 | 13.070 | 583.500 | 164.200 | 496.300 | 86.440 | -1.37E+15 | 2.35E+13 | -8.56E+13 | 2.81E+13 | -1.75E+14 | -4.548E+03 | 2.657E+05 | -7.289E+04 | 2.225E+05 | -3.569E+04 |
| 158b | 0.56 | 503.600 | 482.700 | 494.200 | 508.700 | 505.2 | 7.146 | 124.600 | 139.200 | 312.000 | 44.700 | 1.73E+15 | -1.04E+14 | -9.07E+13 | 3.93E+13 | -2.76E+14 | 3.599E+03 | -6.015E+04 | -6.881E+04 | 1.587E+05 | -2.258E+04 |
| 158c | 0.56 | 106.600 | 107.300 | 107.800 | 108.300 | 108.6 | 1.028 | 2.118 | 2.322 | 0.374 | 4.513 | 5.70E+16 | 2.75E+16 | -2.49E+16 | -1.54E+17 | 1.27E+16 | 1.096E+02 | 2.272E+02 | -2.503E+02 | -4.047E+01 | 4.903E+02 |
| 158d | 0.56 | 99.980 | 101.000 | 101.600 | 102.400 | 102.8 | 0.237 | 0.009 | 11.430 | 4.447 | 0.748 | 2.64E+17 | 7.09E+18 | -5.37E+15 | -1.37E+16 | 8.12E+16 | 2.367E+01 | 8.800E-01 | -1.162E+03 | -4.554E+02 | 7.689E+01 |
| 159 | 0.56 | 8.921 | 7.971 | 8.421 | 8.532 | 8.313 | 318.700 | 118.000 | 32.920 | 37.370 | 9.661 | -2.20E+15 | 6.64E+15 | -2.25E+16 | -1.96E+16 | -7.77E+16 | -2.843E+03 | 9.404E+02 | -2.772E+02 | -3.188E+02 | -8.031E+01 |
| 164a | 0.239 | 762.100 | 6.191 | 2988.000 | 436.200 | 746.1 | 5499.000 | 31880.000 | 402.400 | 482.000 | 2538.000 | 1.49E+12 | -3.16E+13 | 5.19E+12 | 2.97E+13 | 3.30E+12 | 4.191E+06 | -1.974E+05 | 1.202E+06 | 2.103E+05 | 1.893E+06 |
| 164c | 0.239 | 3667.000 | 3690.000 | 3703.000 | 3692.000 | 3974 | 725.600 | 342.400 | 281.600 | 307.000 | 113.000 | 2.35E+12 | 4.94E+12 | 5.99E+12 | 5.51E+12 | -1.39E+13 | 2.660E+06 | 1.264E+06 | 1.043E+06 | 1.134E+06 | -4.493E+05 |
| 164d | 0.239 | 1062.000 | 909.300 | 1043.000 | 1067.000 | 1028 | 76.210 | 3025.000 | 321.800 | 1235.000 | 438.800 | 7.71E+13 | -2.27E+12 | -1.86E+13 | 4.74E+12 | 1.38E+13 | 8.094E+04 | -2.751E+06 | -3.356E+05 | 1.317E+06 | 4.511E+05 |
| 167a | 0.394 | 31.260 | 34.530 | 35.700 | 36.640 | 37.39 | 0.960 | 0.659 | 0.040 | 0.623 | 0.182 | -2.08E+17 | 2.74E+17 | -4.35E+18 | 2.73E+17 | -9.18E+17 | -3.000E+01 | 2.275E+01 | -1.434E+00 | 2.283E+01 | -6.804E+00 |
| 167b | 0.394 | 35.960 | 37.920 | 39.080 | 40.030 | 40.78 | 0.027 | 2.206 | 0.222 | 0.148 | 0.663 | 6.32E+18 | 7.46E+16 | -7.19E+17 | -1.06E+18 | -2.31E+17 | 9.874E-01 | 8.364E+01 | -8.684E+00 | -5.908E+00 | -2.704E+01 |
| 167c | 0.394 | 42.540 | 43.810 | 44.650 | 45.610 | 46.8 | 0.401 | 0.248 | 0.271 | 0.810 | 0.212 | 3.66E+17 | 5.74E+17 | 5.15E+17 | 1.69E+17 | -6.30E+17 | 1.707E+01 | 1.087E+01 | 1.212E+01 | 3.694E+01 | -9.913E+00 |
| 168a | 0.328 | 222.300 | 247.100 | 236.700 | 238.800 | 246.8 | 204.900 | 407.400 | 198.800 | 377.900 | 81.630 | -1.37E+14 | -6.20E+13 | -1.33E+14 | -6.92E+13 | 3.10E+14 | -4.554E+04 | -1.007E+05 | -4.706E+04 | -9.025E+04 | 2.014E+04 |
| 168b | 0.328 | 338.700 | 350.100 | 349.600 | 334.900 | 359.9 | 468.300 | 4.303 | 2063.000 | 2015.000 | 409.800 | 3.94E+13 | -4.14E+15 | -8.66E+12 | -9.25E+12 | -4.23E+13 | 1.586E+05 | -1.507E+03 | -7.212E+05 | -6.749E+05 | -1.475E+05 |
| 168c | 0.328 | 106.000 | 108.500 | 110.400 | 112.300 | 113.7 | 0.294 | 1.752 | 0.135 | 0.422 | 0.129 | 2.00E+17 | 3.28E+16 | -4.19E+17 | -1.32E+17 | -4.27E+17 | 3.116E+01 | 1.901E+02 | -1.491E+01 | -4.733E+01 | -1.461E+01 |
| 168d | 0.328 | 115.900 | 117.400 | 118.300 | 119.200 | 119.9 | 3.113 | 2.681 | 36.590 | 2.627 | 3.332 | -1.73E+16 | 1.98E+16 | 1.44E+15 | 1.99E+16 | -1.56E+16 | -3.608E+02 | 3.146E+02 | 4.330E+03 | 3.131E+02 | -3.996E+02 |
| 169a | 0.557 | 22.580 | 23.400 | 23.580 | 23.710 | 23.83 | 0.678 | 0.525 | 0.446 | 0.758 | 0.159 | 4.08E+17 | 5.08E+17 | 5.94E+17 | 3.47E+17 | -1.64E+18 | 1.532E+01 | 1.228E+01 | 1.051E+01 | 1.798E+01 | -3.799E+00 |
| 169b | 0.557 | 22.930 | 23.610 | 24.040 | 24.410 | 24.73 | 0.099 | 0.091 | 0.490 | 0.534 | 0.154 | 2.74E+18 | -2.90E+18 | -5.30E+17 | 4.79E+17 | 1.64E+18 | 2.281E+00 | -2.154E+00 | -1.177E+01 | 1.304E+01 | 3.797E+00 |
| 169c | 0.557 | 13.600 | 13.790 | 13.910 | 14.010 | 14.1 | 0.463 | 1.170 | 0.047 | 1.917 | 5.428 | -9.92E+17 | 3.87E+17 | -9.47E+18 | 2.32E+17 | 8.16E+16 | -6.292E+00 | 1.613E+01 | -6.593E-01 | 2.686E+01 | 7.654E+01 |
| 169d | 0.557 | 18.150 | 18.610 | 18.940 | 19.180 | 19.39 | 0.839 | 0.475 | 0.015 | 0.127 | 0.696 | 4.10E+17 | 7.06E+17 | 2.24E+19 | -2.57E+18 | -4.63E+17 | 1.523E+01 | 8.848E+00 | 2.782E-01 | -2.431E+00 | -1.350E+01 |